Subpicosecond Pulse Generation Using Modelocked Semiconductor Laser Diodes

by

Roger Jonathan Helkey

A Dissertation submitted in partial satisfaction
of the requirements for the degree of

Doctor of Philosophy
in
Electrical and Computer Engineering

July 1993

Committee Members

Professor John E. Bowers, Chair
Professor Larry A. Coldren
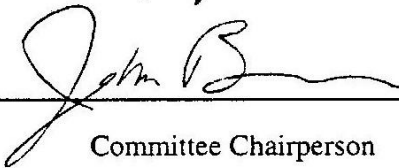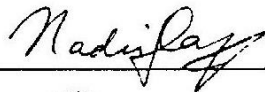Professor Nadir Dagli
Professor Mark J. Rodwell

Subpicosecond Pulse Generation Using

Modelocked Semiconductor Laser Diodes

The dissertation of Roger Jonathan Helkey

is approved

_____

_____

_____

_____
Committee Chairperson

July 1993

ii

To Martha
Daniel and Christopher

ABSTRACT

Subpicosecond Pulse Generation Using Modelocked Semiconductor Laser Diodes

by

Roger Jonathan Helkey

This dissertation deals with short pulse generation by passive modelocking of semiconductor lasers. A partial integration method for numerical simulation is developed, which reduced computation time by >2 orders of magnitude over previous modelocked laser simulations. The effects of higher order correction terms are included, and the finite gain-bandwidth of the laser medium is shown to be a limiting factor in producing subpicosecond pulses with active modelocking. Numerical modeling techniques are compared under strong gain saturation. Simplified expressions under various asymptotic limits are developed. The importance of the colliding pulse effect on the passive modelocking process is investigated both theoretically and experimentally. The results show how parameters can be optimized for short pulsewidth or high output power.

Curved waveguide devices are shown to eliminate secondary pulses, and tapered waveguide devices are shown to increase the output power. Using quadratic phase compensation, pulses have been compressed to 0.45 ps.

The generation and distribution of millimeter-wave reference signals by semiconductor lasers is considered. The optimum conditions for harmonic generation are examined. Feedback stabilization of monolithic devices is proposed, and demonstrated for an external cavity passively modelocked laser. Timing jitter is reduced from 1 ns to 4 ps for a one second measurement.

ACKNOWLEDGMENTS

I would like to thank my dissertation advisor Professor John Bowers for initiating my work on modelocking, and for his enthusiasm and commitment to this project.

I would like to thank my thesis committee Professor Larry Coldren, Professor Mark Rodwell, and Professor Nadir Dagli for their time and input. The ECE faculty also deserves commendation for facilitating an environment of cooperation between research groups. I indirectly benefitted from the efforts of many fellow graduate students, particularly those involved in building processing equipment and fabricating lasers.

I would like to thank my collaborators Alan Mar who developed much of the modelocking technology at UCSB, and Dennis Derickson with whom I have had many discussions on modelocking and phase noise measurement. Judy Karin supplied results and insight on the absorption recovery dynamics in GaAs/AlGaAs devices, and Wenbin Jiang provided valuable assistance with pulse compressors. I would like to thank John Wasserbauer who fabricated InGaAsP laser diodes for the modelocking group, Robert Thornton of Xerox who supplied the GaAs-AlGaAs laser diodes on which part of this work is based, and Wei-Xiong Zou for fabricating the extremely low threshold InGaAs-GaAs lasers on which the rest of this work is based. I would like to thank Bruce Young for growing the InGaAs/AlGaAs material, and Ralph Logan and Tawee Tan-bun Ek for suppling InGaAsP/InP material and lasers to the group.

I would like to thank Tom Reynolds for sputtering some of the antireflection coatings and for keeping the laboratory running smoothly, and Jim Dudley for teaching me how to use the laser coating system. Rich Mirin, Pat Corvini, and Phil

PUBLICATIONS

1. R. J. Helkey, "Mode-Locked Semiconductor Lasers", to be presented at IEEE Lasers and Electro-optics Society Annual Meeting, San Jose CA (1993), **Invited Paper**.

2. A. Mar, R. J. Helkey, J. E. Bowers, D. Mehuys, D. Welch, "Mode-locked Operation of a Master Oscillator Power Amplifier", to be presented at IEEE Lasers and Electro-optics Society Annual Meeting, **MSFL4.2**, San Jose CA (1993).

3. R. Nagarajan, S. Levy, R. J. Helkey, P. Humphrey, J. E. Bowers, "Fiber-Optic BPSK Subcarrier Transmission at 35 GHz over 6.3 km using a Grating External Cavity Semiconductor Laser", IEEE Optical Microwave Interactions Conference, **T2.2,** Santa Barbara (1993).

4. A. Mar, R. J. Helkey, T. Reynolds, J. E. Bowers, D. Botez, C. Zmudzinski, "Mode-Locked Multi-Segment Resonant-Optical-Waveguide Diode Laser Arrays", IEEE Optical Microwave Interactions Conference, **PD2**, Santa Barbara (1993).

5. R. J. Helkey, W. X. Zou, A. Mar, D. B. Young, J. E. Bowers, "Curved and Tapered Waveguide Mode-Locked InGaAs/AlGaAs Semiconductor Lasers Fabricated by Impurity Induced Disordering", Device Research Conference, Santa Barbara (1993).

6. S. Levy, R. Nagarajan, R. J. Helkey, P. Humphrey, J. E. Bowers, "Millimeter Wave Fiber-Optic PSK Subcarrier Transmission at 35 GHz over 6.3 km Using a Grating External Cavity Semiconductor Laser", Electronics Letters, **29**, p. 690-691 (1993).

7. D. J. Derickson, R. J. Helkey, A. Mar, J. G. Wasserbauer, J. E. Bowers, "Mode-Locked Semiconductor Lasers", Microwave Journal, **36**, 76-90 (1993).

8. R. J. Helkey, A. Mar, W. X. Zou, D. B. Young, J. E. Bowers, "Mode-Locked Repetition Rate Feedback Stabilization of Semiconductor Diode Lasers", Society of Photo-Optical Instrumentation Engineers, Optoelectronic Packaging and Interconnects Proceedings, **1861**, (1993), **Invited Paper**.

9. R. J. Helkey, D. J. Derickson, A. Mar, J. G. Wasserbauer, J. E. Bowers, "Millimeter Wave Signal Generation Using Semiconductor Diode Lasers", Microwave and Optical Technology Letters, **6**, 1-5, Jan. (1993), **Invited Paper**.

10. R. J. Helkey, D. J. Derickson, A. Mar, J. G. Wasserbauer, J. E. Bowers, R. L. Thornton, "Stabilization of Passively Mode-Locked Semiconductor Laser Repetition Frequency", IEEE Lasers and Electro-optics Society Annual Meeting, **DLTA4.2**, Boston (1992).

11. D. J. Derickson, R. J. Helkey, A. Mar, J. R. Karin, J. G. Wasserbauer, J. E. Bowers, "Short Pulse Generation Using Multi-Segment Mode-Locked Semiconductor Lasers", IEEE Journal of Quantum Electronics, **28**, p. 2186-2202, Oct. (1992), **Invited Paper**.

12. R. J. Helkey, D. J. Derickson, A. Mar, J. E. Bowers, R. L. Thornton, "Repetition frequency stabilization of passively mode-locked semiconductor lasers", Electronics Letters, **28**, 1920-1922, Sept. (1992).

13. A. Mar, D. J. Derickson, R. J. Helkey, J. E. Bowers, D. Botez, "Mode-Locking of High-Power Resonant-Optical-Waveguide Diode Laser Arrays", Semiconductor Laser Conference, **N-7**, Takamatsu Japan (1992).

14. J. G. Wasserbauer, D. J. Derickson, K. Giboney, R. J. Helkey, J. R. Karin, A. Mar, J. E. Bowers, "Integrated Optical Transmitters and Receivers Using Multi-Segment Laser Processes", IEEE Lasers and Electro-optics Society Meeting on Integrated Optoelectronics, **ThC1**, Santa Barbara CA, August (1992).

15. J. R. Karin, D. J. Derickson, R. J. Helkey, J. E. Bowers, R. L. Thornton, "Field-Enhanced GaAs/AlGaAs Waveguide Saturable Absorbers", Ultrafast Phenomena VIII, **MC21,** France (1992).

16. D. J. Derickson, R. J. Helkey, A. Mar, J. G. Wasserbauer, W. B. Jiang, J. E. Bowers, "Mode-locked semiconductor lasers: Short Pulse, Small Package", Optics and Photonics News, **3**, p. 14-20, May (1992).

17. A. Mar, D. J. Derickson, R. J. Helkey, J. E. Bowers, R. T. Huang, D. Wolf, "Actively Mode-Locked External-Cavity Semiconductor Lasers with Transform-Limited Single Pulse Output", Optics Letters, **17**, p. 868-870 June (1992).

18. D. J. Derickson, R. J. Helkey, A. Mar, J. G. Wasserbauer, J. E. Bowers, "Microwave and Millimeter Wave Signal Generation Using Mode-Locked Semiconductor Lasers with Intra-Waveguide Saturable Absorbers", IEEE MTT International Microwave Symposium Digest, p. 753-756, June (1992).

19. D. J. Derickson, R. J. Helkey, A. Mar, J. E. Bowers, "Suppression of Multiple Pulse Formation in External Cavity Mode-locked Semiconductor Lasers using Intra-Waveguide Saturable Absorbers", IEEE Photonics Technology Letters, **4**, p. 333-335, April (1992).

20. R. J. Helkey, D. J. Derickson, A. Mar, J. G. Wasserbauer, J. E. Bowers, R. L. Thornton, "Colliding Pulse Effects in Mode Locked Semiconductor Diode Lasers", Conference on Lasers and Electro-Optics, **JTHB2** , Anaheim CA (1992).

21. D. J. Derickson, R. J. Helkey, A. Mar, J. G. Wasserbauer, J. E. Bowers, "Design of Multisection Mode-Locked Semiconductor Lasers with Intra-Waveguide Saturable Absorbers", IEEE Lasers and Electro-Optics Society Integrated Photonics Research Topical Meeting, **WC3**, New Orleans LA, April (1992).

22. D. J. Derickson, J. G. Wasserbauer, R. J. Helkey, A. Mar, J. E. Bowers, "A Comparison of Colliding Pulse and Self-Colliding Pulse Monolithic Cavity Mode-Locked Semiconductor Lasers", Optical Fiber Communication Conference, **ThB3**, Feb. (1992).

23. J. E. Bowers, D. J. Derickson, R. J. Helkey, A. Mar, J. G. Wasserbauer, Y. G. Wey, "Comb and Signal Generation Above 100 GHz Using Optoelectronics", Photonic Systems for Antenna Applications Conference, Monterey CA, Dec. (1991).

24. A. Mar, D. J. Derickson, R. J. Helkey, J. E. Bowers, "Picosecond Pulses Directly Generated Using a Tandem-Contact Actively Mode-Locked 1.3 μm Semiconductor Laser", Laser and Electro-Optics Society Annual Meeting, **SDL14.1**, Nov. (1991).

25. D. J. Derickson, R. J. Helkey, A. Mar, R. L. Thornton, J. E. Bowers, "Benefits of Intra-Waveguide Saturable Absorbers in External Cavity Mode-Locked Semiconductor Lasers", Optical Society of America Annual Meeting, **MG5**, San Jose, Nov. (1991).

26. P. A. Morton, D. J. Derickson, R. J. Helkey, A. Mar, J. E. Bowers, "Mode Locked Semiconductor Lasers", Laser Optics of Condensed Matter, **2**, Plenum Press, New York, (1991).

27. R. J. Helkey, "A New Receiver Filter Transformation", Microwave Journal, p. 207-212, Sept. (1990).

28. J. E. Bowers, D. J. Derickson, R. J. Helkey, J. R. Karin, A. Mar, P. A. Morton, R. Nagarajan, "Picosecond Dynamics in Semiconductor Lasers", IEEE International Semiconductor Laser Conference, **A.3**, Switzerland, Sept. (1990).

29. P. A. Morton, D. J. Derickson, R. J. Helkey, A. Mar, J. E. Bowers, "Mode Locked Semiconductor Lasers", US-USSR Symposium on the Physics of Optical Phenomena and their Use as Probes of Matter, UC Irvine, 401 (1990).

30. R. J. Helkey, P. A. Morton, J. E. Bowers, "A Novel Analysis Method for Mode Locked Semiconductor Lasers", IEEE LEOS Topical Meeting on Integrated Photonics Research, **TuC2**, March (1990).

31. R. J. Helkey, P. A. Morton, J. E. Bowers, "A New Partial Integration Method for Analysis of Mode Locked Semiconductor Lasers", Optics Letters, **15**, p. 112-114, Jan. (1990).

32. P. A. Morton, R. J. Helkey, A. Mar, D. J. Derickson J. E. Bowers, "Monolithic Mode Locked Laser Arrays in Optical Computing", SPIE Digital Optical Computing Conference, **1215**, Los Angeles, Jan. (1990).

33. D. J. Derickson, R. J. Helkey, A. Mar, P.A. Morton, J. E. Bowers, "Self Mode Locking of a Semiconductor Laser Using Positive Feedback", Applied Physics Letters, **56**, 7-9, Jan. (1990).

34. P. A. Morton, R. J. Helkey, J. E. Bowers, "Dynamic Detuning in Actively Mode Locked Semiconductor Lasers", IEEE Journal of Quantum Electronics, **QE-25**, 2621-2633 (1989).

35. J. Ashjaee, R. Lorenz, R. Sutherland, J. Dutilloy, J. Minazio, R. Abtahi, J. Eichner, J. Kosmalska, R. J. Helkey, "New GPS Developments and Ashtech M-XII", Proceedings of the Institute of Navigation, **GPS-89**, 195 (1989).

36. J. E. Bowers, P. A. Morton, R. J. Helkey, D. J. Derickson, A. Mar, "High Speed Semiconductor Lasers and Applications in Subpicosecond Mode Locking", IEEE Lasers and Electro-Optics Society Conference, **OE7.1** (1989).

37. D. J. Derickson, R. J. Helkey, A. Mar, P.A. Morton, and J. E. Bowers, "Self Mode Locking of a Semiconductor Laser Using Positive Feedback", IEEE Lasers and Electro-Optics Society Conference, **OE4.4** (1989).

38. P. A. Morton, R. J. Helkey, S. W. Corzine, J. E. Bowers, "Subpicosecond Multiple Pulse Formation in Actively Mode-Locked Semiconductor Lasers",

Optical Society of America Proceedings on Picosecond Electronics and Optoelectronics, **4**, 87 (1989).

39. J. Ashjaee, D. Bourn, R. J. Helkey, R. Lorenz, J. Minazio, B. Remondi, R. Sutherland, "Ashtech XII GPX Receiver, the All-In-One All-In-View", International Symposium on Global Positioning System, Queensland Australia, Oct. (1988).

40. R. Eschenbach and R. J. Helkey, "Performance/Cost Ratio Optimized for GPS Receiver Design", Microwave System News, 43-52, Nov. (1984).

41. J. Ashjaee and R. J. Helkey, "Precise Positioning Using a 4-Channel C/A Code GPS Receiver", IEEE Plans Conference (1984).

42. J. Ashjaee, R. Eschenbach, R. J. Helkey, "C/A Code Receivers for Precise Positioning Applications", Institute of Navigation, June (1984).

43. J. Ashjaee, R. J. Helkey, R. Hyatt, "A New Precision Time and Frequency Source for Stationary PTTI Applications", Precise Time and Interval Applications and Planning Meeting, Dec. (1983).

PATENTS

R. Lorenz, R. J. Helkey, K. Abadi, "Global Positioning System Receiver Digital Processing Technique", U.S. patent #5,134,407, issued 1992.

J. Ashjaee, R. J. Helkey, R. Lorenz, R. Sutherland, "Global Positioning Receiver with Improved Radio Frequency and Digital Processing", U.S. patent #4,928,106, issued 1990.

TABLE OF CONTENTS

LIST OF FIGURE CAPTIONS

xvi

CHAPTER 1

INTRODUCTION

1.1 Optical Pulse Applications

Modelocked semiconductor diode lasers are important as small, reliable and inexpensive sources of subpicosecond optical pulses with moderate peak powers over wide wavelength ranges. They can be used for telecommunications systems, high speed A/D converters, electro-optic sampling systems, optical computing, phased array radar systems, optical microwave frequency sources, and multiple wavelength high speed physics experiments.

Some advantages of semiconductor diode lasers as optical pulse sources are that they are compact, available over a wide range of wavelengths using bandgap engineering, allow integration with other optoelectronic devices, and are electrically pumped.

Currently, the other compact system for producing short optical pulses is modelocked Er-fiber lasers. Fiber lasers have two disadvantages. One disadvantage is that modelocked fiber lasers require optical pumping at relatively high optical powers (500 mW pump power used to produce 180 fs pulses) [1]. This problem is being addressed with lower threshold fibers with reduced core size, and higher power semiconductor diode pump sources using the Master Oscillator Power Amplifier (MOPA) technique [2]. The other disadvantage is that fiber lasers are only available over a narrow wavelength window. This problem is being partially addressed with other fiber technologies such as Pr-doped fiber [3]. Semiconductor lasers are available over a much broader wavelength range, from <0.7 µm to >2 µm.

1

High speed data communication can be achieved by time division multiplexing a number of modelocked lasers [4-6] as shown in Fig. 1.1. This technique has been demonstrated up to 100 Gbit/sec over 50 km using ring lasers at a moderate bit rate (~6.3 Gbit/s) and combining the optical outputs [5]. The receiver can process high data rate signals by demultiplexing using four-wave mixing in a fiber [7]. Because the pulse width of a modelocked laser can be a few picoseconds or less, very high bit rates are possible using this method of time division multiplexing. This is expected to become a very important technique to get the maximum data transmission performance out of an optical fiber.
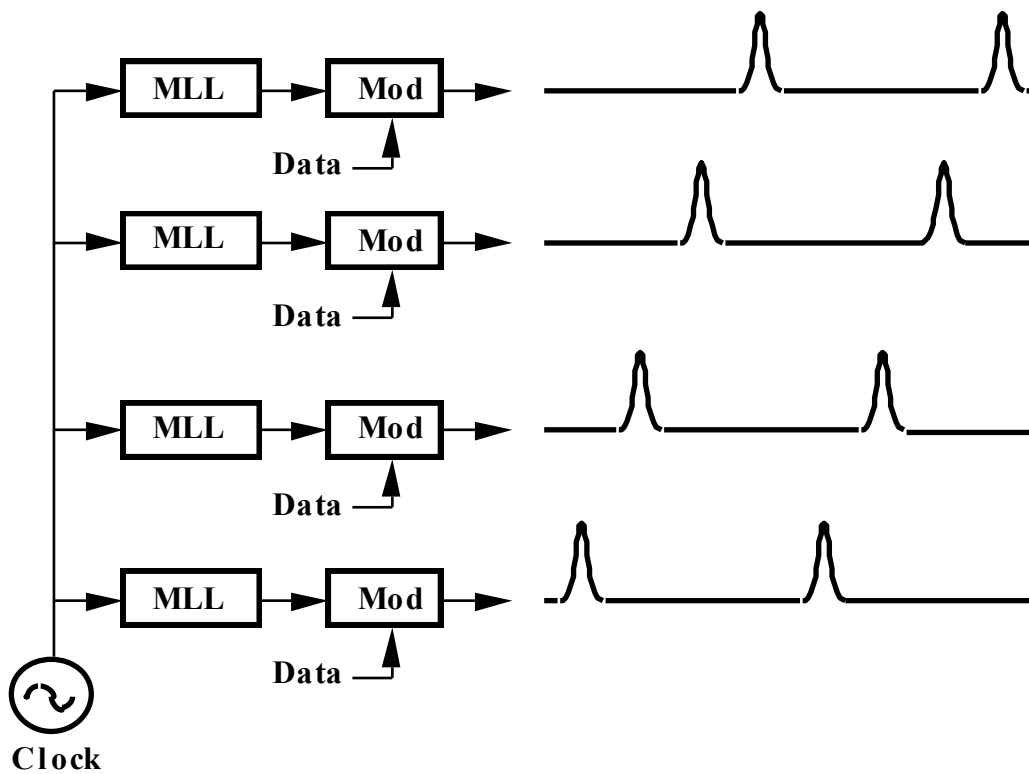
Fig. 1.1   Time division multiplexing using interleaved optical pulses.

For long distance communications, soliton propagation allows the nonlinear index of the fiber to compensate for the wavelength dispersion, and maintain the

2

pulse shape for thousands of kilometers [6]. Soliton propagation requires a relatively unchirped pulse. When the pulse is chirped, different optical spectral components do not add together with the correct phase, leading to pulse broadening. This implies that the pulses are not transform limited, or that the pulsewidth cannot be found from the Fourier transform of the optical power spectrum.

Optical pulses from modelocked semiconductor lasers are usually chirped, because the carrier induced index change during the pulse causes self phase modulation (SPM). Chirping can be reduced by restricting the optical bandwidth with a grating. Transform limited pulses as short as 1.4 ps have been achieved by strong active modulation of a multisegment modelocked laser [8] using a grating for spectral control. The optimum pulse width for optical soliton transmission is from 6 ps to 60 ps, depending on the pulse energy.

Another important application for modelocked lasers is electro-optic sampling. The voltage on an electro-optic material such as GaAs can be measured with a short optical pulse by detecting change in light polarization after it passes through the substrate. A 1 ps optical pulse provides a measurement bandwidth of ~300 GHz. In the past, modelocked Nd:YAG lasers frequently were used as the optical source for electro-optic sampling. The output is typically compressed from 75 ps down to 1.5 ps using nonlinear fiber interactions. This large compression ratio leaves substantial optical power outside of the main pulse, which degrades the measurement process. The pulse compression produces a medium power output (>100 mW) with both large amplitude and large pulsewidth jitter. Semiconductor lasers can produce a much lower noise source at a lower power, but with a similar signal to noise ratio. A semiconductor laser is a smaller, less expensive, lower noise measurement system for electro-optic sampling. Recently Ti:sapphire lasers have

become available which also can provide high power, subpicosecond pulses directly for electro-optic sampling. However, these devices are large and expensive, require a large and expensive optical pump, and are unsuitable for portable instrumentation.

Modelocked semiconductor lasers are also useful as optical microwave sources. Monolithic passive modelocked devices have been demonstrated as free running oscillators up to 350 GHz [9]. However, many applications require that the oscillation frequency be stabilized to an external source. Active monolithic modelocked devices have been modulated to 40 GHz [10]. Applications include microwave frequency distribution with high isolation, clock generation for optical computing, and microwave signal transmission to remote locations. Optical microwave signal transmission components have been developed for an optical phased array radar system [11].

1.2 Modelocking Overview

Modelocking is a technique of generating distinct optical pulses by modulation of a resonant cavity. Fig. 1.2 illustrates the operation of a laser with periodic modulation applied at the round trip time of the optical cavity. The optical signal at the peak of the amplitude modulation receives the most gain, with the loss to the optical signal increasing away from this point. This causes the formation of optical pulses. Each time a pulse travels through the cavity, the pulse tails receive less gain than the pulse peak, leading to pulsewidth shortening. The optical pulsewidth decreases until the pulse shortening per pass is balanced by the pulse broadening per pass due to other mechanisms.
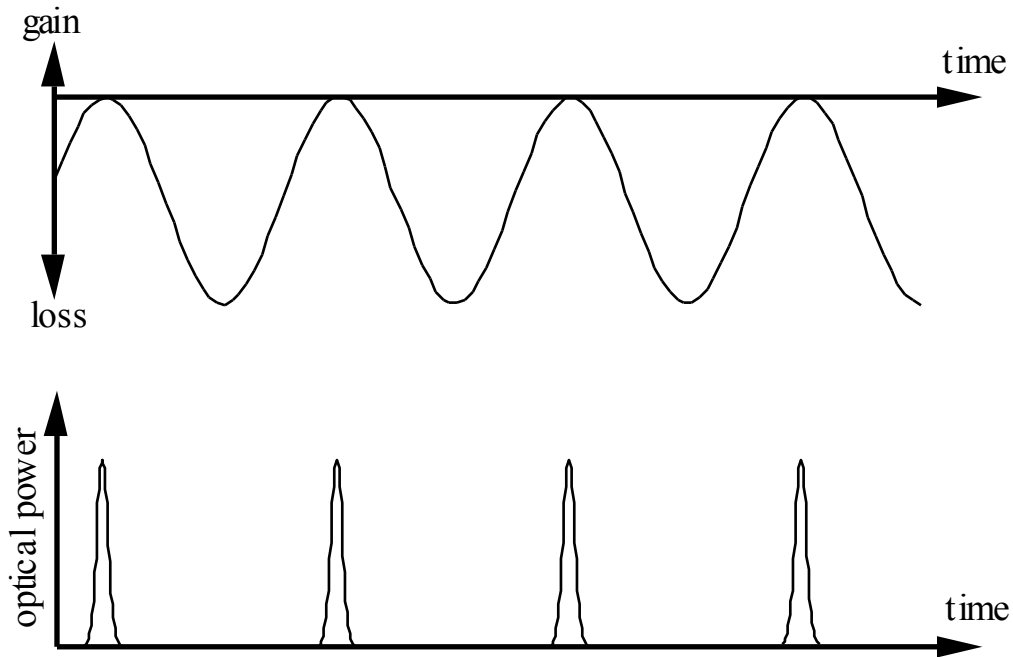
Fig. 1.2   Time dependence of gain modulation and optical output of modelocked laser.
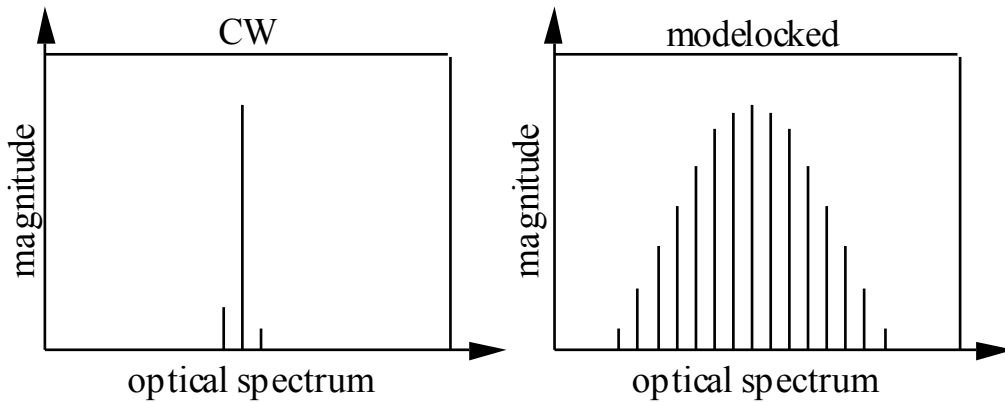
Fig. 1.3   Optical spectrum of a CW laser and modelocked laser.

The optical spectrum of a modelocked laser is a series of modes corresponding to the Fabry-Perot cavity modes of the laser (Fig. 1.3). However, short optical pulses only result from this optical spectrum if the optical modes add up in phase. The term modelocking is a frequency domain description in which optical

5

cavity modes are coupled in phase to produce a short pulse. However, under CW conditions the maximum spectral gain occurs at one mode, so the laser tends to operate at one main mode for a homogeneously broadened laser or a few modes for an inhomogeneously broadened laser. In addition to coupling the modes in phase, the modelocking mechanism must also couple energy from each mode to the adjacent modes.

1.3 Active Modelocking

Active modelocking is a technique in which the modulation is externally applied. Semiconductor lasers are well suited for this technique, as the electrical contact allows for high frequency gain modulation (Fig. 1.4).
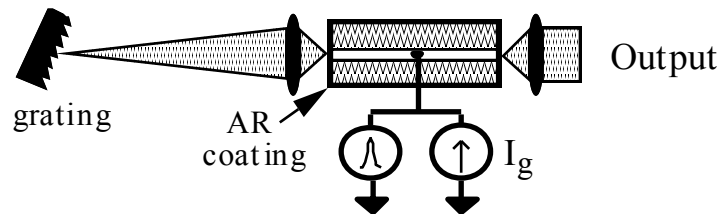
Fig. 1.4   Active modelocking of a semiconductor laser diode. Time varying gain is applied by external current modulation.

Frequency modulation (FM) modelocking has also been demonstrated in semiconductor lasers [12]. For FM modelocking, during every round trip of the cavity the frequency modulation shifts the optical frequency up or down depending on the position in the modulation waveform. Optical pulses are formed because a self consistent solution only allows optical energy at the stationary points in the modulation waveform.

1.4 Passive Modelocking

Passive modelocking uses a saturable absorber in order to operate under the same gain modulation principle, but the gain modulation is supplied by the optical pulse itself. The absorber attenuates the beginning of the optical pulse (Fig. 1.5), which leads to overall pulse shortening. After the absorber saturates, the center of the pulse experiences net gain. As the pulse continues to propagate, saturation of the gain medium reduces the gain to below threshold and shuts off lasing.
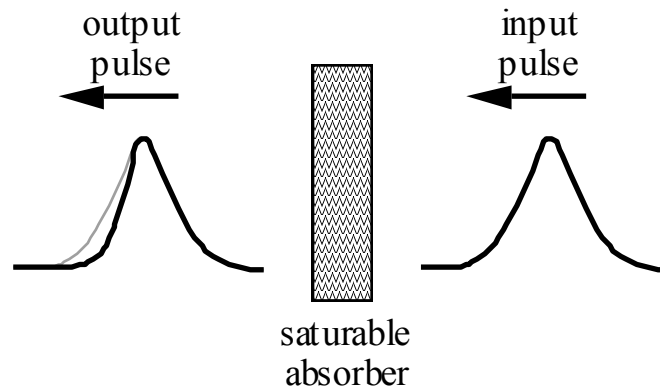
Fig. 1.5   Passive modelocking with a slow saturable absorber. Time varying loss is internally generated by the interaction of the pulse with the saturable absorber.

In addition to active modelocking, semiconductor lasers also allow two methods of passive modelocking with an integrated saturable absorber. One method is ion implantation to introduce recombination centers at one facet, which decreases the carrier recombination time and forms a saturable absorber. However, this can reduce the reliability of the devices [13,14].

The other approach is to split the gain contact (Fig. 1.6) and reverse bias one segment to form an integrated waveguide saturable absorber [15].

7
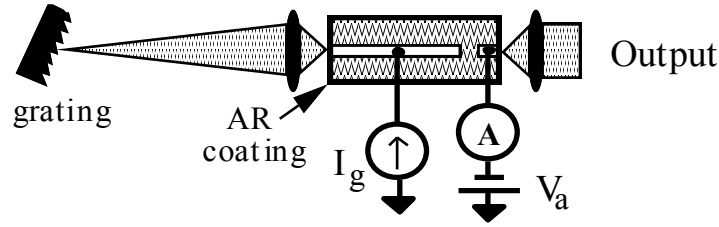
Fig. 1.6   Passive modelocking of a semiconductor laser diode using a separately reversed biased region to form an integrated waveguide saturable absorber.

The optical mode spacing of the modelocked laser can be found by Fourier analysis to be:

$$\Delta f = \frac{c}{2\, n_g\, L}$$

where Δf is the spacing between each mode, c is the velocity of light, n_g is the group index of the pulse, and L is the cavity length. (Fig. 1.7). The optical mode spacing frequency Δf of the laser under CW operation is given by:

$$\Delta f(\lambda) = \frac{c}{2\, n_g(\lambda)\, L}$$

where $n_g(\lambda)$ is the local group velocity at the wavelength λ. The group index n_g and spacing Δf are given explicit wavelength dependence, because in general the gain medium will be dispersive and n_g will not be constant with wavelength.

These two equations look the same, but they are actually different. The mode spacing of the optical pulse is constant over the bandwidth of the pulse, but the laser mode spacing is not constant (Fig. 1.7). This means that the pulse modes cannot all line up exactly with the cavity modes. If the cavity modes were infinitely narrow, modelocking would not be possible in the presence of dispersion. However the

8

cavity modes have a finite width, and the effect of dispersion is to cause the modes to start to shift somewhat out of phase. This shift causes a gradual 'unlocking' of the modes and leads to pulse broadening. The 'unlocking' must be counterbalanced by the modelocking mechanism.
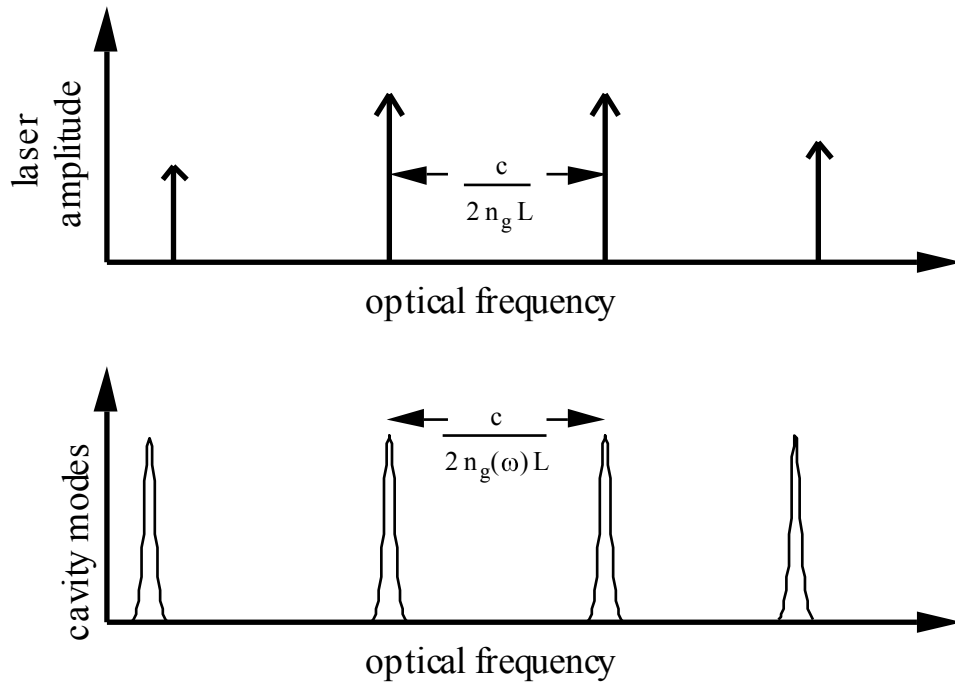
Fig. 1.7   (a) Mode spacing of the optical output pulse train   (b) Mode spacing of the laser cavity modes.

1.5 Scope and Organization of the Dissertation

The Introduction has discussed applications of short optical pulses, and the modelocking technique of generating short optical pulses using a resonant cavity. In addition to the Introduction, this Dissertation is organized into five other chapters and one appendix.

In *Chapter II*, numerical simulation techniques for analyzing modelocked laser systems are discussed. The partial integration method is developed, which reduced computation time by >2 orders of magnitude over previous modelocked laser simulations. The effects of higher order correction terms are considered, and the finite gain-bandwidth of the laser medium is shown to be a limiting factor in producing subpicosecond pulses with active modelocking.

In *Chapter III*, passive modelocking is examined. Numerical modeling techniques are compared under the strong gain saturation occurring in passive modelocking. Simplified expressions under various asymptotic limits are developed. The effect of absorber parameters is considered. Curved waveguide devices are demonstrated to virtually eliminate multiple pulsation due to facet reflections. Tapered waveguide devices are shown to directly increase the output power from the modelocked device without external amplification. Self phase modulation causes spectral broadening and highly chirped 2-5 ps pulses. Using quadratic phase compensation, these pulses have been compressed to 0.45 ps. This was the first demonstration of a compact system for generating <0.5 ps pulses with a semiconductor laser.

In *Chapter IV*, the importance of the colliding pulse effect on the passive modelocking process is investigated both theoretically and experimentally. The colliding pulse effect can be changed both by varying both the facet reflectivity, which varies the standing wave ratio, and the absorber offset from the facet, which decreases the colliding pulse effect for short pulses. It is shown that output pulse width is not strongly affected by the standing wave ratio, but that the absorber position is important in pulse formation. The facet reflectivity can be optimized for short pulsewidth or high output power.

10

In *Chapter V*, the generation and distribution of millimeter-wave reference signals by semiconductor lasers is considered. The optimum conditions for harmonic generation are examined. Feedback stabilization is proposed for stabilizing the repetition rate of monolithic passively modelocked lasers well past the electrical parasitic cutoff frequency of the contacts. Stabilization is demonstrated for an external cavity passively modelocked laser, and is shown to reduce the timing jitter for 1 second measurement from 1 ns to 4 ps using an unoptimized loop bandwidth.

Chapter VI summarizes the Dissertation, and presents some areas of interest and further research.

Appendix A examines chirped pulse compression techniques utilizing manipulation of the phase of the optical pulses.

References

1.   M. E. Fermann, M. J. Andrejco, Y. Silberberg, A. M. Weiner, "Generation of pulses shorter than 200 fs from a passively mode-locked Er fiber laser", Optics Lett., **18**, p. 48-50 (1993).

2.   G. Bendelli, K. Komori, S. Arai, Y. Suematsu, "A new structure for high-power TW-SLA", IEEE Photonics Tech. Lett. **3**, p. 42-44 (1991).

3.   Y. Ohishi, T. Kanamori, T. Nishi, S. Takahashi, and E. Snitzer, "Gain characteristics of Pr^{3+}-Yb^{3+} codoped fluoride fiber for 1.3μm amplification", Photon. Technol. Lett., **3**, p. 990-992 (1991).

4.   M. Nakazawa, K. Suzuki, E. Yamada, and Y. Kimura, "20 Gbit/s Soliton Transmission Over 200 km Using Erbium-Doped Fibre Repeaters", Electron. Lett., **26**, p. 1592 (1990).

5.   S. Kawanishi, H. Takara, K. Uchiyama, T. Kitoh, M. Saruwatari, "100 Gbit/s, 50 km optical transmission employing all-optical multi/demultiplexing and PLL timing extraction", Optical Fiber Communications Conference, **PD2-1**, San Jose (1993).

6.   N. A. Olsson, P. A. Andrekson, J. R. Simpson, T. Tanbun-Ek, R. A. Logan, K. W. Wecht, "Bit-error-rate investigation of 2-channel soliton propagation over more than 10000 km", Electron. Lett., **27**, p. 695-697 (1990).

7.   P. A. Andrekson, N. A. Olsson, J. R. Simpson, D. J. Digiovanni, P. A. Morton, T. Tanbun-Ek, R. A. Logan, K. W. Wecht, "64 GBit/s all-optical demultiplexing with the nonlinear optical-loop mirror", IEEE Photon. Tech. Lett., **4**, p. 644-647 (1992).

8.   A. Mar, D. J. Derickson, R. J. Helkey, J. E. Bowers, R. T. Huang, D. Wolf, "Actively Modelocked External-Cavity Semiconductor Lasers with

Transform-Limited Single Pulse Output", Optics Letters, **17**, p. 868-870 (1992).

9. Y. K. Chen, M. C. Wu, T. Tanbun-Ek, R. A. Logan, and M. A. Chin, "Subpicosecond monolithic colliding-pulse modelocked multiple quantum well lasers", Appl. Phys. Lett., **58**, p. 1253 (1991).

10. R. S. Tucker, U. Koren, G. Raybon, C. A. Burrus, B. I. Miller, T. L. Koch, G. Eisenstein, and A. Shahar, "Monolithic extended cavity laser", Electron. Lett., **25**, p. 621 (1989).

11. J. F. Coward, T. K. Yee, C. H. Chalfant, P. H. Chang, "A high performance integrated optic system to control RF phase and amplitude for phase array antennas", Optical Millimeter-Wave Interactions: Measurements, Generation, Transmission and Control Conference, **FB.2**, p. 59 (1991)

12. R. Nagar, D. Abraham, G. Eisenstein, "Pure phase-modulation mode locking in semiconductor lasers", Optics Letters, **17**, p. 1119-1121 (1992)

13. J. P. Van Der Ziel, W. T. Tsang, R. A. Logan, R. M. Mikulyak, W. M. Augustyniak, "Subpicosecond pulses from passively mode-locked GaAs buried optical guide semiconductor lasers", Appl. Phys. Lett., **39**, 525 (1981).

14. E. L. Portnoi and A. V. Chelnokov, "Characteristics of heterostructure lasers with a saturable absorber fabricated by deep ion implantation", Soviet Tech. Phys. Lett., **15**, p. 432 (1989).

15. C. Harder, J. S. Smith, K. Y. Lau, A. Yariv, "Passive mode-locking of buried heterostructure lasers with non-uniform current injection", Appl. Phys. Lett., **42**, p. 772 (1983).

CHAPTER 2

PARTIAL INTEGRATION MODEL

2.1 Semiconductor Gain Medium Models

Actively mode locked lasers can be analyzed by analytic or numeric methods. *Analytic* solutions are based on the "self-consistent profile" (SCP) approach [1-3], and provide closed form solutions based on a simplified laser model. These models can be very useful for understanding qualitative behavior of pulse formation. However, the models neglect the dominant effects of gain variations due to photon-electron interactions, finite reflectivity of the anti-reflection (AR) coated laser diode facet, additional pulse formation due to gain recovery [4], spontaneous emission, and length dependent gain effects that occur if the active medium is long compared to the pulse width. Consequently, the results of these models do not agree with experimental sub-picosecond mode locked semiconductor laser results [5] where the round trip time of the laser cavity was seven times as long as the pulse width.

Numeric solutions to mode locked laser systems have been presented by several authors [6-10]. The sub-picosecond results reported in [5] have been successfully predicted with a numerical model based on a finite difference traveling wave rate equation analysis [9,10]. This model includes finite facet reflectivity, optically induced gain variations, and spontaneous emission which are ignored in most analytic models, but the model neglects the bandwidth of the semiconductor gain.

Computer models based on finite difference equations have the advantage of being able to include many additional effects such as nonuniform current injection,

14

inhomogeneous material structure, dispersion, and gain bandwidth limitations. These models are limited only by the accuracy to which the physical mechanisms can be determined. Finite difference solutions can be useful for determining the range of validity of analytic models, as well as the validity of simpler numeric models. The main drawback of finite difference solutions is the excessive computational requirements. The results reported for an analysis of a 16 GHz linear cavity mode locked laser required 20 billion finite difference computations [10].

In this chapter a mode locking model is developed based on a traveling wave rate equation numerical analysis [6]. This model can be solved numerically with effects such as finite internal facet reflectivity, inhomogeneous pumping, and photon-electron interactions that have not been included in analytic solutions. However, it is much more computationally efficient than earlier traveling wave solutions, requiring typically 1% of the computation time of a full finite difference solution.

Short pulses generated by active modelocking occur at low pulse energy in order to minimize pulse broadening due to self phase modulation. Consequently, gain saturation is also small. The solution of the traveling wave rate equations under large gain saturation will be discussed further in Chapter 3.

2.2 Traveling wave rate equations

The photon and carrier populations in a semiconductor laser can be described by rate equations. These are a pair of differential equations which describe the two quantities, and are cross-coupled by stimulated and spontaneous emission. This simple model neglects longitudinal variations in the carrier density and photon density. The spatially averaged rate equations are:

15

$$\frac{\partial N}{\partial t} = \frac{J}{qd} - \frac{N}{\tau_n} - g(N - N_{tr})S$$

$$\frac{\partial S}{\partial t} = \left[\Gamma g(N - N_{tr}) - v_g \alpha_i\right]S + \frac{\Gamma\beta'}{\tau_n}$$

where N is the time dependent carrier density, N_{tr} is the carrier density for transparency, S is the photon density, J is the injected current density, g is the differential gain coefficient of the laser, α_i is the internal loss, β' is the fraction of the spontaneous emission coupled into the lasing mode, d is the active layer thickness, Γ is the optical confinement factor, τ_n is the lifetime of the carriers, and q is the electron charge.

This approximation is accurate in cases where the mirror reflectivity is large, so the gain in the cavity is small. Even though in-plane lasers have a cleaved-facet power reflectivity of ~0.3, the constant photon density approximation can still be fairly accurate and is commonly used due to its simplicity. Applications of this model include small signal current modulation and long optical pulse generation by gain switching, where the variation in the photon density is slow compared to the optical transit time through the lasing cavity. Analytic solutions to these coupled equations can be obtained using a small signal perturbation expansion around a steady state solution.

For modelocked lasers where the optical pulse is shorter than the transit time through the device, the spatially averaged rate equations are inadequate. Traveling wave rate equations are needed where the carrier and photon densities have spatial dependence. The optical waveform must be described by traveling waves with

16

forward and backward components. The traveling wave rate equations for a single lateral and transverse mode inside a semiconductor diode are [9]:

$$\frac{\partial N}{\partial t} = \frac{J}{qd} - \frac{N}{\tau_n} - g(N - N_{tr})(S^+ + S^-)$$

$$\frac{\partial S^+}{\partial t} + v_g \frac{\partial S^+}{\partial z} = \left[\Gamma g(N - N_{tr}) - v_g \alpha_i\right]S^+ + \frac{\Gamma \beta' M}{\tau_n}$$

$$\frac{\partial S^-}{\partial t} - v_g \frac{\partial S^-}{\partial z} = \left[\Gamma g(N - N_{tr}) - v_g \alpha_i\right]S^- + \frac{\Gamma \beta' M}{\tau_n}$$

where in addition to the previous parameters, S^+ and S^- are the forward and reverse traveling photon densities, J is the injected current density, and v_g is the material group velocity.
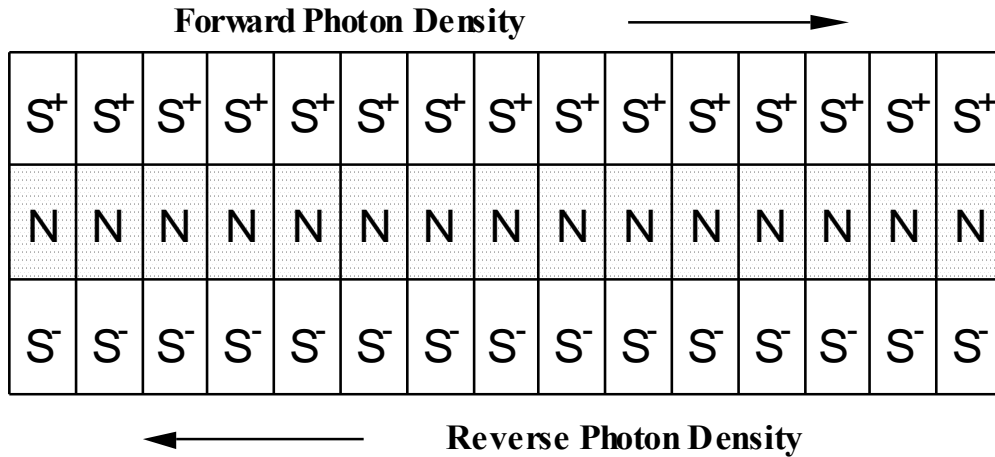
Fig. 2.1 Finite difference semiconductor gain model. The medium is broken into a number of segments each using a linear gain approximation. The photon density is broken up into the same length segments.

2.3 Finite Difference Solution

17

The traveling wave rate equations can be solved by sampling the optical field and the carrier density in space and time as shown in Fig. 2.1, with the time step Δt and distance step Δz related by:

$$\Delta t = \frac{\Delta z}{v_g}$$

The photon density shifts over Δz in the integration time interval Δt. The differential equations can be converted to a series of finite difference equations that can be solved numerically [8,10].

One consequence of this finite difference solution is that the time and distance step are locked together. The computation time is inversely proportional to square of time step. The interval Δz is set by the criterion that the gain over the length is small so that a linear approximation is valid. The interval Δt is set by the necessary resolution in sampling the optical wave. The integration time-step Δt is the more stringent criterion for sub-picosecond optical pulses, so that the necessary computation time goes up as the optical pulsewidth decreases. Since Δz decreases as Δt increases, the computation time is inversely proportional to the square of the time-step.

The model discussed so far applies only to the gain region. Boundary conditions also are needed to account for cavity reflections and loss. An external cavity can be included with a region where the photon density propagates without changing.

2.4 Partial Integration Solution

The small signal semiconductor gain has an exponential solution, illustrated in Fig. 2.2. The finite difference solution is a linear gain solution, and requires many segments to model exponential gain. It would be more efficient to use an exponential gain model as a basis function for analysis.
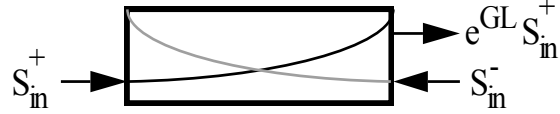
Fig. 2.2   Semiconductor gain medium is best modeled by an exponential gain.

When the carrier density varies slowly with distance the rate equations can be analytically spatially integrated. If the photon-electron interactions are assumed to occur in the center of the segment, the result is a thin, spatially uniform semiconductor model given by the rate equations:

$$\frac{\partial N}{\partial t} = \frac{J}{qd} - \frac{N}{\tau_n} - \frac{v_g}{\eta \Gamma L}\left(e^{GL} - 1\right)\left(S_{in}^+ + S_{in}^-\right)$$

$$S_{out}^+ = e^{GL}S_{in}^+ + \left(\frac{e^{GL} - 1}{G}\right)\left(\frac{\Gamma \beta' N}{v_g \tau_n}\right)$$

and S_{in} and S_{out} are the photon densities at the input and output of the laser segment and G and η are defined by:

$$G \equiv \frac{g\Gamma\left(N - N_{tr}\right)}{v_g} - \alpha_i$$

$$\eta \equiv 1 - \frac{v_g \alpha_i}{g\Gamma\left(N - N_{tr}\right)}$$

19

Forward Photon Density $\longrightarrow$

$\longleftarrow$ **Reverse Photon Density**
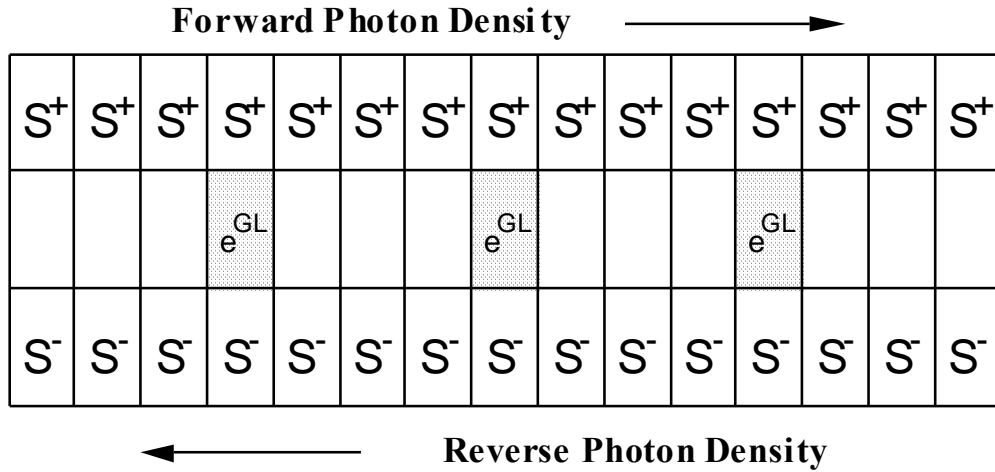
Fig. 2.3   Partial integration model.   The photon density is broken up into segment lengths determined by the optical bandwidth.   The semiconductor medium can be modeled by fewer segments separated by free space.

A mode locked laser can be broken up into several segments, if necessary. Each segment is described by the previous equations, where the length dependence has been solved explicitly.   The result is a partially integrated analysis that can be solved numerically.
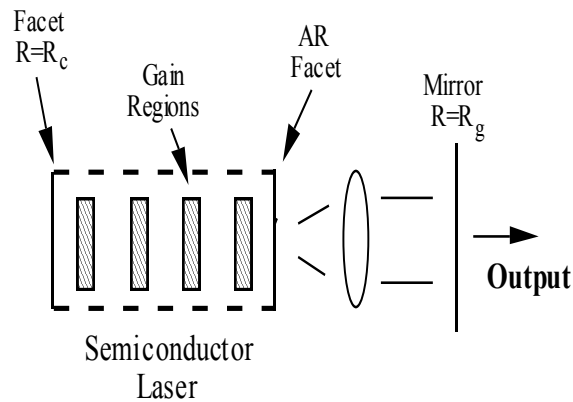
Fig. 2.4   Partial integration model of a modelocked semiconductor laser with external boundary conditions. Gain region is modeled with four exponential gain regions.

20

The model for a four segment mode locked laser is shown in Fig. 2.4. The semiconductor segments are spaced between mirrors representing the facet reflectivity of the actual laser diode. The AR coated mirror couples the forward and reverse traveling optical waves, while the lens acts as a cavity loss element.

In the free space regions of the external cavity, the photon density does not change shape with time, but does change position:

$$S^{\pm}(x{\pm}\Delta x, t+\Delta t)= S^{\pm}(x,t)$$

The addition of external cavity elements is handled by applying the appropriate boundary conditions for loss and reflection:

$$S^{-}(L,t) = \left(c_{L}\right)^{2} R_{c}\ S^{+}(L,t)$$

$$S^{+}(0,t) = R_{g}\ S^{-}(0,t)$$

where L is the length of the cavity, R_c is the cavity output reflectivity, R_g is the gain medium mirror reflectivity, and c_L is the coupling efficiency of the collimating lens. For simplicity, the coupling lens loss is lumped together with the mirror loss in one computational step. An important advantage of this method is that the step of the carrier distribution can be much greater than the distance step of the optical distribution.

This analytical technique is used to examine the effect of detuning the modulation frequency from the cavity resonance frequency [15]. The solution calculated using one infinitesimal laser segment (a fully integrated analysis) is

21

somewhat different than the solution using four laser segments (Fig. 2.5), indicating the importance of length-dependent carrier variation and gain interactions that are neglected in analytic models. The solution using four segments matches the solution using 20 segments, indicating that only a few segments are required. The four segment solution also matches the results of the traveling wave finite difference solution if those results are extrapolated to a zero optical time step. The calculations are in good agreement with experimental results. The minimum pulse width is close to the experimental value of 0.67 ps reported by Corzine et al. [5].
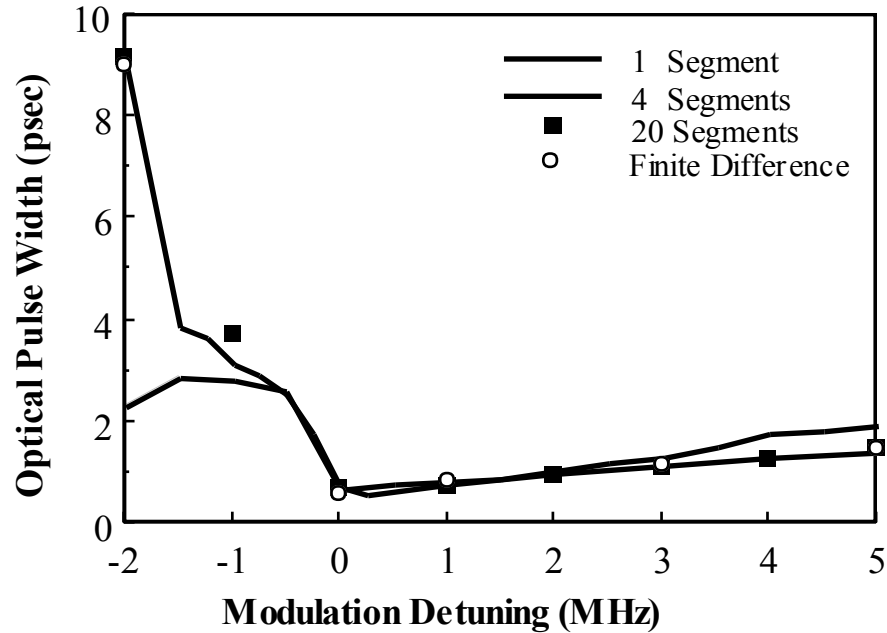
Fig. 2.5   Comparison of detuning with varying number of gain segments. The finite difference method requires many segments. Four segments are sufficient with the partial integration method.

The analysis parameters are 16 GHz cavity frequency, 16.001 GHz sinusoidal modulation frequency, 260 μm laser length, 1 μm waveguide width, 0.15 μm active

region thickness, g=0.34, mirror power reflectivity 0.7, AR coating 0.5%, lens coupling 0.42, α_i=25 cm^{-1}, β'=2.5x10^{-6}, N_{tr}=1.2x10^{18} cm^{-3}, g=1.8x10^{-6} cm^2/sec, I_{dc}=4 mA over threshold, and I_{rf}=40 mA. When the laser was reversed biased by the applied modulation, the maximum reverse current was 660 A/cm^2, limited by thermionic emission [14].
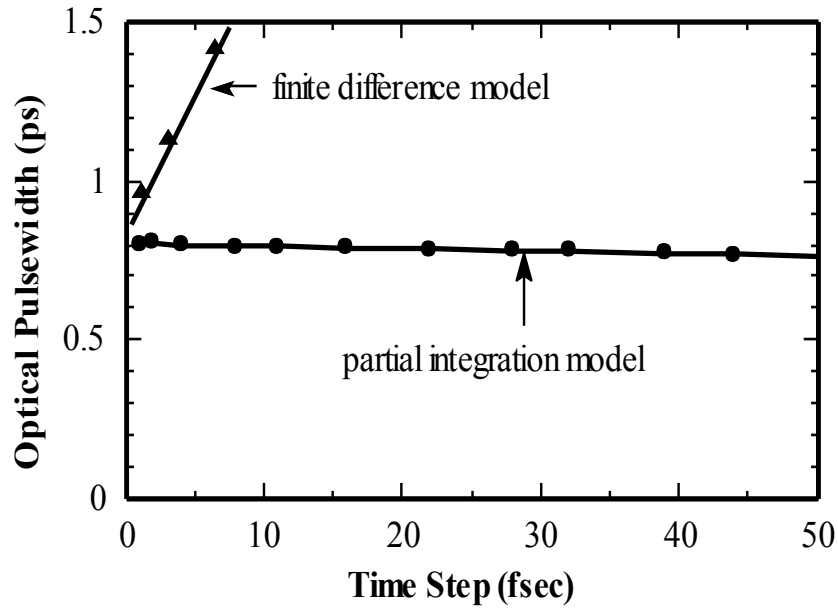
Fig. 2.6   Comparison of optical pulsewidth with integration time for the partial integration and finite difference method. The finite difference method has >2 orders of magnitude improvement in computation time by using an exponential basis function.

The dependence of output pulse width on computation time step is compared in Fig. 2.6 to a finite difference traveling wave rate equation analysis of the same 16 GHz linear cavity [9, 10]. Both models assume uniform current injection and incoherent addition of photon fluxes at the AR facet. The accuracy of the finite difference model falls off quite rapidly for time steps greater than 3 fs, while a much larger time step can be used with the partial integration method. For either method

the required time step decreases as the optical pulse width decreases, so computational efficiency becomes critically important for femtosecond mode locked systems.

The improved convergence due to an exponential basis function gives >1 order of magnitude improvement in computation time. Uncoupling of the time and distance steps also gives >1 order of magnitude improvement by condensing the gain medium into small regions. This leaves regions of free space propagation which do not require any computation.
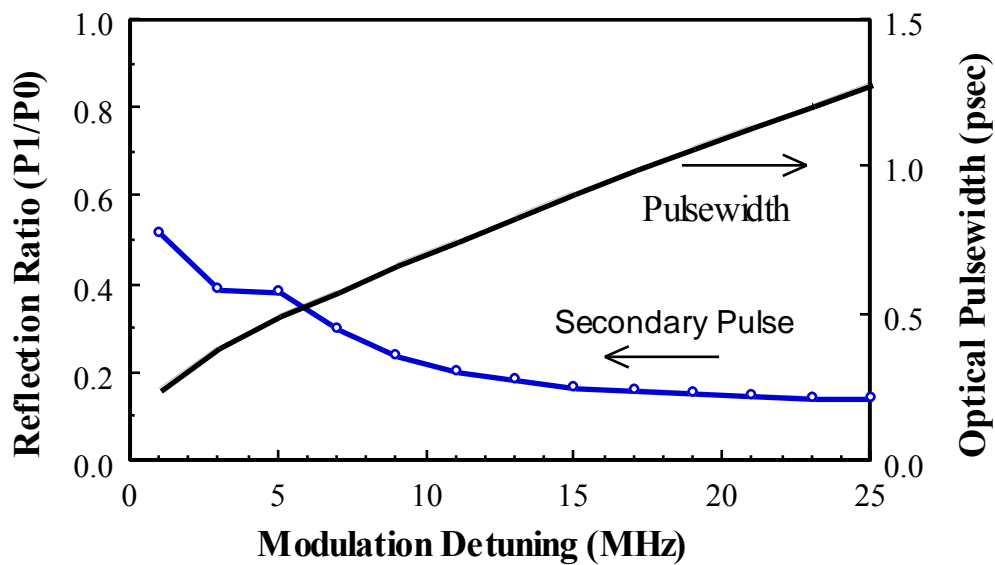
Fig. 2.7   Secondary pulse suppression as a function of modulation detuning. Detuning leads to improved pulse suppression but poorer pulsewidth shaping.

In external cavity active modelocking, the small residual reflectivity of the AR coated facet can seed a series of satellite pulses. In many applications, the critical requirement is not the width of the first pulse, but the width of the pulse envelope which includes the secondary pulses. The dependence of the reflection

24

ratio on modulation detuning is shown in Fig. 2.7 for a 10 ps pulse with 1.4 pJ energy per pulse. The power reflection ratio can be reduced to <0.15 by detuning the modulation frequency, which moves the main pulse near the trailing edge of the drive current, and reduces the gain available to the reflected satellite pulses. At the same time, the pulse moves to a position on the modulation waveform with poorer pulsewidth shaping, so the pulsewidth gets wider.

2.5 Higher Order Correction Terms

The steady state modelocked optical pulsewidth is determined by the condition that the pulse is unchanged after each round trip through the optical cavity. This means that the pulsewidth reduction due to gain modulation must be balanced by an equal pulsewidth broadening mechanism. Since no bandwidth limiting mechanisms have yet been introduced, the dominant pulse broadening mechanism is gain saturation.

Stationary pulse profiles can exist in the absence of any bandwidth-limiting component [10,16]. For active modelocking, pulse shortening is caused by quadratic change in the carrier density and gain. Since the carrier density is the integral of the injected current, this gain modulation is produced by the rate of change in current. Large modulation produces a large rate of change of current, and therefore short pulses. The external modulation is a pulse shortening mechanism that decreases width decreasing optical pulsewidth. However, gain saturation has a pulse broadening effect that is constant with pulsewidth. The pulsewidth decreases until the two effects balance. At this point, the average gain profile must be stationary across the optical pulse. This mechanism has been termed dynamic detuning [10].

25

The photon density rate equations so far have not included higher order effects, such as chirping due to self-phase modulation or the finite material gain-bandwidth. In active modelocking, self phase modulation broadens the pulses at high optical power. Consequently, the shortest pulses are produced at low optical power, where self-phase modulation is not very important. In contrast, passive modelocking must take place at higher optical power, in order to get pulse shaping by saturating the absorber. In Chapter 3, self-phase modulation will be shown to be very important pulsewidth broadening effect for passive modelocking.
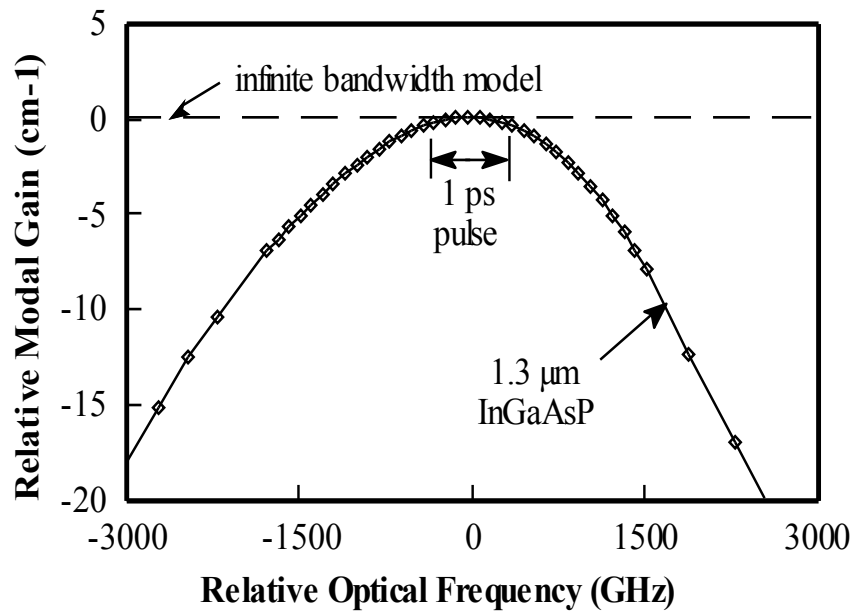
Fig. 2.8   Comparison of the bandwidth of an InGaAsP laser with the bandwidth of an unchirped 1 ps optical pulse. The semiconductor modal gain is calculated for 1.3 μm InGaAsP material with $N=1.8 \times 10^{18} cm^{-3}$ and $\Gamma=0.34$ [11].

Pulse broadening due to finite gain-bandwidth will become important when the optical pulse fills a significant portion of the semiconductor bandwidth. Fig. 2.8 compares the semiconductor bandwidth in 1.3 μm InGaAsP to the bandwidth of an

unchirped optical pulse [11]. The optical pulse bandwidth is given for the FWHM of the electric field assuming a 1 ps Gaussian pulse. For subpicosecond pulses, higher order effects in the gain medium can be expected to become important.

The effect of higher order terms on the wave propagation can be described by a Taylor series expansion of the propagation constant:

$$\beta = \beta_g + \beta''(\omega - \omega_o)^2 + (\alpha + j)\frac{\Gamma g}{2}(N - N_{tr}) - \frac{j\alpha_i}{2} - \frac{j\Gamma g_{bw}}{2}(\omega - \omega_o)^2$$

where β_g is the group index at the center frequency, ω is the optical frequency, ω_o is the optical frequency of peak gain, g_{bw} is the gain-bandwidth parameter, β'' gives the material and waveguide dispersion, and α is the ratio between phase changes and gain changes in the active medium.

These higher order effects can be added with a digital filter in the time domain [17] or a split-step Fourier method in the frequency domain [18]. In the split-step method, the optical pulse first propagates though a time domain rate equation model with infinite bandwidth. The output is converted to the frequency domain with a Fourier transform, where the spectrum is multiplied by the frequency dependent optical gain function $\beta(\omega)$. This is then converted back to the time domain with an inverse Fourier transform. The split-step Fourier method can solve for a wide variety of systems. Rather than being limited to a power series expansion, $\beta(\omega)$ can include an arbitrary gain function such as a Gaussian or Lorentzian.

Converting these terms into the time domain and including them in a partial integration solution gives:

$$\frac{dN}{d\tau} = \frac{J}{qd} - \frac{N}{\tau_n} - \frac{v_g}{\eta\Gamma L}\left[e^{(G + \Delta G_{bw})L} - 1\right]|E_{in}|^2$$

$$E_{out} = e^{(G+\Delta G_{bw}+j\Delta G_{im})L/2} E_{in} + \Delta E_{sp}$$

where E is the electric field amplitude normalized to the square root of optical power, and G and η are the same gain and quantum efficiency definitions given previously. The effects of bandwidth, dispersion and chirp can be treated as real and imaginary gain perturbations ΔG_{bw} and ΔG_{im}, and are given by:

$$\Delta G_{bw} \equiv -\frac{\Gamma g_{bw}}{v_g}\left(\frac{1}{E_{in}}\frac{\partial^2 E_{in}}{\partial \tau^2}\right)$$

$$\Delta G_{im} \equiv -\alpha\frac{\Gamma g}{v_g}\left(N - N_{tr}\right) - \frac{\partial^2 \beta}{\partial \omega^2}\left(\frac{1}{E_{in}}\frac{\partial^2 E_{in}}{\partial \tau^2}\right)$$

The bandwidth-induced gain correction is proportional to the normalized quadratic component of the arbitrary input waveform E,

$$\Delta G_{bw} \propto \left(\frac{1}{E_{in}}\frac{\partial^2 E_{in}}{\partial \tau^2}\right)$$

which is independent of the amplitude of E, and is a measure of the curvature of the input waveform. A Gaussian input pulse is shown in Fig. 2.9. At the peak of the pulse between the two inflection points, ΔG_{bw} is negative. Outside the two inflection points, ΔG_{bw} is positive. The gain-bandwidth term decreases the gain at the peak of the pulse, and increases the gain in the tails. This time dependent gain causes pulsewidth broadening.
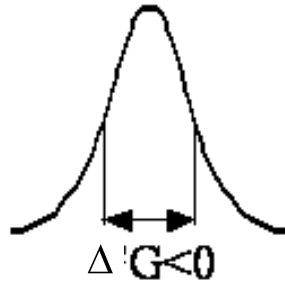
Fig. 2.9   Bandwidth correction term ∆G is negative between the pulse inflection points.   The reduced gain in the center of the pulse causes pulsewidth broadening.

Spontaneous emission can be important in the initial pulse formation, as the pulse builds up to a steady state solution. It also is important for analyzing timing jitter [19].   Using a full field analysis instead of a photon density model, it is necessary to consider the random phase of the spontaneous emission events.   The remainder of the simulations will be analyzing pulsewidth, so spontaneous emission will be neglected.

The numerical solution using these equations is shown in Fig. 2.10, where the effect of finite gain-bandwidth is computed in the time domain. This is compared to the quadratic analytical model for 1.3 μm InGaAsP material shown in Fig. 2.7. Over the bandwidth represented by a 1 ps pulse, this quadratic model is sufficiently accurate. For pulses significantly shorter than this, the model can be easily extended to include cubic and higher order gain terms.
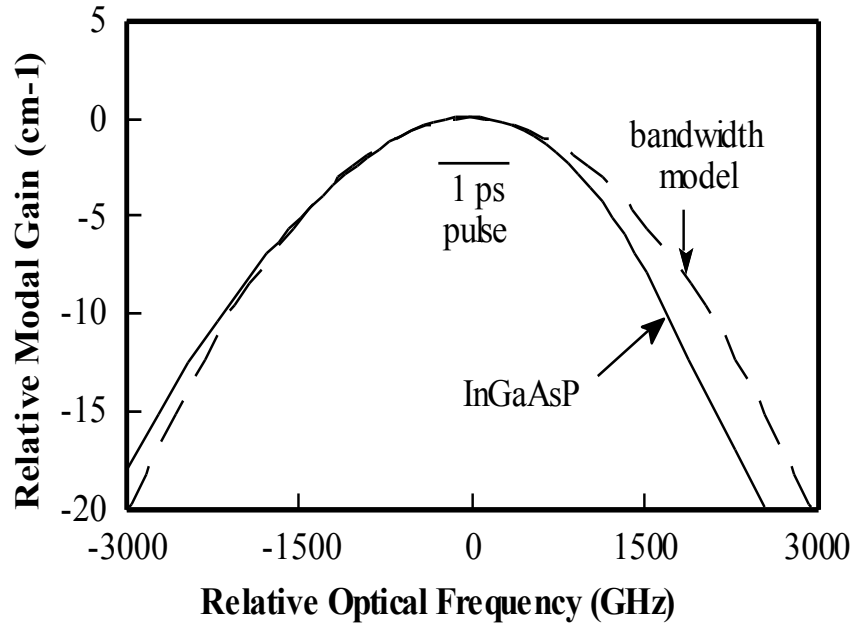
Fig. 2.10   Comparison of the bandwidth of InGaAsP with the partial integration time domain bandwidth model. Cubic gain terms can be ignored for a 1 ps pulse.
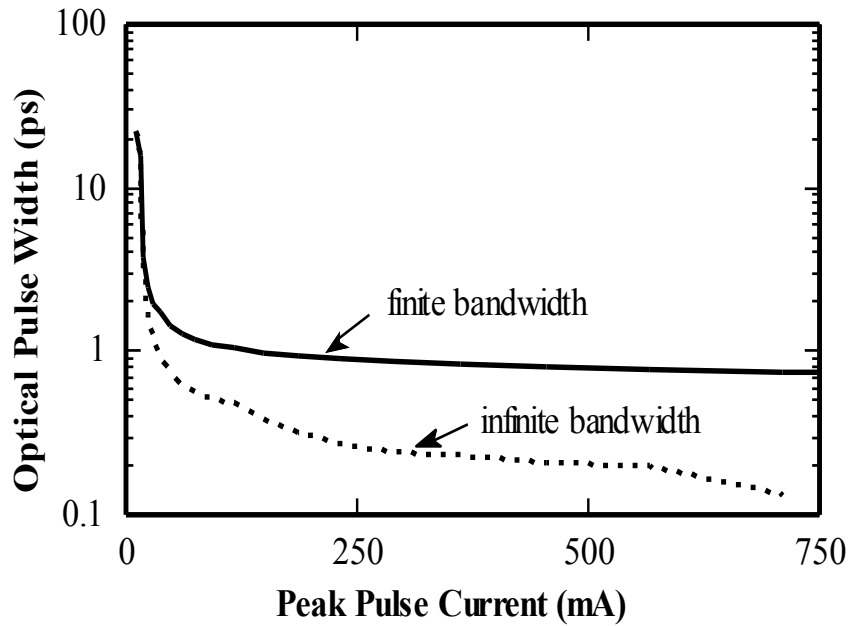
Fig. 2.11   Effect of optical bandwidth on active mode-locking. The optical bandwidth limits the optical pulsewidth to ~1 ps even for very strong amplitude modulation.

30

The effect of the finite bandwidth on the mode-locking process is shown in Fig. 2.11 [17]. This is compared to the simple photon density model previously illustrated in Fig. 2.4 and Fig. 2.5. In the case of the infinite bandwidth model, as the amplitude modulation increases, the pulsewidth becomes shorter without limit. As expected, the effect of the finite gain-bandwidth becomes important for pulses ~1 ps. For pulsewidths <1 ps, the pulsewidth broadening per pass increases rapidly, so that a large increase in modulation is required in order to achieve a small decrease in pulsewidth.

2.6 Summary

A partial integration model has been developed which allows efficient numerical analysis of active and passive semiconductor mode locked lasers. It includes important features such as imperfect facet coating and spontaneous emission that are neglected in analytic solutions, but requires much less computation time than finite difference numeric solutions. It can be extended to include many additional effects that have not been previously modeled, and can be used to analyze other systems such as passive mode locking configurations. The model was extended to include higher order effects. The gain-bandwidth of the laser has been shown to limit the production of subpicosecond pulses.

The partial integration method demonstrated more than 2 orders of magnitude improvement in computation time over a finite difference solution. Each simulation of a 16 GHz cavity configuration took one week on a Sun IV workstation to give a solution within 30% of the correct pulsewidth. With the partial integration method, analyzing the same configuration took 15-30 minutes of computation time to give an answer within 2-4% of the correct pulsewidth.

31

References

1. A. E. Siegman and D. J. Kuizenga, "Simple Analytic Expressions for AM and FM Mode-Locked Pulses in Homogeneous Lasers", Appl. Phys. Lett., **14**, p. 181 (1969).

2. J. R. Creighton and J. L. Jackson, "Simplified Theory of Picosecond Pulses in Lasers", J. Appl. Phys., **42**, p. 3409 (1971).

3. H. A. Haus, "A Theory of Forced Mode Locking", J. Quantum Electron., **QE-11**, p. 323-330 (1975).

4. C. P. Ausschnitt and R. K Jain, "Pulse-width dependence on intracavity bandwidth in synchronously mode-locked cw dye lasers", Appl. Phys. Lett., **32**, p. 727 (1978).

5. S. W. Corzine, J. E. Bowers, G. Przybylek, U. Koren, B. I. Miller, and C. E. Soccolich, "Active mode locked GaInAsP laser with subpicosecond output", Appl. Phys. Lett., **52**, p. 348 (1988).

6. J. A. Fleck, "Mode-Locked Pulse generation in passively switched lasers", Appl. Phys. Lett., **12**, p. 178 (1968).

7. G. J. Aspin and J. E. Carroll, "Simplified theory for mode-locking in injection lasers", Proc. Inst. Elect. Eng., **3**, p. 220-223 (1979).

8. M. S. Demokan, "A model of a diode laser actively mode-locked by gain modulation", Int. J. Electronics , **60**, p. 67-85 (1986).

9. J. E. Bowers, P. A. Morton, A. Mar, S. W. Corzine, "Actively Mode Locked Semiconductor Lasers", J. Quantum Electron., **QE-25**, p. 1426-1439 (1989).

10. P. A. Morton, R. J. Helkey, and J. E. Bowers, "Dynamic Detuning in Actively Mode-Locked Semiconductor Lasers", J. Quantum. Electron., **QE-25**, p. 2621-2633 (1989).

11. G. P. Agrawal and N. K. Dutta, <u>Long-Wavelength Semiconductor Lasers</u>, Van Nostrand Reinhold, New York (1986).

12. J. E. Bowers, U. Koren, B. I. Miller, C. Soccolich, and W. Y. Jan, "High speed polyimide based semi-insulating planar buried heterostructures", Electron. Lett., **24**, p. 1263 (1988).

13. Y. Suematsu and K. Furuya, "Theoretical spontaneous emission factor of injection lasers", Trans. IECE Japan, **E 60**, p. 467 (1977).

14. S. M. Sze, <u>Physics of Semiconductor Devices</u>, 2nd ed., New York:Wiley, (1981).

15. R. J. Helkey, P. A. Morton, J. E. Bowers, "A New Partial Integration Method for Analysis of Mode Locked Semiconductor Lasers", Optics Lett., **15**, p. 112-114 (1990).

16. G. H. C. New and J. M. Catherall, "Problems in the self-consistent profile approach to the theory of laser mode locking", Opt. Comm., **50**, p. 111-116 (1984).

17. R. J. Helkey, P. A. Morton, J. E. Bowers, "A Novel Analysis Method for Mode Locked Semiconductor Lasers", IEEE LEOS Topical Meeting on Integrated Photonics Research, **TuC2**, March (1990).

18. G. P. Agrawal, <u>Nonlinear Fiber Optics</u>, Academic Press, San Diego (1989).

19. A. J. Lowery, N. Onodera, R. S. Tucker, "Stability and spectral behavior of grating-controlled actively mode-locked lasers", J. Quantum Electron., **27**, p. 2422-2430 (1991).

CHAPTER 3

Subpicosecond Pulse Generation

3.1 Gain Region Saturation Model

In Chapter 3, subpicosecond pulse generation using passive modelocking will be explored. The convergence of rate equation solutions under strong gain saturation occurring in passive modelocking will be examined. Optimum gain and absorber parameters for pulse-shortening are considered. The first compact system for generating <0.5 ps pulses is demonstrated.

In order to analyze passive modelocking, it is helpful to simplify the traveling wave rate equations of Chapter 2 by using normalized parameters [1]. This normalization reduces the number of material and waveguide parameters, so that a few numerically generated plots can be used to predict the behavior of a wide variety of modelocked lasers and optical amplifiers. These parameters are particularly well suited for modelocking analysis:

$$h(\tau) \equiv \frac{g\Gamma[N(\tau) - N_{tr}]L}{v_g}$$

$$P_{in}(\tau) \equiv S_{in}(\tau)\frac{A}{\Gamma}v_g E_{ph}$$

where h is the logarithm of the gain function, found by integrating the gain/unit length over the gain region, and P_{in} is the input power. The power gain is given by $G(\tau) = \exp[h(\tau)]$. The input power is found by multiplying the photon density by the

34

mode cross-section area and group velocity to get the photon arrival rate, which is multiplied by the photon energy E_{ph} to get the input power.

The parameters P_{in} and h are defined in terms of the previous rate equation parameters given in Chapter 2, where S_{in} is the input photon density, A is the active region area, Γ is the optical mode confinement factor, g is the differential gain, N is the carrier density, N_{tr} is the transparency carrier density, L is the length of the gain segment, and v_g is the optical group velocity.

Using these parameters in an exponential gain model and neglecting the waveguide internal loss gives:

$$\frac{dh(\tau)}{d\tau} = \frac{g_oL - h}{\tau_c} - \frac{g/v_g}{A/\Gamma}\frac{P_{in}(\tau)}{E_{ph}}\left[\exp(h(\tau)) - 1\right]$$

where g_oL is the steady state logarithmic gain in the absence of an input signal, and τ_c is the carrier recovery time.

A further useful normalization parameter is:

$$E_{sat} \equiv \frac{A/\Gamma}{g/v_g}E_{ph} = \frac{optical\ mode\ area}{differential\ gain} * photon\ energy$$

The parameter E_{sat} is essentially the saturation energy of the gain region. The role that E_{sat} plays in determining the saturated gain will be explored later in this chapter.

The rate equation solutions now reduce to the following pair of coupled differential equations which will be studied in the remainder of this chapter:

$$P_{out}(\tau) = P_{in}(\tau)\exp[h(\tau)]$$

$$\frac{dh(\tau)}{d\tau} = \frac{g_o L - h}{\tau_c} - \frac{P_{in}(\tau)}{E_{sat}}\left[\exp(h(\tau)) - 1\right]$$

This exponential gain model has been used in the analysis of traveling wave semiconductor amplifiers [1].

For amplification of short optical pulses the gain recovery term is not important. When the optical pulsewidth is much less than τ_c, the first term due to gain relaxation in the second equation can be neglected during the pulse, resulting in the simplified form:

$$\frac{dh(\tau)}{d\tau} = \frac{P_{in}(\tau)}{E_{sat}}\left[\exp(h(\tau)) - 1\right]$$

Under these conditions, a section of semiconductor gain medium can be characterized solely by P_{in}/E_{sat} (the normalized input pulse energy) and $h(0)$ (the initial unsaturated gain). Using this normalization approach, it is possible to analyze general modelocking configurations and predict results for whole classes of problems.

This simplified coupled differential equation has the analytical solution [1]:

$$G(\tau) \equiv \exp[h(\tau)] = \frac{G_o}{G_o - (G_o - 1)\exp(-U_{in}(\tau)/E_{sat})}$$

where $\quad U_{in}(\tau) \equiv \int_{-\infty}^{\tau} P_{in}(\tau')d\tau'$,

and $G(\tau)$ is the amplifier gain, $G_o=\exp[h(0)]$ is the gain before the pulse, and U_{in} is the energy of the input pulse up to time τ.

The energy gain is the ratio of the output pulse energy to the input pulse energy:

$$G_E \equiv \frac{E_{out}}{E_{in}} = \frac{1}{E_{in}} \int_{-\infty}^{\infty} P_{in}(\tau)G(\tau)d\tau$$

where $E_{in} \equiv U_{in}(\infty)$. Expanding this equation with the previous analytic gain expression gives:

$$G_E = \frac{1}{E_{in}} \int_{-\infty}^{\infty} \frac{G_o P_{in}(\tau)d\tau}{G_o - (G_o - 1)\exp(-U_{in}(\tau)/E_{sat})}$$

G_E has the analytic solution [1]:

$$G_E = \frac{\ln[(G_o - 1)/(G_f - 1)]}{\ln[(G_o - 1)/(G_f - 1)] - \ln[G_o/G_f]}$$

where $\quad G_f \equiv G(\infty) = \dfrac{G_o}{G_o - (G_o - 1)\exp(-E_{in}/E_{sat})}$

G_f is the saturated gain after the passage of the pulse. The calculated energy gain is shown in Fig. 3.1 for several values of initial unsaturated gain.

37
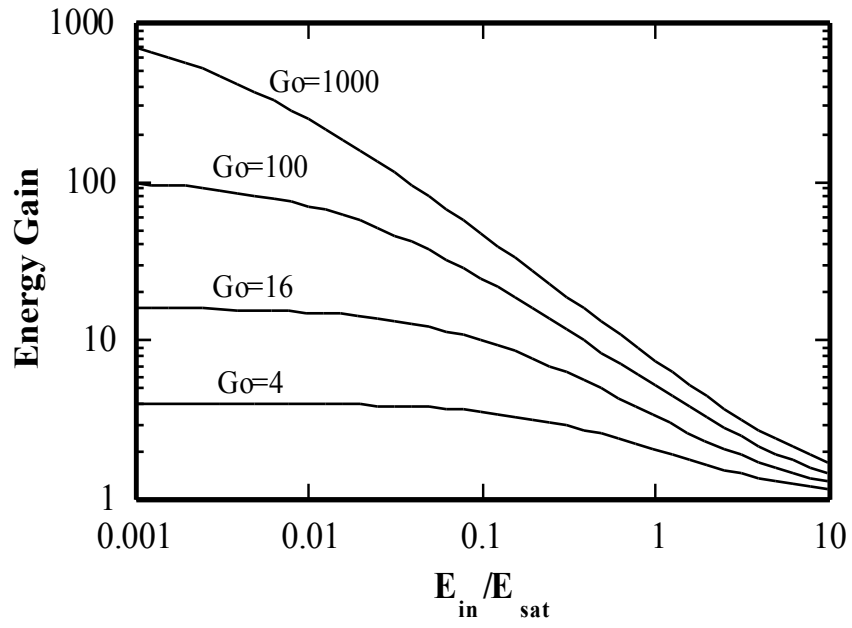
Fig. 3.1   Pulse energy gain as a function of the normalized input energy E_{in}/E_{sat}.
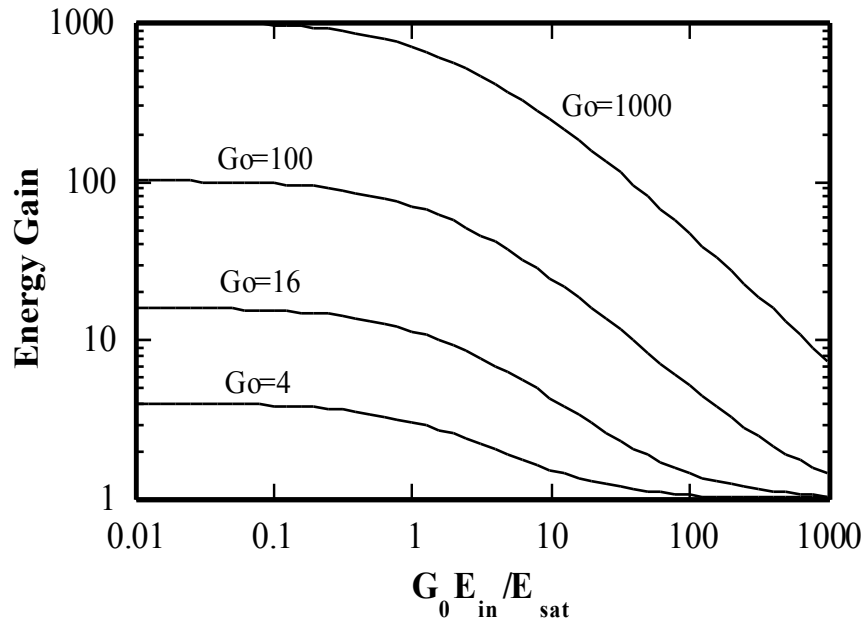
Fig. 3.2   Pulse energy gain as a function of extrapolated output pulse energy G_oE_{in}.

38

When G_o is large, the output of the amplifier will begin to saturate while the input pulse energy is still small compared to E_{sat}. By expanding the exponential term in the denominator, G_f can be approximated by:

$$G_f \approx \frac{G_o}{1-(G_o-1)E_{in}/E_{sat}} \approx \frac{G_o}{1-G_oE_{in}/E_{sat}}$$

The meaning of E_{sat} can clearly be seen from this expression. G_oE_{in} is the value of the output energy extrapolated from low input energy where the gain saturation is negligible. E_{sat} is the value of the extrapolated output energy G_oE_{in} at which the gain is reduced by 3dB. E_{sat} is thus the 3dB compression point referenced to the output energy.

The energy gain is plotted against G_oE_{in} in Fig. 3.2. The gain compression can be seen to start near where the output energy approaches E_{sat}.

3.2 Numerical Integration of Gain Equation

Active modelocking typically operates with low pulse energy, where pulse broadening due to self phase modulation is minimized. As a result, the gain region is under weak saturation. In contrast, passive modelocking requires higher pulse energy in order to bleach the absorber. Gain saturation also is needed to meet the modelocking requirement that the round trip gain be less than unity after the passage of the pulse.

The previous equations give analytical solutions for energy gain for the entire pulse. These results can be used in approximate solutions assuming Gaussian input and output pulses. However, a Gaussian pulse shape is not preserved during gain and absorber saturation, and the instantaneous gain must be found in order to

determine pulse shaping. Most of the numerical computation involves solving the differential equation:

$$\frac{dh(\tau)}{d\tau} = \frac{P_{in}(\tau)}{E_{sat}}\left[\exp(h(\tau)) - 1\right]$$

Euler's method estimates of the actual change in gain Δh based on the infinitesimal derivative $\Delta h \approx dh \equiv (dh/d\tau)\Delta\tau$, where dh is the linear approximation. This is a linear slope estimate to a function which in general has higher order terms. Consequently, the error in estimating the slope $\Delta h/\Delta\tau$ using $dh/d\tau$ has an error which is proportional to order $O(\Delta\tau)$, making it a first order integration algorithm.

3.3 Taylor Series Expansion of Gain Equation

A Taylor series solution can be found by expanding the gain function $h(t)$ in a power series, and substituting the result into the differential equation:

$$h(\tau_o + \Delta\tau) = h_0 + h_1\Delta\tau + h_2\Delta\tau^2 + \ldots$$

$$\left.\frac{dh}{d\tau}\right|_{\tau_o + \Delta\tau} = h_1 + 2h_2\Delta\tau + 3h_3\Delta\tau^2 + \ldots = -\frac{P_{in}}{E_{sat}}\left(e^{h(\tau_o + \Delta\tau)} - 1\right)$$

Matching coefficients in the power series gives:

$$h_1 = -\frac{P_{in}}{E_{sat}}\left(e^{h_0} - 1\right) \qquad h_2 = -\frac{P_{in}e^{h_0}}{2E_{sat}}h_1$$

$$h_3 = -\frac{P_{in}e^{h_0}}{6E_{sat}}\left(2h_2 + h_1^2\right) \quad h_4 = -\frac{P_{in}e^{h_0}}{24E_{sat}}\left(6h_3 + 6h_1h_2 + h_1^3\right)$$

Substituting these coefficients back into the power series gives:

$$h = h_o - dh\left[1 - \frac{E_{out}}{2E_{sat}}\left(1 - \frac{E_{out} + dh}{3E_{sat}} + \frac{E_{out}^2 + 4E_{out}dh + dh^2}{12E_{sat}} - \ldots\right)\right]$$

40

where $dh = -h_1 \Delta \tau$ gives the Euler approximation and $E_{out} = P_{in} \exp[h_o] \Delta \tau$ would be the output energy over the integration time $\Delta \tau$ in the absence of gain saturation. Not surprisingly, this equation clearly shows that numerical integration is accurate for time steps small enough that $E_{out} \ll E_{sat}$. The output energy emitted during the integration time interval needs to be small compared to the amplifier saturation energy.

The Taylor expansion can be simplified by recognizing that $dh \approx E_{out}$ for large gain, which gives:

$$h \approx h_o - dh + \frac{dh^2}{2} - \frac{dh^3}{3} + \frac{dh^4}{4} - \frac{dh^5}{5} + ...$$

For small gain, only the first term of the expansion is important anyway, so this formula is still applicable. Although the coefficients for this series were only computed to order $[dh]^5$, up to this order it matches to the Taylor series for a logarithmic function (it will be seen later that the solution does indeed have this logarithmic form):

$$h \approx h_o - \log[1 + dh] = h_o - \log\left[1 + \frac{P_{in}}{E_{sat}}\left(e^{h_0} - 1\right)\Delta\tau\right]$$

The Taylor series approximations to the logarithmic function $\log[1+dh]$ are shown in Fig. 3.3, and compared to the analytic function. Using a Taylor series solution, for small dh it is easy to approximate the differential equation solution to arbitrary accuracy by increasing the order of series. However, as $dh \rightarrow 1$, the Taylor series becomes a slowly converging function of limited usefulness. The error term changes sign each time another term is added, but the convergence is slow. An accurate solution should not be expected for $dh > 1$, or alternately

$$\Delta\tau > \frac{1}{\dfrac{P_{in}}{E_{sat}}(G_0 - 1)} \qquad \text{or} \quad E_{out} > E_{sat}$$

regardless of the order of the Taylor series that is used.
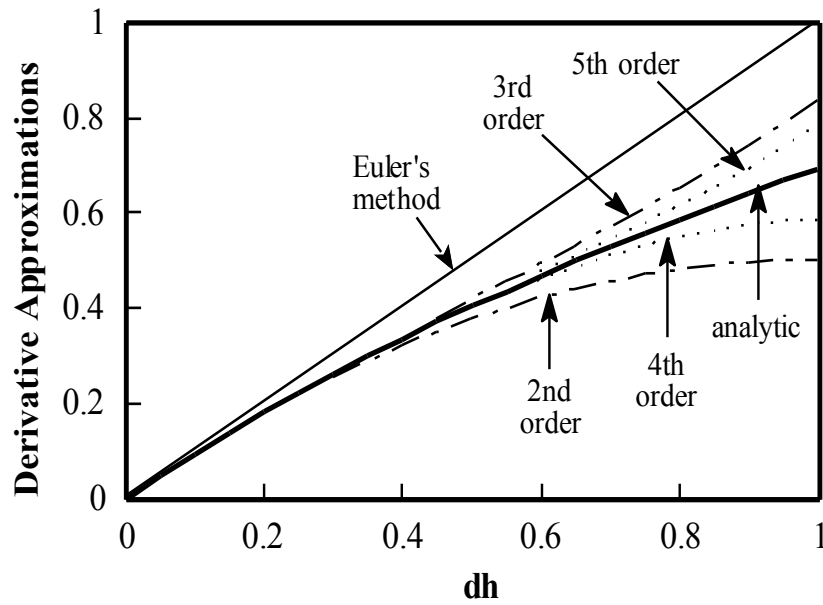
Fig. 3.3   Derivative approximation Δh computed using Taylor series of various order, compared to the logarithmic expression (heavy solid line). Results are plotted vs. the Euler's method approximation dh=-(dh/dτ)$\Delta\tau$.

3.4 Runge-Kutta Integration of Gain Equation

A powerful and general numerical method for solving differential equations is a Runge-Kutta method [2]. Like the Taylor expansion, this technique also makes a series of iterative estimates of the effective slope $\Delta h / \Delta \tau$ for a finite step size $\Delta \tau$. The differential equation for gain considered here has no explicit dependence on t, so a simplified form of the Runge-Kutta equations can be used:

$$dh_1 = -\frac{P_{in}}{E_{sat}} \left(e^{h_i} - 1 \right) \Delta \tau$$

$$dh_2 = -\frac{P_{in}}{E_{sat}} \left(e^{h_i + dh_1 \Delta \tau / 2} - 1 \right) \Delta \tau$$

$$dh_3 = -\frac{P_{in}}{E_{sat}} \left(e^{h_i + dh_2 \Delta \tau / 2} - 1 \right) \Delta \tau$$

$$dh_4 = -\frac{P_{in}}{E_{sat}} \left(e^{h_i + dh_3 \Delta \tau} - 1 \right) \Delta \tau$$

Euler's method is first order integration using only the first parameter dh_1, which is a linear estimate of the slope:

$$h_{i+1} = h_i + dh_1 \Delta \tau = h_i + \left. \frac{dh}{dt} \right|_{\tau_o} \Delta \tau$$

The modified Euler's method is a form of second order Runge-Kutta method, which uses Euler's method to project the solution at that midpoint value of h and τ, and then estimates the slope at the midpoint of the integration step.

$$h_{i+1} = h_i + dh_2 \Delta \tau \approx h_i + \left. \frac{dh}{d\tau} \right|_{\tau_o + \Delta \tau / 2} \Delta \tau$$

43

The fourth-order Runge-Kutta integration method is a weighted average of the series slope estimates, such that the error in the slope estimates cancel up to fourth order in $\Delta\tau$:

$$h_{i+1} = h_i + \frac{1}{6}\left(dh_1 + 2dh_2 + 2dh_3 + dh_4\right)$$

This fourth-order technique is sufficiently accurate for solving most differential equations, and is frequently used for numerical analysis.

3.5 Logarithmic Gain Equation Approximation

The closed form gain solution given earlier in this chapter was:

$$G(\tau) \equiv \exp[h(\tau)] = \frac{G_o}{G_o - (G_o - 1)\exp\left(-U_{in}(\tau)/E_{sat}\right)}$$

where U_{in} is the integral of the input power. This solution has an analytic form in the case where the input power is a function with a known integral. In the case of time evolution of a modelocked pulse, $U_{in}(\tau)$ is not an analytic function. As a consequence, this form of the differential equation requires the same numerical integration as the previous techniques. However, since the only unknown parameter is $U_{in}(\tau)$, this solution should converge for a larger time step under the conditions of large gain and a slowly varying input power.

When there is not an analytic function for $U_{in}(\tau)$ and this formula is used for numerical analysis, $U_{in}(\tau)=P_{in}\Delta\tau$ so:

$$\Delta h \equiv \log[G(\tau)] - \log[G_o] = -\log\left[G_o - (G_o - 1)\exp\left(-P_{in}\Delta\tau/E_{sat}\right)\right]$$

This is the exact solution in the absence of a time varying input power. In many cases $P_{in}\Delta\tau << E_{sat}$ so the exponential term can be expanded:

44

$$h = h_o - \log\left[1 + \frac{P_{in}}{E_{sat}}\left(e^{h_0} - 1\right)\Delta\tau\right]$$

which is the same result obtained earlier by summing the terms generated by the Taylor series expansion. This is the logarithmic approximation, which is independent of the amplifier gain G_o.

3.6 Comparison of Numerical Integration Techniques

In order to compare these numerical techniques, a good test case is an amplifier under strong gain saturation by a Gaussian pulse. In this example, $G_o=100$ and $E_{in}=0.1E_{sat}$. The extrapolated gain without saturation is $G_oE_{in}\gg E_{sat}$. Fig. 3.4 shows the accuracy of the various methods of calculating the final gain as a function of optical time step. The actual energy gain$=9.596\ll E_o$. Ideally, the calculated final gain should not change as the integration time is increased. The rate of convergence with decreasing integration time-step is given by how quickly the numerical result approaches the value of 1.

All of the other methods exhibit dramatic improvement in numerical convergence over Euler's method. The logarithmic approximation is not as good as the other approximations, because the input pulse energy is not sufficiently small. The fourth-order Runge-Kutta solution is particularly accurate for this type of analysis. Over the maximum integration time step of 150 fs, the fourth-order Runge-Kutta solution is indistinguishable from the exact solution.
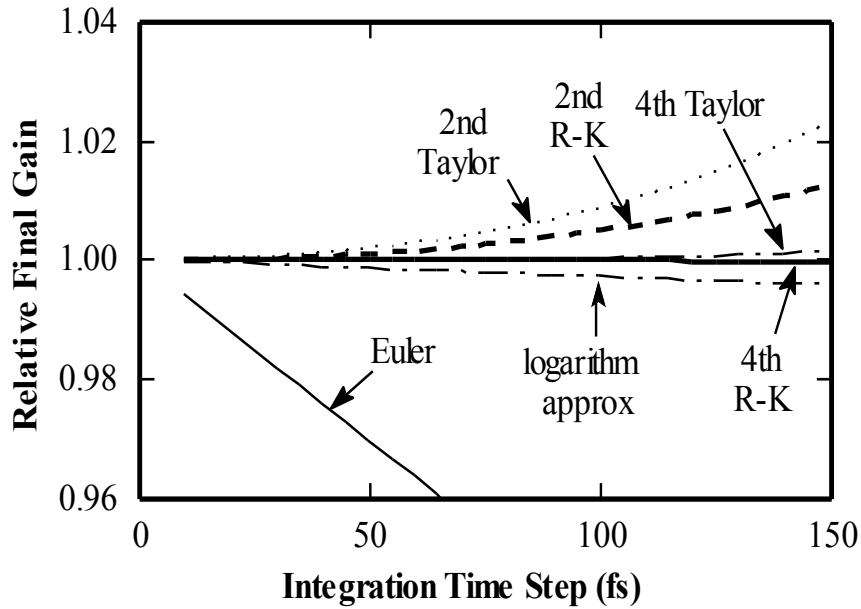
Fig. 3.4   Gain saturation numerical convergence for strong gain saturation by a Gaussian pulse with $E_{in}=0.1E_{sat}$ and unsaturated amplifier gain $G_o=100$.   Final energy gain is normalized to the expected value of G=9.596.

The next example compares these approximations under weak saturation using a Gaussian pulse, as would be found in active modelocking. In this example, $G_o=100$ and $E_{in}=0.01E_{sat}$. The extrapolated gain without saturation is $G_oE_{in}\approx E_{sat}$. Fig. 3.5 shows the accuracy of the various methods of calculating the final gain as a function of optical time step. The actual energy gain=50.376, which is close to the original unsaturated gain. In this plot, the vertical scale is the same, but the integration time step is plotted over a wider range of 500 fs. The improved time step convergence was expected based on the power series formulation developed earlier in this chapter. The relative accuracy of the other approximations with respect to each other is similar, except for the logarithmic approximation which is much better in this

46

example.   Unlike   the   other   approximations,   the   logarithmic   approximation   is
dependent only on the ratio E_{in}/E_{sat}, and not on the unsaturated amplifier gain.
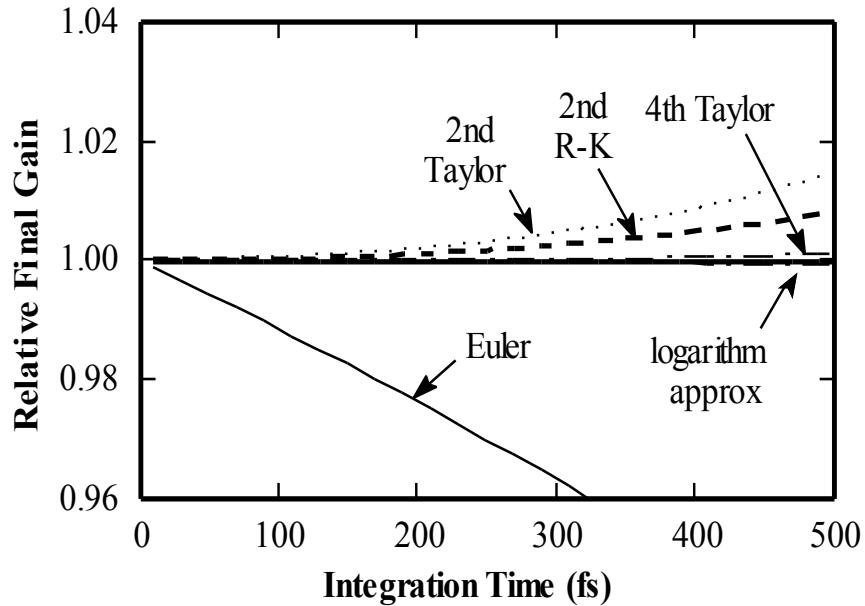
Fig. 3.5   Weak gain saturation by a Gaussian pulse with $E_{in}=0.01E_{sat}$ and unsaturated amplifier
gain $G_o=100$. Final energy gain is normalized to the expected value of $G=50.376$.

A   much   more   stringent   test   of   convergence   occurs   with   a   waveform   with   a
steep rising edge.   The last example compares these approximations under strong
saturation using a square wave input pulse.   This situation can happen in passive
modelocking, where the saturable absorber removes the front edge of the pulse.   For
this example, $G_o=100$ and $E_{in}=0.01E_{sat}$, the same parameters used in the first
example.   Fig. 3.6 shows the accuracy of the various methods of calculating the final
gain as a function of optical time step.

47
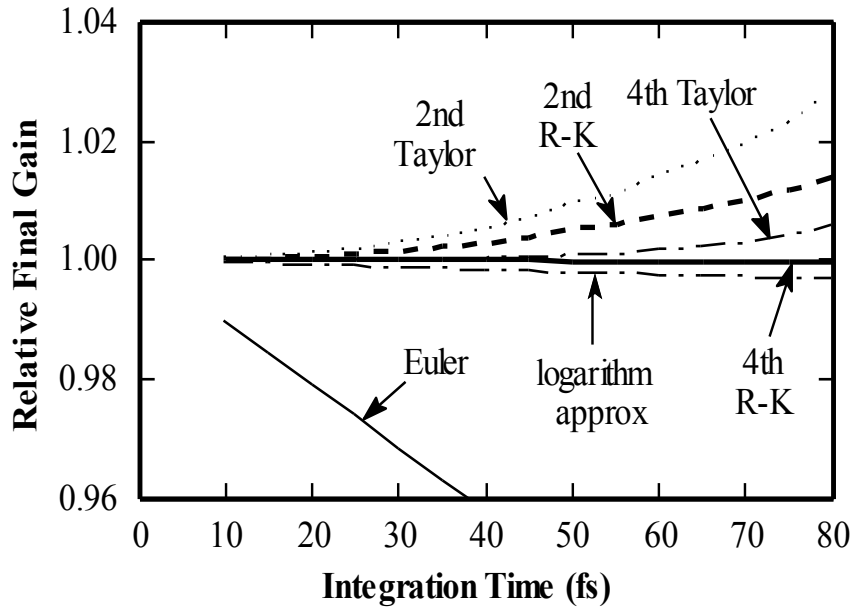
Fig. 3.6   Strong gain saturation by a square pulse with $E_{in}=0.1E_{sat}$ and unsaturated amplifier gain $G_o=100$. Final energy gain is normalized to the expected value of $G=9.596$.

In this plot, the integration time step is plotted over 80 fs, which is the smallest range for these examples. A square wave is the worst pulse shape for computation of gain saturation, as most of the saturation occurs right at the beginning of the input pulse. In contrast, a Gaussian pulse begins to saturate the gain gradually, before the optical input reaches its peak, so less saturation occurs in a single integration time step.

The required time step depends strongly on the amplifier conditions and the input pulse shape. The only reliable method of choosing an integration time step is to redo the calculation with a reduced time step and verify that the answer does not change.

3.7 Absorber Region Modeling

Passive modelocking requires a saturable absorber to generate the modelocking gain/loss modulation from the optical pulse itself. Passive modelocking requires that the saturation energy in the gain region be larger that in the absorber [3]. In previous cases with an integrated saturable absorber, the saturation energy has been proportional only to the differential gain. The saturable absorber can be formed from the same material as the gain region, due to the sub-linear dependence of differential gain on the carrier density illustrated in Fig. 3.7 [4]. However, later in this chapter new devices based on tapered waveguides will be demonstrated. By changing the optical mode area between the gain and absorber regions, these devices can either enhance or degrade the gain to absorber saturation energy ratio σ.
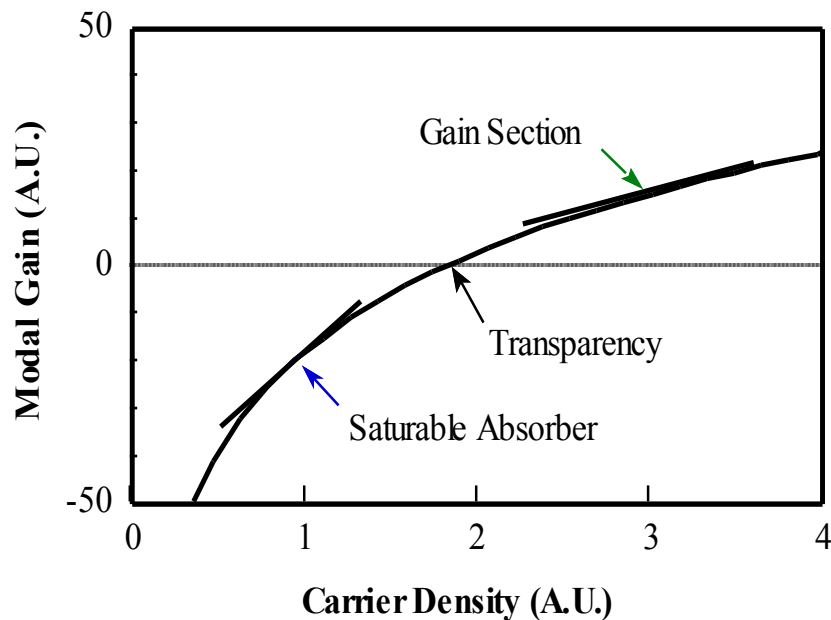
Fig. 3.7   The differential gain in a semiconductor laser has a sublinear dependence on carrier density.

49

The rate equations for the absorber section are similar to that for the gain region, and are given by:

$$P_{out}(\tau) = P_{in}(\tau) \exp[h(\tau)]$$

$$\frac{dh}{d\tau} = \frac{g_o L - h}{\tau_c} - \sigma \frac{P_{in}(\tau)}{E_{sat}}[\exp(h) - 1]$$

The only difference from the gain equations is that here E_{sat} still refers to the saturation energy of the gain region and the absorber saturation energy is E_{sat}/σ. The ratio of the saturation energy in the absorber to the saturation energy in the gain region is given by σ. As will be seen in the next section, it is convenient to use this definition as important pulsewidth shaping mechanisms are dependent on this saturation energy ratio. Carrier grating effects induced by the optical standing wave in the absorber will be covered in next chapter

Rewriting the previous analytic energy gain solution G_E in terms of the input parameters of the absorber equation gives:

$$G_E = 1 + \frac{\ln\left[G_o - (G_o - 1)\exp\left(-\sigma E_{in}/E_{sat}\right)\right]}{\sigma E_{in}/E_{sat}}$$

Under the normal operation of the absorber, $E_{in} > E_{sat}$. Under this condition, the energy gain can be approximated by:

$$G_E \approx 1 + \frac{\ln(G_o)}{\sigma E_{in}/E_{sat}}$$

Bleaching energy is a useful value that can be defined for the absorber, which is the energy lost under strong saturation of the absorber. This value is limited to the

energy which can be supplied by the gain region, which is on the order of E_{sat}. The bleaching energy E_{bl} is given by:

$$E_{bl} \equiv E_{in} - E_o = E_{in}(1 - G_E) \approx -E_{in}\frac{\ln(G_o)}{\sigma E_{in}/E_{sat}}$$

where the unsaturated absorption $\alpha_o = 1/G_o$. The approximate bleaching energy is:

$$E_{bl} \approx \frac{\ln(\alpha_o)}{\sigma}E_{sat}$$

For a given absorber bleaching energy, the unsaturated absorption increases as the differential gain increases. This approximate formula for the bleaching energy is compared to numerical calculations in Fig. 3.8. The accuracy of the analytic approximation is very good for $\sigma \geq 3$.
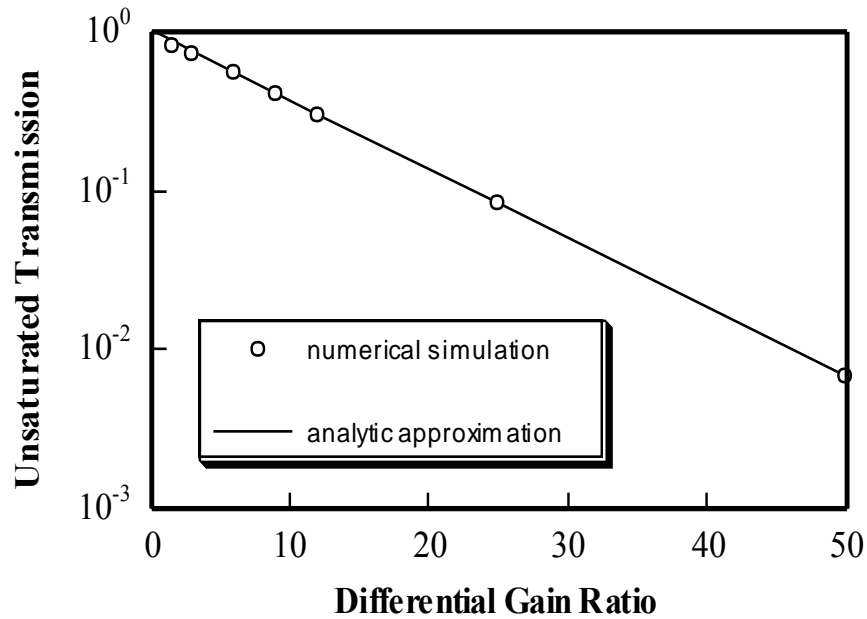
Fig. 3.8   Unsaturated absorber transmission needed to give a bleaching energy of $E_{bl}=0.1E_{sat}$ as a function of the differential gain ratio σ for an input pulse energy of $E_{in}=E_{sat}$. Circles are computed values, solid line is the analytic approximation of $E_{bl} \approx \log(\alpha_o)/\sigma = 0.1$.

51

Increasing the differential gain parameter σ improves pulse shaping by sharpening the leading edge of the pulse. A larger value of σ also satisfies the modelocking condition over a wider range of parameters by increasing the unsaturated absorption and suppressing CW lasing.
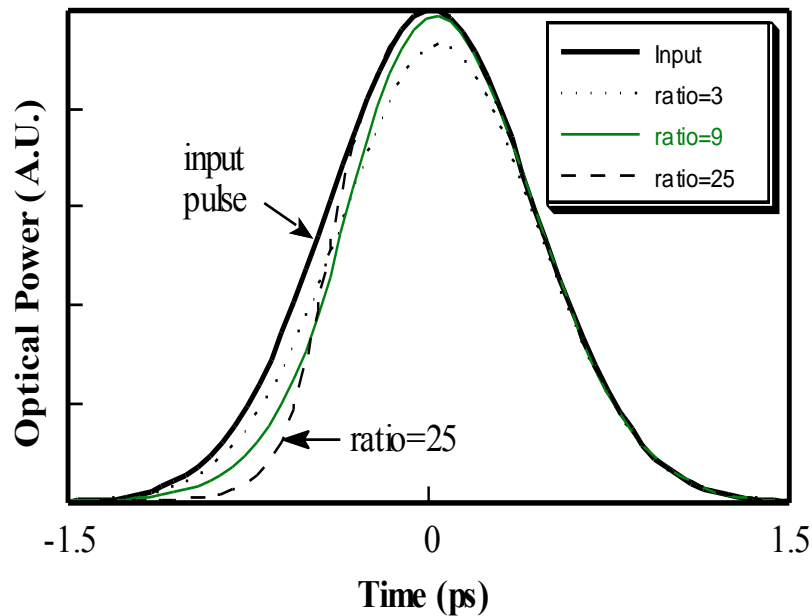
Fig. 3.9   Gain shaping provided by the saturable absorber for varied values of differential gain ratio between absorber and gain region. Input pulse energy $E_{in}=E_{sat}$ of the gain region.

3.8 Pulse Shaping by Passive Modelocking

In order to understand the effect of the gain and absorber, it is helpful to examine a unidirectional case illustrated in Fig. 3.10. Here the effects of pulse shortening and energy gain occur independently in the gain and absorber region. The absorber contribution is calculated by taking the ratio of the case of gain alone and the case of the gain/absorber cascade. As a result, the input pulse energy for the absorber contribution is not the E_{in}/E_{sat} as labeled on the graph, but rather the amplifier output energy at that given input energy.

52

The pulse energy gain through the gain and absorber regions (the chip gain) must equal the round trip coupling loss in the external cavity. This can be fairly high in the GaAs devices used here. The loss contributions come from the optical beam at the waveguide output having a high numerical aperture, non-ideal phase variations across the beam-front, and astigmatism/elliptical shape due to differences in the horizontal and vertical directions of the waveguide. Semiconductor lasers such as these have an optical mode which is small compared to the optical wavelength. Consequently, the emission angle from the cleaved facet is large, so that even high numerical aperture lenses do not capture all of the output beam. In an external cavity device, this coupling loss also occurs in the reverse direction, due to mode mismatch as the input beam is focused back down into the laser.

Non-ideal phase/amplitude variations occur due to the optical mode not having a planar phase-front and a Gaussian shaped amplitude. As a result, the collimating lens does not produce an ideal collimated beam. The ellipticity of the beam arises from the asymmetry in the optical waveguide mode. The mode is strongly confined to a small size in the vertical direction by the material layer structure. The confinement in the horizontal direction is given by photolithography, and is due to the index step caused by the aluminum inter-diffusion from impurity-induced disordering.

All of these coupling problems can be substantially reduced with buried heterostructure devices in the InP material system. Here, a nearly square active region can be formed which is surrounded by a relatively uniform material with a small index step. This technique has been used to produce polarization insensitive semiconductor optical amplifiers [5].

53

In the example shown in Fig. 3.10, the single pass absorber transmission is 0.04. Assuming a net chip gain of 20 in order to allow for loss in coupling to an external cavity and a saturation energy ration σ of three, the unsaturated amplifier gain must be 130. At low input energy, both the gain and absorber region are unsaturated. At an intermediate energy, the absorber is beginning to be bleached before the amplifier saturates, giving a higher net gain for pulsed operation,. As the input energy is increased further, the absorber becomes completely bleached, and increased amplifier saturation leads to less overall gain. The gain region gives some pulsewidth broadening. The absorber gives stronger pulse shaping by removing the leading edge of the pulse, leading to overall pulsewidth shaping.

In an actual device, the optical wave makes a round trip through the gain and absorber. In order to be equivalent to the unidirectional example, the absorption per pass in this case is reduced to 0.2, in order to give an equal round trip absorption of 0.04. It might be expected that reducing the amplifier gain to the square root of the single pass gain in the previous example also would produce the desired energy gain of 20. This would be a single pass gain=sqrt[130]≈11.4. However, the gain and absorber saturation characteristics in the bi-directional case are somewhat more complicated. For an unsaturated single pass gain of 17, Fig. 3.11 shows the calculated energy gain for forward and backward propagation. The results are qualitatively similar to the unidirectional case. The pulsewidth broadening contribution from the gain region has a somewhat different shape. This is due to the saturation of the absorber, which changes the relative amplitude of the optical wave on the return path.
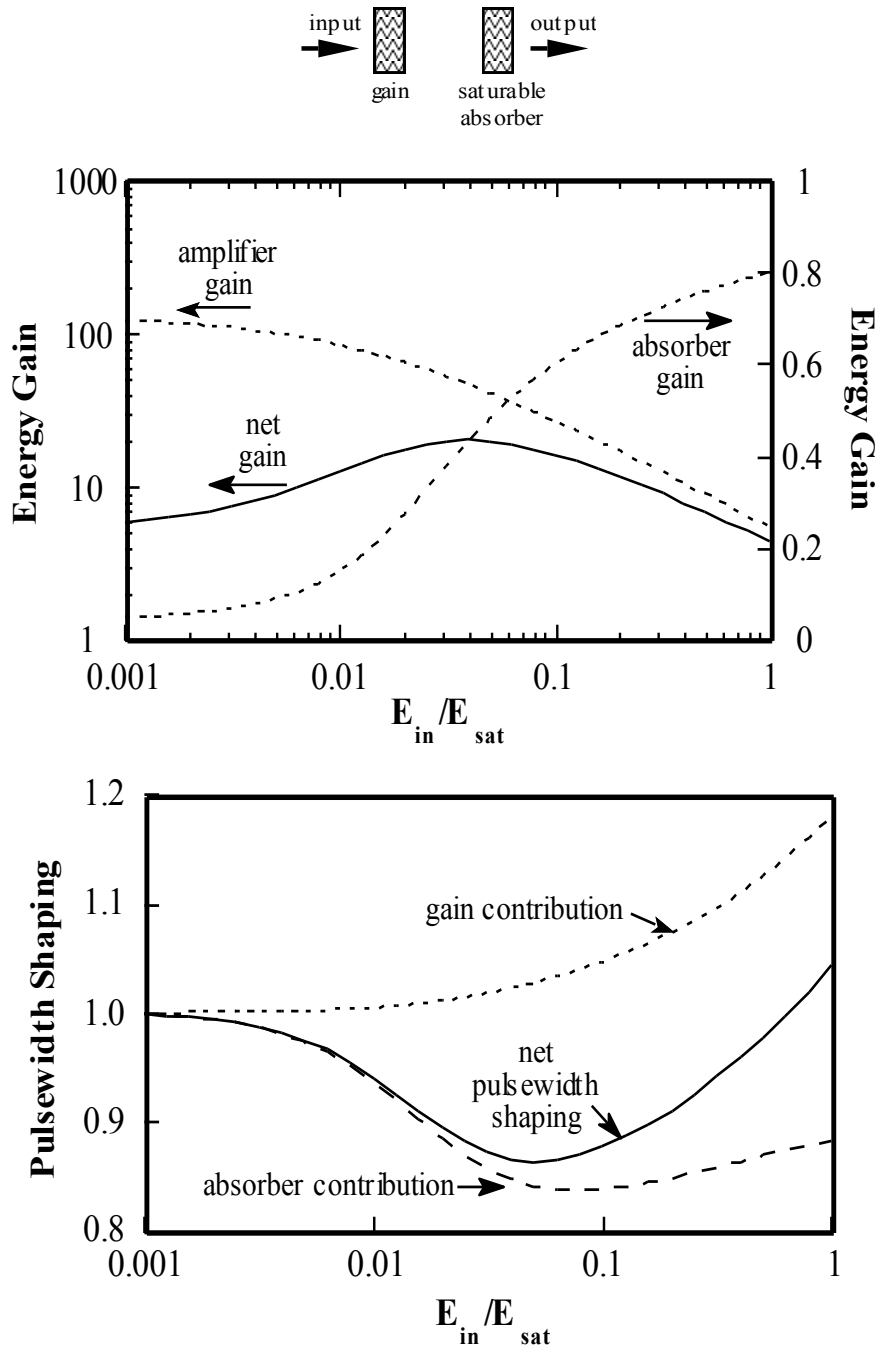
Fig. 3.10   Energy gain and pulse shortening per pass as a function of input power for unidirectional
propagation with $\sigma=3$, $G_{amp}=130$ and $G_{abs}=0.04$ for a single pass.
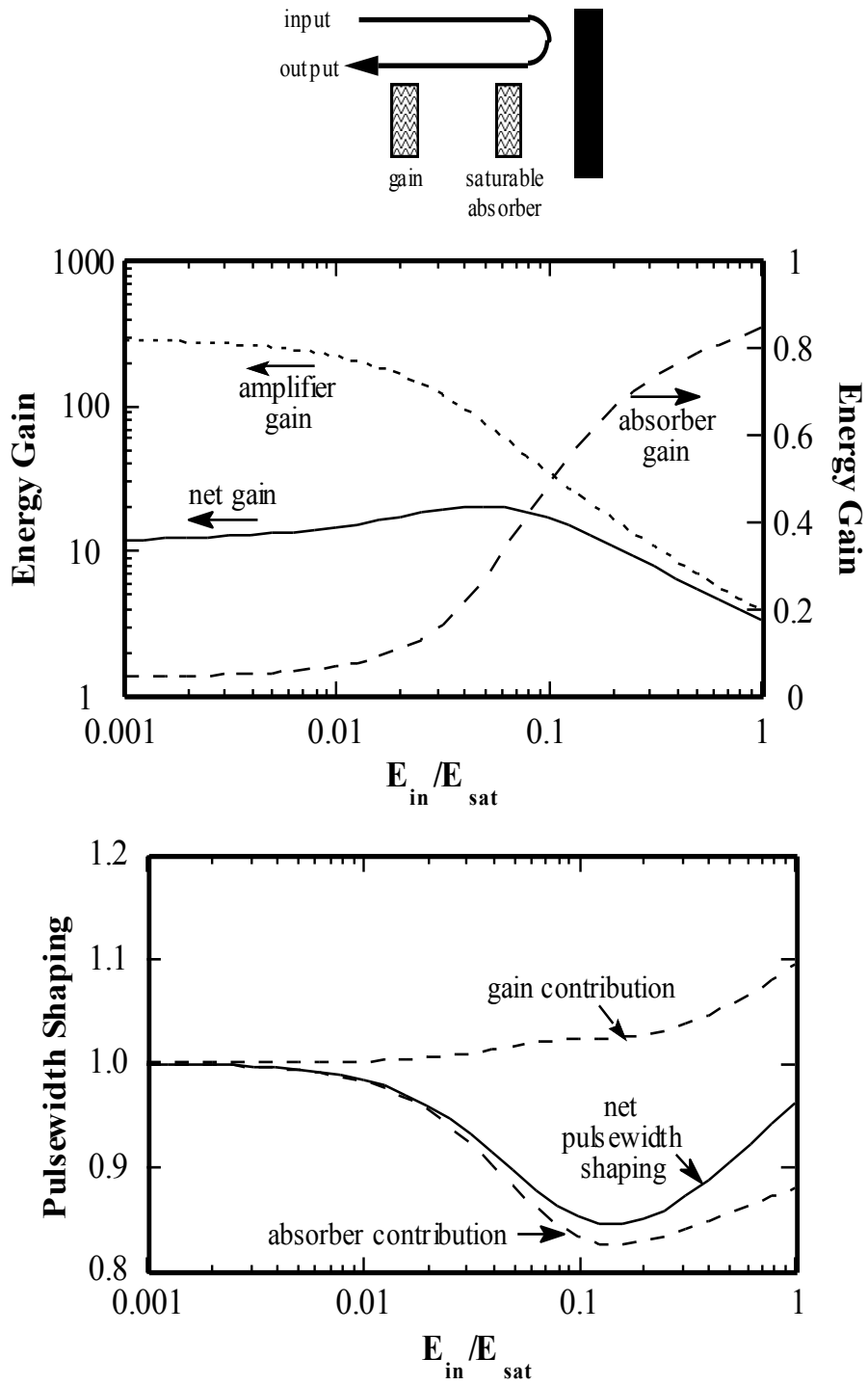
Fig. 3.11   Energy gain and pulse shortening per pass as a function of input power for round trip propagation with $\sigma=3$, $G_{amp}=17$ and $G_{abs}=0.2$ per pass. Maximum energy gain ~20.

There are several requirements for achieving modelocking. There needs to be a net pulsewidth reduction mechanism, to counterbalance the pulsewidth broadening mechanisms of dispersion and bandwidth broadening. There also needs to be net cavity loss before and after the pulse, to prevent a CW mode from taking over.
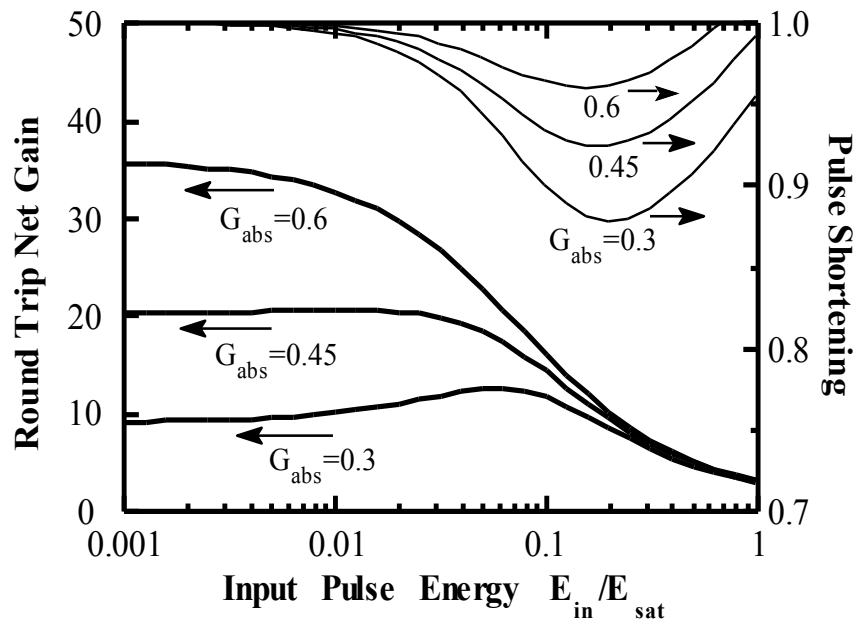
Fig. 3.12   Round trip net gain and pulsewidth shortening vs. input pulse energy for various values of unsaturated absorber transmission, using a round trip propagation model with G_{amp}=10 per pass. Energy saturation ratio σ=3.

In the previous example, the energy gain for pulsed operation was higher than at low pulse energy when the gain and absorber region were not saturated. As a result, the CW mode had a higher threshold than for a modelocked pulse. Fig. 3.12 examines the case of absorber regions with lower bleaching energy (higher unsaturated transmittance G_{abs}), using a single pass amplifier gain G_{amp}=10. For G_{abs}=0.3 (E_{bl}=0.417), the gain still peaks for higher energy pulses. For G_{abs}=0.45 (E_{bl}=0.28), the gain function is relatively flat, and approximately equal to the

57

assumed external cavity loss. However, for $G_{abs}=0.6$ ($E_{bl}=0.183$) the energy gain is monotonically decreasing with input pulse energy. The CW mode with the gain and absorber regions unsaturated will have a lower threshold than for pulse operation.

Dye lasers and solid state lasers can operate with a gain per pass which is much lower than in a semiconductor laser. These lasers do not have the large coupling loss due to an intracavity waveguide. In addition, the lasers operate with higher mirror reflectivity to give a high-Q cavity. Semiconductor lasers require lower mirror reflectivity to achieve sufficient output power. As a result of the lower gain, dye lasers and solid state lasers can operate with much smaller absorption per pass. The higher gain of semiconductor lasers has important consequences, as is shown later in this chapter with regards to increased self-phase modulation and in Chapter 4 with regards to the colliding pulse effect. Fig. 3.13 shows a similar calculation with the single-pass unsaturated amplifier gain reduced to 2.5 per pass. With the lower amplifier gain, an unsaturated absorber transmission $G_{abs}=0.6$ is low enough to cause modelocking. The plots are for $G_{abs}=0.6$ and $G_{abs}=0.8$, corresponding to $E_{bl}=0.183E_o$, and $E_{bl}=0.0085E_o$.

For a given absorber value, the necessary unsaturated amplifier gain to give a pulse energy gain of 20 is shown in Fig. 3.14, along with the pulsewidth shortening ratio at the this peak energy gain. When varying the saturation energy ratio σ, it is a more direct comparison to use the absorber bleaching energy E_{bl} than unsaturated transmission G_{abs}. Using a constant bleaching energy, as the saturation energy ratio σ increases the pulsewidth shortening increases. However for a given absorber bleaching energy, the required unsaturated amplifier gain remains the same. Only one gain curve is shown for both values of σ.

58

A high saturation energy ratio is desirable for increasing the pulsewidth shortening, but also for increasing the modelocking parameter range. For the case of $\sigma=3$, as the bleaching energy is reduced, the pulsewidth shortening ratio goes to 1. At the same bleaching energy the modelocking condition requiring net cavity loss before the pulse is no longer satisfied.

In the other extreme, as the bleaching energy increases beyond E_{sat} the required unsaturated amplifier gain becomes extremely large. This is because the amplifier can only supply pulse energies on the order of E_{sat}.
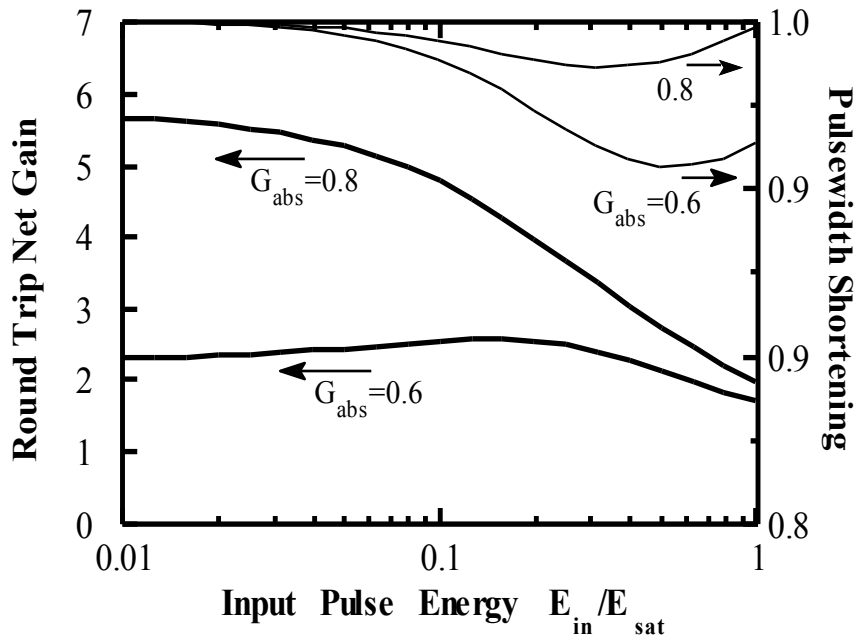
Fig. 3.13   Round trip net gain and pulsewidth shortening vs input pulse energy, using a round trip propagation model with G_{amp}=2.5 per pass. Energy saturation ratio σ=3.
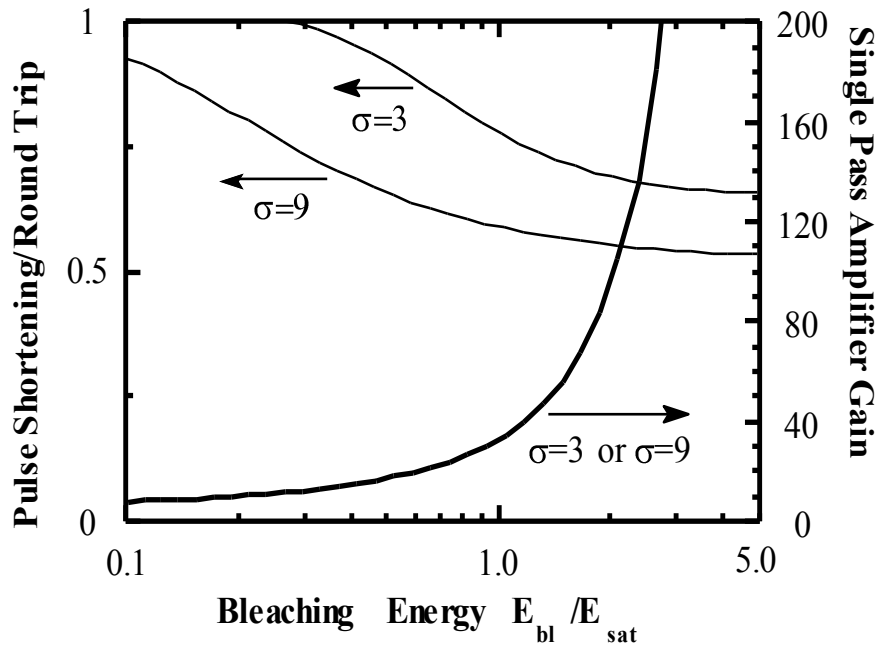
Fig. 3.14   Pulsewidth shortening and required unsaturated amplifier gain as a function of bleaching energy in order to give a round-trip energy gain of 20.

3.9 Curved Waveguide for Secondary Pulse Suppression

A fundamental limitation in coupling a semiconductor diode laser into an external cavity is the finite facet reflectivity that remains after applying an antireflection coating. The minimum facet reflectivity is limited by the control of the thickness and index of the material being used to match the effective mode impedance of the laser to the impedance of air. Very tight tolerances are required in order to achieve a power reflectivity $<10^{-4}$.

In tunable lasers, the residual reflectivity can cause ripple and hysteresis in the output power, and discrete steps in the optical frequency during frequency tuning. In addition to the grating that acts as the main tuning element, an interferometer with increased frequency resolution is sometimes used to eliminate the unwanted diode modes.

In modelocked semiconductor lasers, the finite facet reflectivity causes multiple pulses spaced at the round trip time of the cavity. This degrades system performance, since the effective pulsewidth becomes that of the multiple pulse envelope, rather than that of each individual pulse. Using active mode-locking of a single section device, a facet reflectivity as low as 10^{-5} is necessary to prevent multiple pulsation [6]. This low facet reflectivity is impractical for most coating systems [7]. Techniques to reduce the multiple pulsation problem include using frequency detuning (Chapter 1) and increased device length [8] for active modelocking, and absorption recovery in passive mode-locking [9].

One way to further reduce facet reflectivity is with angled facet devices [10]. Traveling wave amplifiers can be fabricated by placing the gain region at an angle to the crystallographic plane, so that the cleaved device has waveguides that are not

perpendicular to the facet. This reduces the effective facet reflectivity, because the most of the reflected light does not couple back within the acceptance angle of the guided mode of the waveguide.

(a) straight device

(b) angled facet device
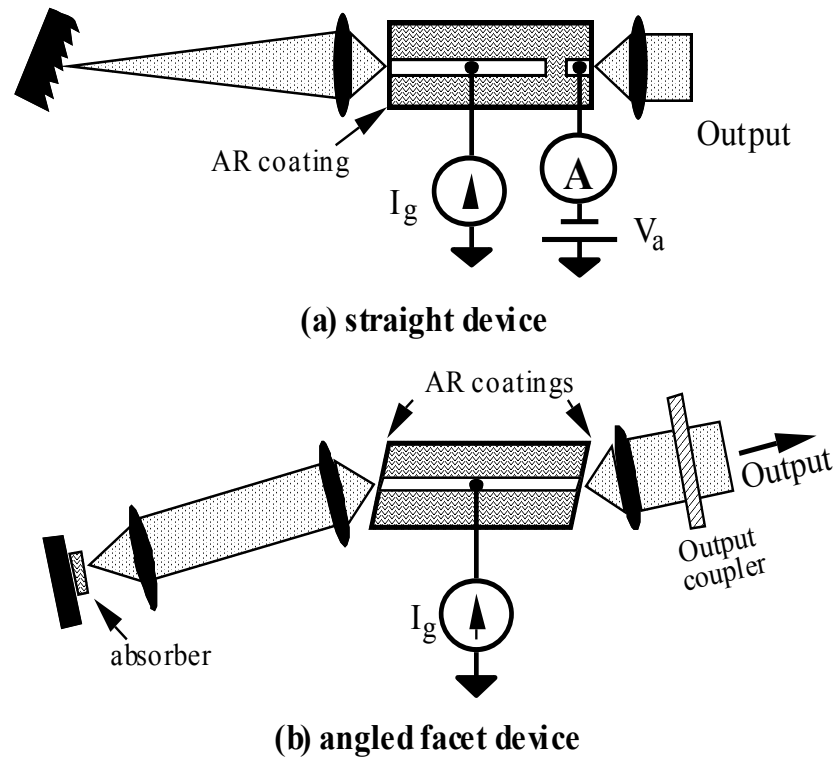
Fig. 3.15   (a) Passive mode-locked semiconductor diode laser using a linear cavity configuration with the gain region at one end of an external cavity. (b) Angled facet device with external absorber.

The standard linear modelocking configuration is shown in Fig. 3.15a. In this configuration, the gain region is at one end of the cavity, and one of the device facets acts as a cavity mirror. As mentioned earlier, a saturable absorber can be formed from an unpumped gain region. Ion implantation can be used to decrease the carrier lifetime. However, a reversed biased segment has the advantage that the carrier removal mechanism is integrated with the processing rather than later requiring a

62

separate processing step. Excitonic absorbers can also be used externally, but work only over a narrow wavelength range, which restricts the wavelength of operation. An excitonic absorber also requires an optical filter to force lasing wavelength to the excitonic transition.

To reduce multiple pulses, angled facet devices have been used [11]. This technique has been applied to passive mode-locking, using a traveling wave amplifier in a cavity between two external mirrors. However, this technique has the disadvantage that the cavity configuration is more complex than the standard linear cavity geometry. Since one of the laser facets is no longer acting as a cavity mirror, an external cavity mirror must be added. This means that the system will require a second cavity alignment, as well as increase the total coupling loss.

As will be shown in Chapter 4, the absorber needs to be placed at one end of the cavity. Since the angled-facet laser is in the middle of the cavity, the absorber cannot be integrated with the laser but must added externally. As was shown earlier in this chapter, the beam size in the absorber must be small to give a low saturation energy. In order to have a small optical spot size in the absorber, a second lens must be added.

The angled facet modelocking configuration eliminates multiple pulses, but the normal facet configuration is simpler. Since only one low reflectivity facet is desired for modelocking, these two techniques can be combined by having only one facet angled with respect to the waveguide. A single angled facet can be realized with an etched facet or curved waveguide.

Two configurations are proposed using devices with a single angled facet (Fig. 3.16). The curved waveguide technique has the advantage that both of the facets are formed by cleaving, without further processing steps. The etched angled

facet approach requires an additional alignment/etching step to form angled facets. Curved waveguides had been reported previously for the generation of chirped gratings in distributed feedback (DFB) lasers [12].

(a) etched angled facet

(b) curved waveguide
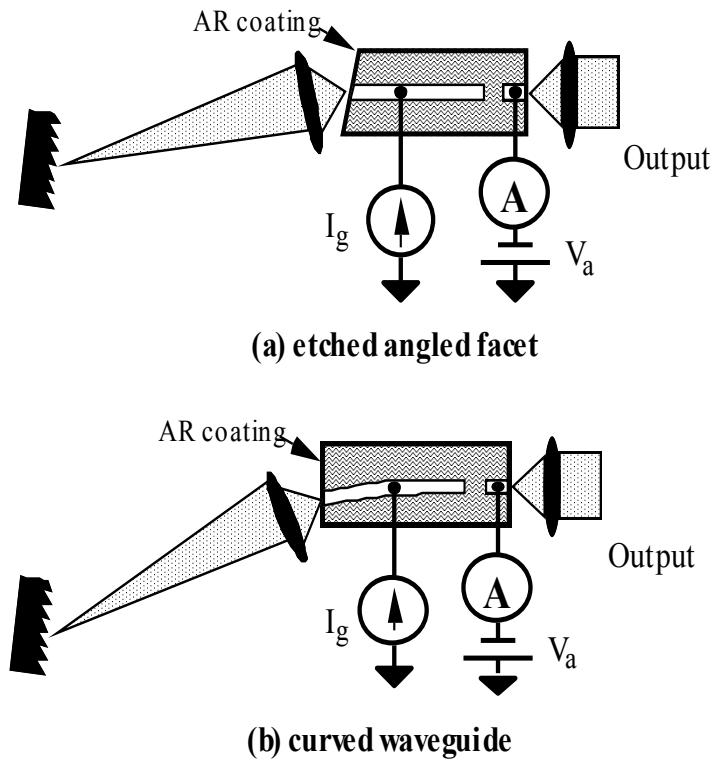
Fig. 3.16   Two proposed angled facet methods for reducing the facet reflectivity for external cavity applications such as modelocked semiconductor lasers.   The output facet should be normal to the waveguide.

The potential problem with the curved waveguide configuration is that the waveguide does not follow a crystallographic axis. As a result, ridge lasers and buried heterostructure lasers require more careful fabrication. Wet etching can produce waveguides with higher edge roughness due to etch anisotropy. Regrowth also can be more difficult due to growth anisotropy.
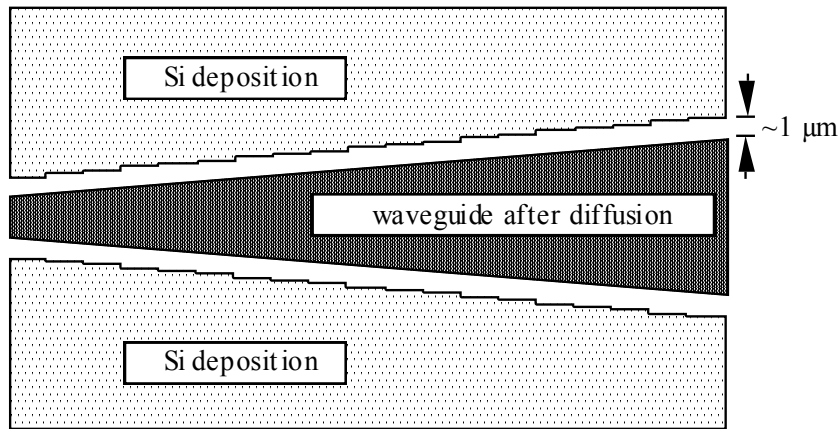
Fig. 3.17   Diffusion-defined waveguides allow smoothing of mask irregularities. Larger waveguide
mask features increase photolithography yield.

Impurity induced disordering [13] is a good fabrication technique for curved and angled gain regions, as it is insensitive to crystal orientation. In this technique, silicon is placed on the surface, except over the waveguide. Silicon enhances the interdiffusion of aluminum from the cladding layers into the separate confinement region (SCH) and quantum wells. This lowers the index for optical confinement and raises the bandgap for electrical confinement [14]. Because the diffusion process occurs at high temperature, there is also interdiffusion in the active region even without silicon present, but it is orders of magnitude smaller. In the diffusion process, the silicon moves inward as well as down, so the original mask pattern must

65

be larger than the final waveguide. This has an advantage of increasing the waveguide mask features, and reducing defects due to photolithography. This diffusion process also smoothes out small mask irregularities (Fig. 3.17).

Two InGaAs/AlGaAs devices were used for comparison, a straight cavity and curved cavity device. Both devices had an absorber length of ~40 μm and a cavity length of 300 μm. The curved device was curved to an angle of 5˚ over a distance of 220 μm, with a radius of curvature of 2.5 mm. The devices were fabricated by W. X. Zou using impurity induced disordering [15]. The active region consisted of 3 $In_{0.2}Ga_{0.8}As$ quantum wells 8 nm thick separated by 10 nm GaAs barriers, between 80 nm $Al_{0.2}Ga_{0.8}As$ separate confinement regions.

The two devices were antireflection coated using a quarter wave layer of non-stochiometric SiN. The coating system has passive index control and active thickness control [16]. The index is calibrated by test runs before deposition. The thickness is set by in-situ monitoring of the optical power from the uncoated device.

The relative reduction in facet reflectivity can be found by measuring the amplitude ripple in the spontaneous emission spectrum due to the undesired Fabry-Perot cavity. In a straight waveguide device, the uncoated facet reflectivity is known. By biasing the device at its original threshold, the total material gain is equal to the uncoated mirror loss, and the coated mirror loss can be determined. The straight device had a gain ripple of 1 dB, corresponding to a facet power reflectivity of 10^{-3}.

66
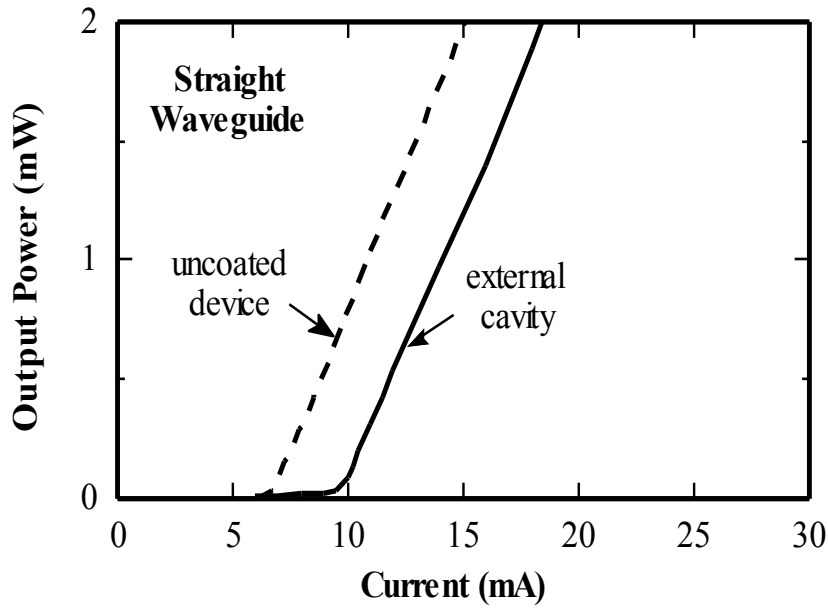
Fig. 3.18 Optical output power for the straight devices coupled to a grating external cavity compared to the output power of the uncoated device.
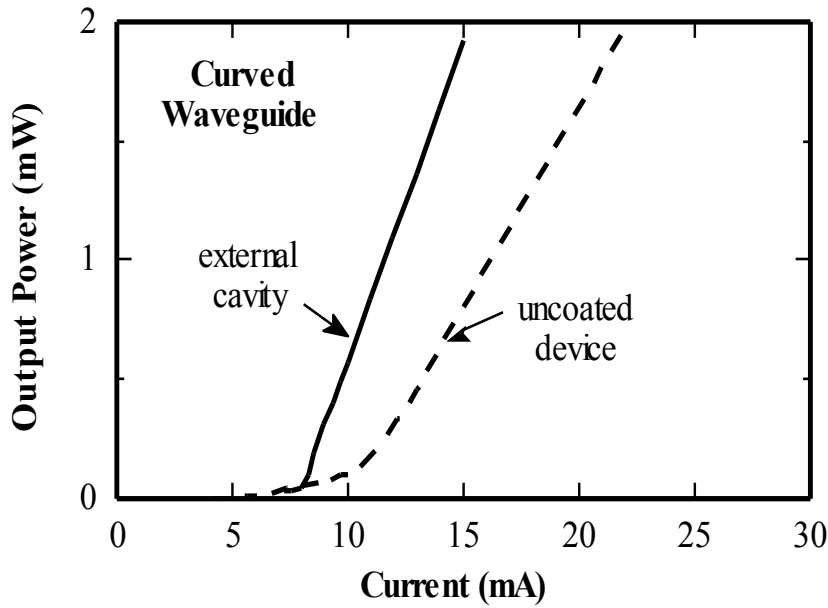
Fig. 3.19 Optical output power for the curved waveguide device coupled to a grating external cavity compared to the original uncoated output from the straight waveguide facet.

67

The original curved facet reflectivity was not known, so finding the reflectivity after coating was somewhat more complicated. The final reflectivity was calculated by using the standard gain ripple procedure twice. The gain ripple at the uncoated threshold gives the reduction in reflectivity due to coating using the previous method. The 'inherent threshold' of the device if the waveguide were straight (R=0.3) was estimated by comparing the external cavity threshold after coating of the curved device with that of the straight device. At this equivalent threshold bias current, the material gain in the curved device is equal to the known mirror loss of a straight waveguide device. The gain ripple at this bias current had been measured before the device was coated, and this ripple was used to find original facet reflectivity. The curved waveguide device had an estimated coated facet reflectivity of $5*10^{-5}$.

The L-I curved for the straight and curved devices are shown in Fig. 3.19, both before coating, and in an external cavity after coating. Passive mode-locking was initiated by reverse biasing the absorber to -0.5 V. The autocorrelation results are shown in Fig. 3.20. The straight device exhibits the small residual trailing pulse which is always seen in these types of structures. The curved device has just a single pulse. This is believed to be the first demonstration of using an integrated waveguide absorber to produce passively modelocked pulses which are shorter than the round trip time of the laser, yet maintain a single pulse output.
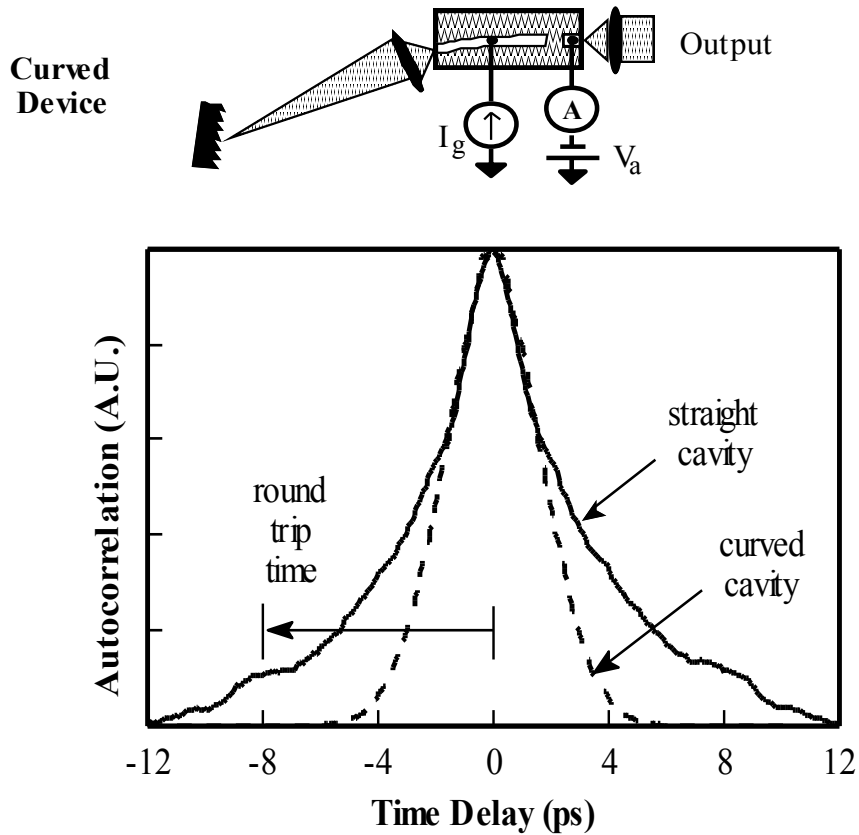
Fig. 3.20   Noncollinear intensity autocorrelation using straight and curved waveguide devices.

3.10 Tapered Waveguide to Increase Pulse Energy

A major limitation of modelocked semiconductor diode lasers is low output power. The average output power is typically a few mW for a single stripe device. By increasing the modal cross-section, the saturation energy can be increased [17]. Techniques to increase the modelocked output power while maintaining a single lateral mode include external cavity spatial filtering of broad area and array structures [11, 18] and resonant optical wave (ROW) coupled arrays [19]. External amplification has also been used [11].   However, these techniques have some problems.   ROW arrays require very precise fabrication in order to meet the

69

transverse resonance condition which couples the individual elements together. The external amplifier approach requires an additional alignment [11]. The simplest approach is to obtain more power from a basic single stripe laser.

Here a modelocked source with a tapered waveguide is demonstrated to give higher energy pulses. Tapered waveguides have previously been used as amplifiers for CW sources [20-22]. The tapered waveguide expands the optical mode from a narrow region which gives a single lateral optical mode, to a wider multimode region for higher power.

The tapered waveguide configuration is shown in Fig. 3.21. The waveguide active region has a linear taper from 2.5 μm to 7.5 μm over a 150 μm distance. The long taper region was used to allow for adiabatic mode expansion. The beam cross-section does not increase as fast as the waveguide width, giving an increase in confinement factor as the waveguide width increases. The absorber lengths were approximately the same, so the pulse energy should be proportional to the saturation energy. The modelocked output pulse energy was increased to 4.1 pJ, which is 2.3 time the 1.8 pJ pulse energy for the 2.5 μm untapered waveguide device. The autocorrelations for the tapered and straight devices also are shown in Fig. 3.21. The pulsewidth is wider by a factor of 1.2 for the tapered device, indicating some modelocking degradation.
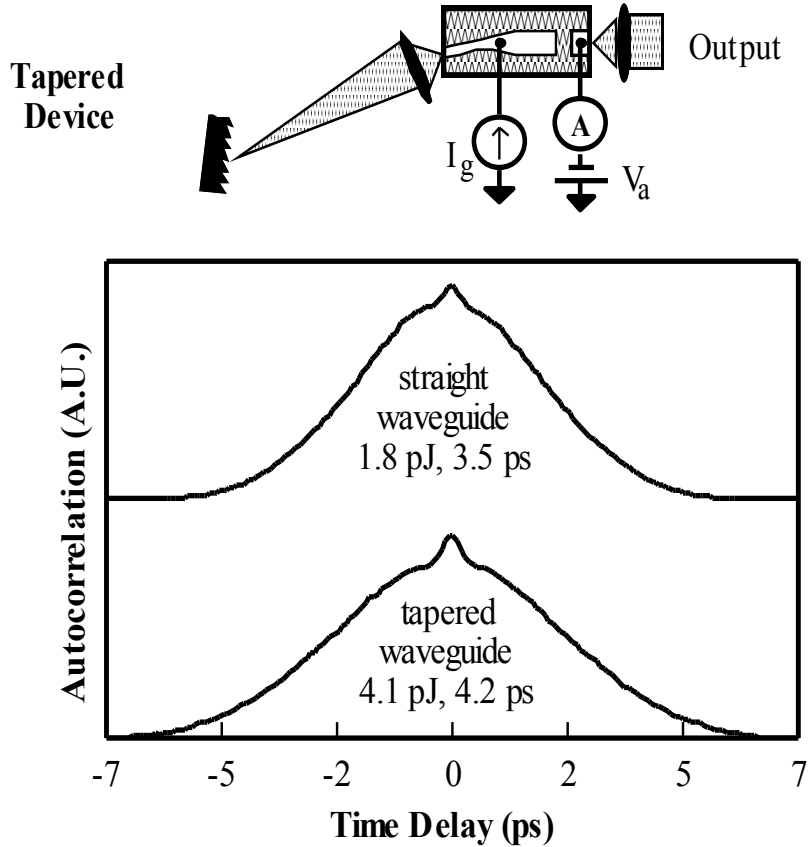
Fig. 3.21   Autocorrelations for straight and tapered waveguide devices.

In principle, this technique could be extended to even higher output energy by tapering to an even broader absorber region. However, there are two limitations to the tapering ratio that can be achieved with this topology. One limitation is heating, and the other is effective increase in the absorber cross-section.

One potential problem with this flared waveguide configuration is that the average beam diameter in the gain region is smaller than in the absorber region. The figure of merit for modelocking is σ, the ratio of the saturation energy of the absorber to the gain defined earlier in the chapter.   This saturation ratio is

proportional to the volume of the optical mode. As a result, σ decreases due to the mode expansion in the waveguide, which degrades the modelocked pulse shaping.

The value of E_{sat} for the amplifier is effectively a weighted value, since the mode area is changing as the pulse propagates. If the taper is near the absorber, the entire amplifier waveguide is single mode, but at the expense of maximum degradation in the amplifier/absorber saturation energy σ. If the taper occurs near the amplifier input, the loss in amplifier saturation energy is small, but the increase in lateral mode selectivity is small. The optimum configuration is for the taper to be as close to the external cavity as possible, while still maintaining single-mode operation.

The main problem with these particular flared devices is in device heating. The passively modelocked devices operate with the gain region biased to strong saturation. The drive current becomes quite large even for modest output power. The drive current for the straight device was ~60 mA. The drive current for the tapered device could thus be expected to be ~150 mA. This high drive current is beyond the failure point of the tapered device when mounted junction-side up. As a result, the absorber bias voltage was increased from -0.5 V where the devices operate best, to +0.5 V for the tapered device. Also, the repetition rate was reduced from 3 GHz to 1.4 GHz in order to reduce the average optical power. The current used for the tapered device was 80 mA.

Mounting devices junction-side down could allow this tapering technique to produce shorter pulses by optimizing bias conditions, as well as extending to larger tapering ratios to give higher output power. However, for large waveguide flaring, the modelocking would be degraded due to the effective reduction in absorber cross-section ratio s. For very high output power, other techniques will be necessary.

72

3.11 Self Phase Modulation Effects on Optical Spectrum

In a semiconductor diode laser, gain saturation produces large refractive index changes. These are caused by the dependence of both the index and gain on the carrier density. This mutual dependence of gain and index is described by the parameter α, known as the linewidth enhancement factor [23]:

$$\alpha \equiv \frac{dn_r}{dn_i} = \frac{dn_r/dN}{dn_i/dN}$$

where n_r is the change in the real index, n_i is the change in the imaginary index (gain), and N is the carrier density. Gain saturation which is induced by the optical pulse causes a corresponding index shift, which modulated the optical frequency:

$$\Delta v(\tau) \equiv \Delta v_{out}(\tau) - \Delta v_{in}(\tau) = \frac{\alpha}{4\pi} \frac{\partial h}{\partial t}$$

where $\Delta v_{in}(\tau)$ and $\Delta v_{out}(\tau)$ are the instantaneous optical offset frequencies at the input and output of the semiconductor region, and $\Delta v(\tau)$ is the change in optical frequency caused by the self-phase modulation. This frequency shift is additive, so it accumulates on each round trip through the optical cavity.

Substituting in the expression for the gain coefficient h gives [1]:

$$\Delta v(\tau) = -\frac{\alpha}{4\pi} \frac{P_{in}}{E_{sat}} (G(\tau) - 1) \approx -\frac{\alpha}{4\pi} \frac{P_{out}}{E_{sat}} \exp\left(-\frac{U_{in}(\tau)}{E_{sat}}\right)$$

For small gain saturation $U_{in}(t) \ll E_{sat}$, so in the absence of gain saturation the chirp is proportional to the output power of the optical pulse.

For a Gaussian input pulse, P_{in} is given by:

$$P(\tau) = \frac{E_{in}}{\pi^{1/2}\tau_o} \exp\left[-\left(\frac{\tau}{\tau_o}\right)^2\right]$$

where τ_o is a parameter which determines the pulsewidth. For this input pulse, the relative optical frequency shift is given by:

$$\Delta v(\tau) = -\frac{\alpha}{4\pi^{3/2}\tau_o} \frac{E_{in}}{E_{sat}} \exp\left[-\left(\frac{\tau}{\tau_o}\right)^2\right](G(\tau)-1)$$

An important feature of the spectral broadening is the term for τ_o in the denominator, which arises because the self-phase modulation is proportional to the optical instantaneous power. As the pulsewidth gets shorter, the spectral broadening due to self-phase modulation increases. This will be shown later to be a very strong pulsewidth limiting mechanism.

Another feature is that the induced frequency shift is always negative. This results in a red-shift of the pulse, so that the modelocked wavelength is longer than the CW wavelength of the same laser. Fig. 3.22 shows the self-phase modulation produced by a 1 ps pulse, for $\alpha=3$ and $E_{in}/E_{sat}=0.05$.
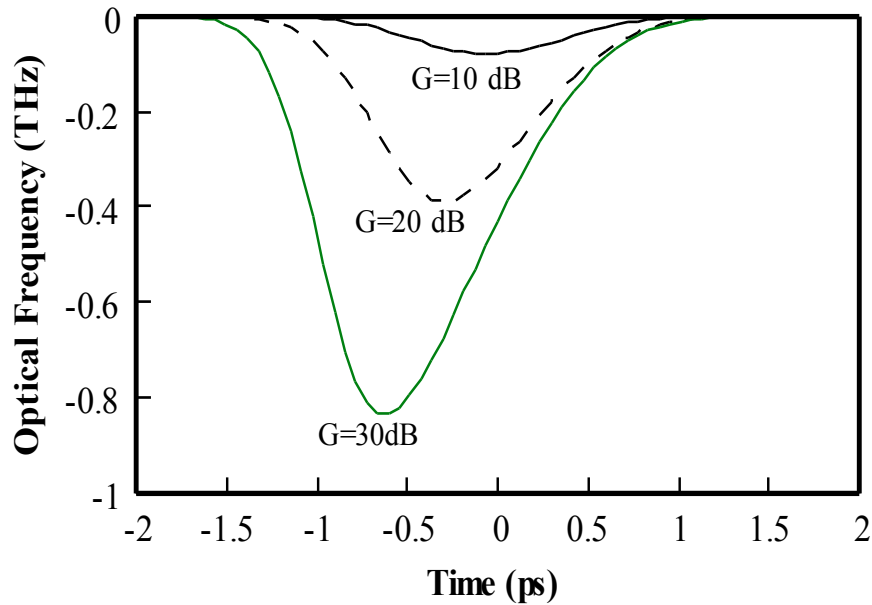
Fig. 3.22   Calculated self-phase modulation in a semiconductor amplifier for a 1 ps input pulse
E_{in}/E_{sat}=0.05, α=3.

The self-phase modulation modifies the phase of the optical signal which leads to spectral broadening, but does not change the shape of the pulse. Consequently, one might expect that the modelocked pulsewidth would be independent of optical power. Fig. 3.23 shows the effect of increasing pulse energy on a modelocked GaAs/AlGaAs device. As the pulse energy increases, the optical spectrum widens, as expected from the equation for self-phase modulation. At the same time however, the optical pulse gets wider. In order to understand this, it is necessary to also consider the finite gain-bandwidth of the material.
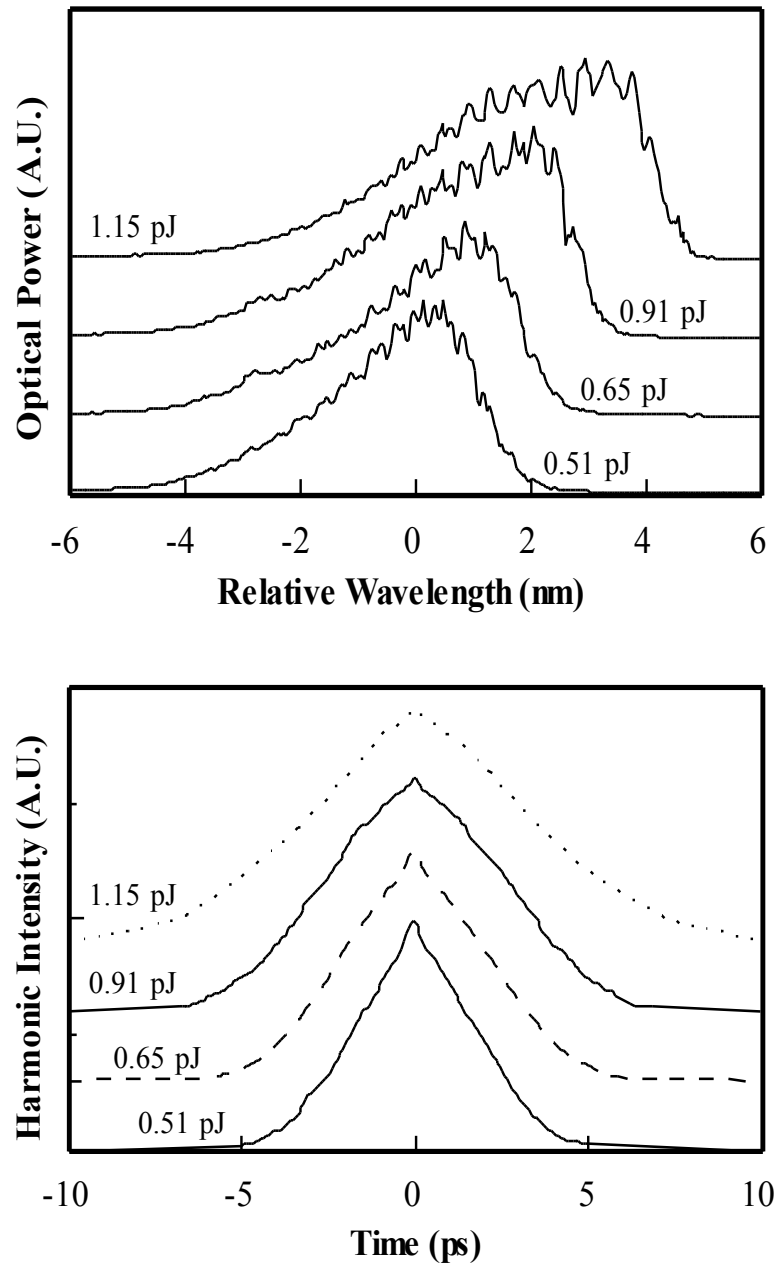
Fig. 3.23   Measured (a) optical spectrum and (b) autocorrelation as a function of pulse energy.

3.12 Bandwidth Shaping Effects on Pulsewidth

Unlike self phase modulation, the amplifier spectral gain function does act as a pulsewidth broadening mechanism. As discussed in Chapter 2, the spectral gain function leads to pulsewidth broadening, which increases as the optical bandwidth increases. Increased optical bandwidth results from decreasing pulsewidth and chirp induced by self-phase modulation.

The self-phase modulation induced by gain saturation widens the optical spectrum without changing the optical pulsewidth. However, this increased optical bandwidth then interacts with the amplifier gain and phase response to cause pulsewidth broadening. As a result the pulsewidth is set by the interaction of self-phase modulation and the amplifier response [24].

Fig. 3.24 shows the calculated pulsewidth and spectral width for a device with a single pass absorber transmission t_{abs}=0.25, saturation energy ratio σ=3, linewidth enhancement factor α=4, and a Lorentzian linewidth=5 THz. The results are compared to experimental values for a 3 QW InGaAs device with a 60 μm absorber.

In the absence of self-phase modulation (α=0), the calculated pulsewidth is 1.18 ps, and the optical bandwidth is 420 GHz. With α=4, the pulsewidth increases to 2.44 ps. However, the optical bandwidth broadens to 890 GHz. The primary goal in ultrashort pulse generation is generating a wide optical spectrum for compression. Even though small α can be used to directly generate shorter pulses, large α can be used to generate a broader spectrum leading to shorter compressed pulses.

In the absence of bandwidth filtering (but still with α=4), there is no strong pulsewidth broadening mechanism and the pulse becomes short. At the same time, there is no bandwidth limiting mechanism so the optical bandwidth gets very large (giving short compressed pulses). This demonstrates that it *is not* important to design lasers for small α to give a smaller uncompressed pulsewidth. It *is* important

77

to maximize the spectral flatness and phase flatness of the amplifier in order to generate large optical spectrum for compression.
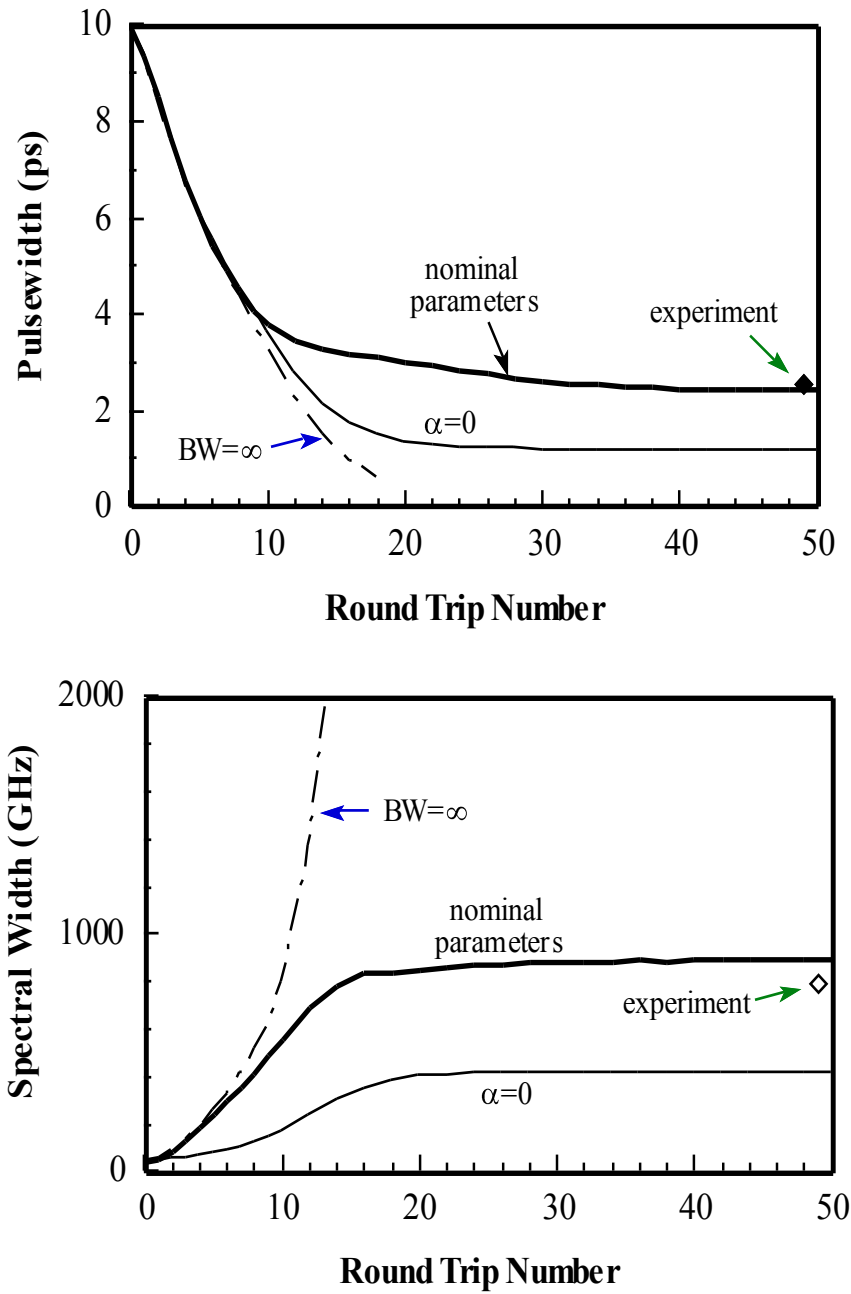
Fig. 3.24   Calculated pulsewidth and spectral width after each round trip of the optical cavity, compared to experimental result using a 3 GHz external cavity.

3.13 Dispersion-Based Pulse Compression

Self-phase modulation and the gain-bandwidth limit combine to give highly chirped 2-3ps pulses. The solution to generating subpicosecond pulses with semiconductor diode lasers is to use dispersion to remove this chirp [11].

The simplest way to provide the necessary dispersion is with gratings. The pulse was up-chirped (from red to blue wavelength shift), and spectral windowing was not used in the compression. This means that a simple 2-grating pulse compressor could be used (Table 3.1). Pulse compression techniques are described further in Appendix A.

chirp		
chirp direction	down-chirp	up-chirp
wavelength shift	blue to red	red to blue
pulse compression		
dispersion type	normal	anomalous
$dv_g/d\lambda$	>0	<0
grating pair	no	yes
grating/telescope	yes	yes
normal fiber	<1.3 µm	>1.3 µm

Table 3.1   Pulse compression methods for down-chirped and up-chirped pulses.

Constructing a compact source requires a relatively high repetition rate (>1 GHz) and a grating pair compressor without the telescope. Fig. 3.25 shows the result using a 10 cm external cavity (1.5 GHz repetition rate). The compressor grating separation was ~12 cm, giving a total source area of 11.4 cm by 35.6 cm. The pulsewidth after compression was 0.45 ps, assuming a hyperbolic secant pulse. At the time, these were the shortest pulses produced by an integrated waveguide saturable absorber, and the first compact pulse source producing <0.5 ps pulses.
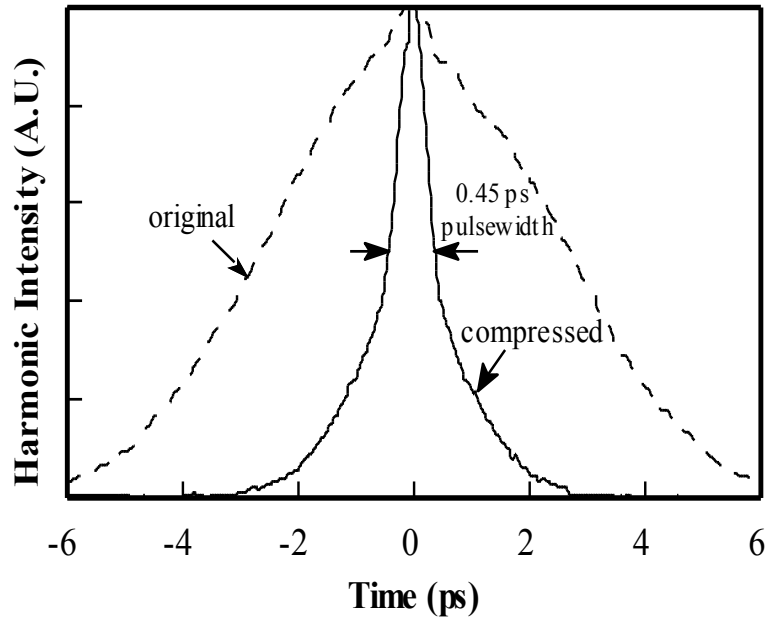
Fig. 3.25   Pulsewidth before and after pulse compression to remove chirp caused by self-phase modulation. Compressed pulsewidth=0.45 ps.

3.14 Summary

Analytic approximations to rate equations to gain and absorption regimes were developed in limiting cases of large amplifier gain and high absorption saturation in order to give more intuitive expressions. Numerical convergence using different differential equation solution algorithms was examined.   A curved waveguide geometry was demonstrated to effectively eliminate secondary pulse formation.   Tapered waveguides were used to increase the output power.   Higher output power should be possible with this tapered waveguide method using devices mounted junction-side down.

The first compact optical source producing pulses <0.5 ps was demonstrated, using external group velocity dispersion to compensate for the laser chirp.   The system produced pulsewidths of 0.45 ps, which at the time were the shortest pulses produced by a semiconductor laser with an integrated saturable absorber.

80

References

1. G. P. Agrawal, N. A. Olsson, "Self-phase modulation and spectral broadening of optical pulses in semiconductor laser amplifiers", J. Quantum Electron., **25**, p. 2297-2306 (1989).

2. B. Carnahan, J. O. Wilkes, <u>Digital Computing and Numerical Methods</u>, John Wiley and Sons, New York, (1973).

3. H. A. Haus, "Theory of modelocking with a slow saturable absorber", J. Quantum Electron., **QE-11**, p. 736-746 (1975).

4. G. P. Agrawal, N. K. Dutta, <u>Long-Wavelength Semiconductor Lasers</u>, Van Nostrand Reinhold, New York, (1986).

5. M. A. Newkirk, B. I. Miller, U. Koren, M. G. Young, M. Chien, R. M. Derosier, C. A. Burrus, "1.5 µm multiquantum-well semiconductor optical amplifier with tensile and compressively strained wells for polarization-independent gain", Photon. Tech. Lett., **5**, p. 406-408 (1993).

6. M. Schell, A. Weber, E. Schol, D. Bimberg, "Fundamental limits of subpicosecond pulse generation by active mode-locking of semiconductor lasers: The spectral gain width and the facet reflectivities", J. Quantum Electron, **27**, p. 1661 (1991).

7. T. Saitoh, T. Mukai, O. Mikami, "Theoretical analysis and fabrication of antireflection coatings on laser-diode facets", J. Lightwave Tech, **LT-3**, p. 288-293 (1985).

8. A. Mar, D. Derickson, R. Helkey, J. Bowers, R. T. Huang, D. Wolf, "Actively mode-locked external-cavity semiconductor lasers with transform-limited single pulse output", Optics Lett., **17**, p. 868-870 (1992).

9. D. J. Derickson, R. J. Helkey, A. Mar, J. E. Bowers, "Suppression of multiple pulse formation in external cavity mode-locked semiconductor lasers using

intra-waveguide saturable absorbers", Photonics Technology Letters, **4**, p. 333-335 (1992).

10. B. L. Frescura, C. J. Hwang, H. Luechinger, J. E. Ripper, "Suppression of output nonlinearities in double heterostructure lasers by use of misaligned mirrors", Appl. Phys. Lett., **31**, p. 770 (1977).

11. P. J. Delfyett, C.-H. Lee, G. A. Alphonse, J. C. Connolly, "High peak power picosecond pulse generation from AlGaAs external cavity modelocked semiconductor laser and traveling wave amplifiers", Appl. Phys. Lett., **57**, p. 971 (1990).

12. H. Hillmer, K. Magari, Y. Suzuki, "Chirped gratings for DFB laser diodes using bent waveguides", Photon. Tech. Lett., **5**, p. 10-12 (1993).

13. R. L. Thornton, R. D. Burnham, T. L. Paoli, N. Holonyak, D. G. Deppe, "Low threshold planar buried heterostructure lasers fabricated by impurity-induced disordering", Appl. Phys. Lett, **47**, p. 1239 (1985).

14. D. G. Deppe, N. Holonyak, "Atom diffusion and impurity-induced layer disordering in quantum well III-V semiconductor heterostructures", J. Appl. Phys., **64**, p. R94-R113 (1988).

15. W. X. Zou, J. L. Merz, L. A. Coldren, "Analysis and optimization of quantum-well thickness for GaAs/AlGaAs and InGaAs/GaAs/AlGaAs quantum-well lasers", J. Applied Physics, **72**, p. 5047-5055 (1992).

16. A. Mar, J. D. Dudley, E. L. Hu, J. E. Bowers, "Reactively Sputtered Silicon Oxynitride for Anti-Reflection Optical Coatings", Electronic Materials Conference, Santa Barbara CA, (1990).

17. J. C. Simon, "GaInAsP semiconductor laser amplifiers for single-mode fiber communications", J. Lightwave Tech., **5**, p. 1286-1295 (1987).

18. L. Pang, J. G. Fujimoto, "Ultrashort-pulse generation from high-power diode arrays by using intracavity optical nonlinearities", **17**, p. 1599-1601 (1992).

19. A. Mar, D. J. Derickson, R. J. Helkey, J. E. Bowers, D. Botez, "Mode-Locking of High-Power Resonant-Optical-Waveguide Diode Laser Arrays", Semiconductor Laser Conference, Takamatsu Japan, **N-7** (1992).

20. G. Bendelli, K. Komori, S. Arai, Y. Suematsu, "A new structure for high-power TW-SLA", Photonics Tech. Lett., **3**, p. 42-44 (1991).

21. P. A. Yazaki, K. Komori, G. Bendelli, S. Arai, Y. Suematsu, "A GaInAsP/InP tapered-waveguide semiconductor laser amplifier integrated with a 1.5 μm distributed feedback laser", Photon. Tech. Lett., **3**, p. 1060-1063 (1991).

22. E. S. Kintzer, J. N. Walpole, S. R. Chinn, C. A. Wang, J. L. Missaggia, "High-power strained-layer tapered traveling wave amplifier", Optical Fiber Communication Conference, vol. 5, **TuH5** (1992).

23. C. H. Henry, "Theory of the linewidth of semiconductor lasers", J. Quantum Electron., **18**, p. 259 (1982).

24. D. J. Derickson, R. J. Helkey, A. Mar, J. R. Karin, J. G. Wasserbauer, J. E. Bowers, "Short pulse generation using multisegment mode-locked semiconductor lasers", J. Quantum Electron., **28**, p. 2186-2202 (1992).

CHAPTER 4

COLLIDING PULSE EFFECTS
ON MODELOCKING

4.1 Optical Pulse Collision

This chapter presents a theoretical and experimental investigation of the effect of pulse collision in modelocked semiconductor diode lasers. In dye lasers, pulse collision in modelocking has been extensively studied and found to play an important pulse shaping role [1-7]. Collision between coherent pulses in a saturable absorber sets up a standing wave absorption grating. This absorption grating reduces the bleaching energy of the absorber, because less total volume of the absorber needs to be saturated for a given change in absorption. Effectively increasing the differential gain in the absorber improves pulse shaping, which was shown in Chapter 3.

Semiconductor lasers have a higher gain and loss per pass than dye lasers, and are physically much smaller. This can lead to differences in the importance of colliding pulse effects, which will be investigated in this chapter. Fig. 4.1 illustrates two optical pulses colliding in an absorber, and shows the total electric field. The field is sampled in this figure to show only a few optical cycles, which is equivalent to having colliding pulses that are only a few cycles long.

Colliding Pulses

Absorber

Distance (A.U.)

Field Amplitude (A.U.)

Distance (A.U.)
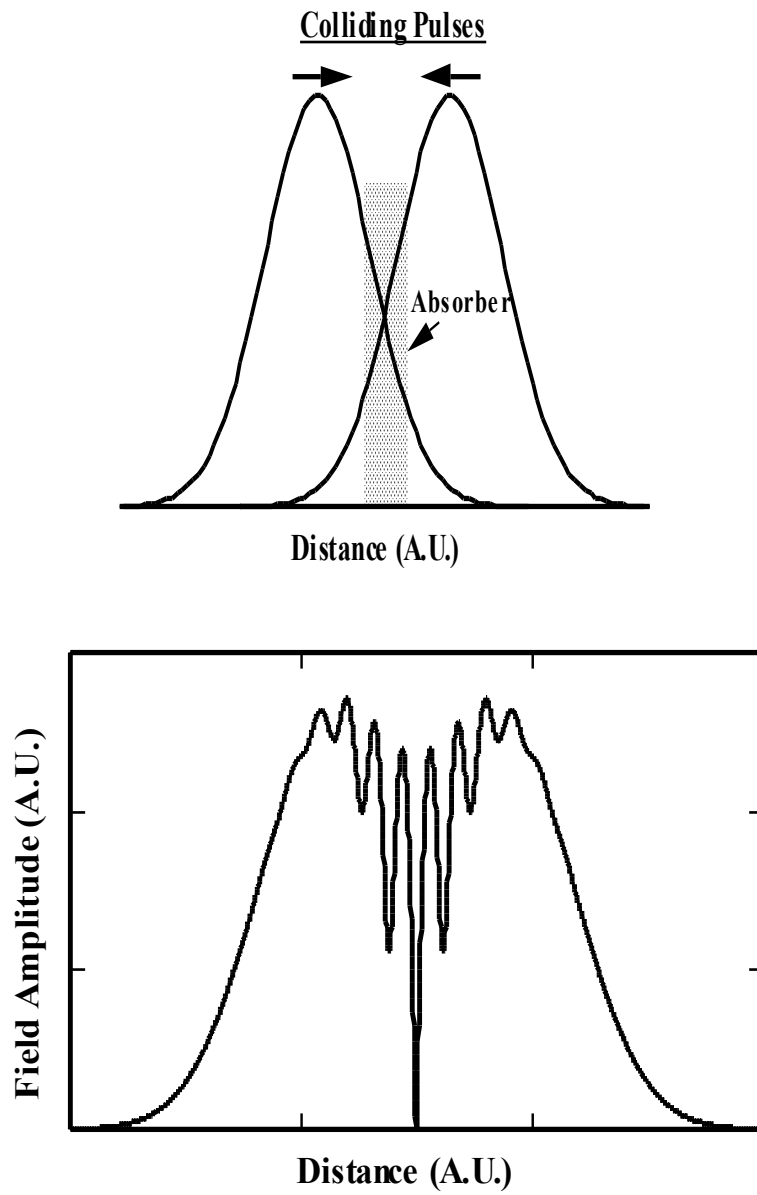
Fig. 4.1 (a) In colliding pulse modelocking, equal energy pulses meet in the saturable absorber.

(b) The total electric field (sampled) due to the sum of the counter-propagating pulses.

85

The standing wave in the optical field will cause spatially dependent carrier generation in the absorber. This will lead to the type of carrier density profile in the absorber shown in Fig. 4.2.
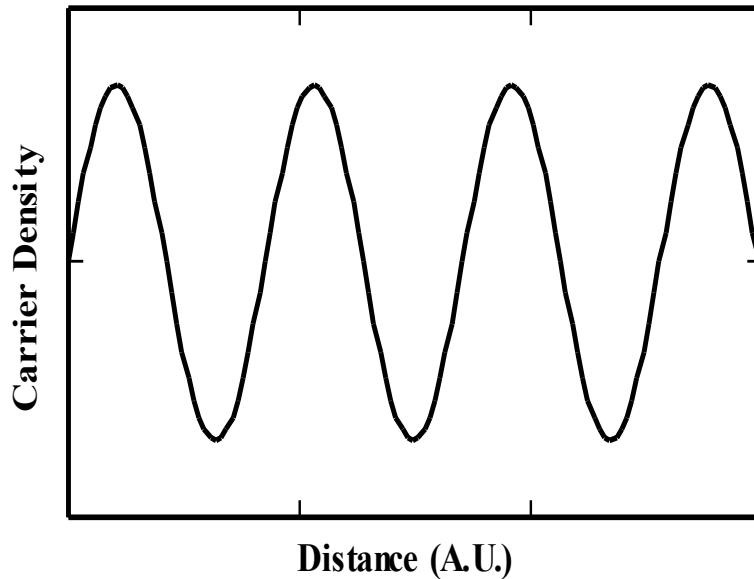
Fig. 4.2   Carrier grating set up by an optical standing wave.

Monolithic semiconductor lasers with an integrated saturable absorber placed at one facet (Fig. 4.1b) have been used for passive modelocking [8-14]. Repetition rates from 5.5 GHz [14] to over 100 GHz [9, 11] have been reported. Monolithic colliding pulse modelocked (CPM) semiconductor lasers with the absorber placed in the center of the device (Fig. 4.1a) have produced pulses at repetition rates up to 350 GHz [15]. The effect of these configurations on the modelocking process is examined. The colliding pulse effect is shown to have two important components - a coherent effect due to grating formation, and an incoherent geometrical effect. Previous experimental work with a dye laser examined both of these effects together [4]. Here these effects are examined separately, both theoretically and

experimentally. It is shown that the carrier grating formation is not an important pulse shaping mechanism. The absorber geometry is important for pulse shaping. The output facet reflectivity and absorber position are optimized for short pulses or high output power.

4.2 CPM Configurations

Early dye and solid state lasers were modelocked in the linear cavity configuration shown in Fig. 4.3a. The ring cavity CPM configuration was developed later (Fig. 4.3b). The minimum energy loss condition for the ring configuration exists when counter-propagating pulses meet in the absorber [16].
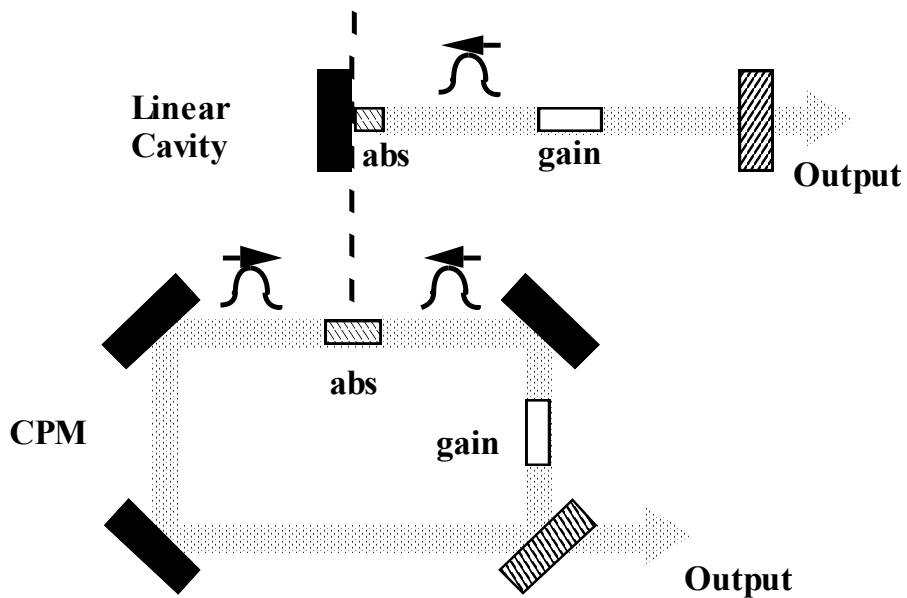
Fig. 4.3   (a) Linear cavity configuration first used for modelocking. (b) Colliding pulse modelocking (CPM) configuration

The CPM configuration has given somewhat shorter pulses, even though the linear cavity configuration has the same coherent interaction [7]. The difference in performance may be due to the absorber in the CPM configuration being easier to fabricate and place. In the linear cavity configuration, the absorber needs to be half as long as the ring configuration, and must be contacted to one mirror.

Semiconductor lasers have been modelocking in a linear cavity colliding pulse modelocked (CPM) configuration (Fig. 4.4a), which has an absorber in the center of the cavity. If the counter-propagating pulses are identical, then by symmetry the CPM configuration is identical to the configuration shown in Fig. 4.4b, which has an absorber of half the length at the end of the cavity.
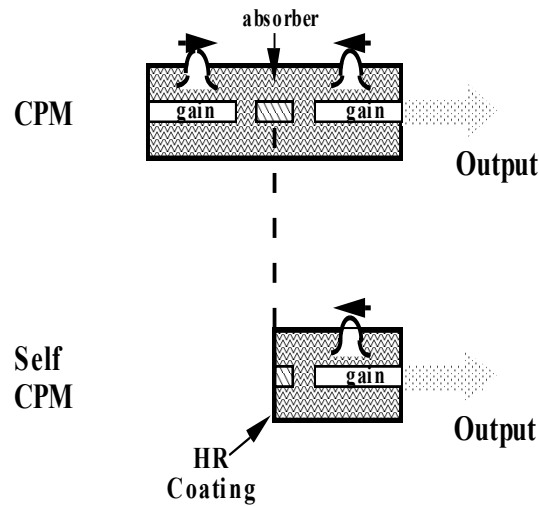
Fig. 4.4   (a) Semiconductor colliding pulse modelocking configuration (CPM). (b) Self-colliding pulse modelocking configuration (SCPM). Here the single pulse collides with itself in an absorber of half the length.

The linear cavity configuration with the absorber at the end of the cavity can be called a self colliding pulse modelocked (SCPM) configuration [17], because the same pulse collision pulse shaping is occurring due to the pulse colliding with itself [5, 7]. Both configurations have been used for passive modelocking of semiconductor diode lasers.

The CPM configuration has two separate optical pulses in the cavity which collide at the absorber in the center of the device. The optical spectrum of each pulse has the mode spacing of the entire device. When the modes from two equal amplitude pulses are summed, every other mode is composed of two out of phase components, so the two components cancel. Output pulses occur at twice the repetition rate of each individual pulse, so the total optical spectrum should have half as many modes. Therefore because of the symmetry about the center of the device, the CPM configuration has the same mode spacing as the SCPM configuration. However, if the symmetry between pulses breaks down, then poor alternate mode suppression will occur. This will be caused by the modes not being equal in amplitude, corresponding to unequal amplitude pulses, or the modes not being exactly opposite in phase, corresponding to the pulses not being equally spaced.

The CPM configuration has the advantage that the absorber length is determined by photolithography rather than cleaving, which can be important for short absorbers. However, it requires that both gain sections be cleaved to the same length in order for the pulses to collide in the absorber. The CPM configuration does not require the deposition of a high reflectivity (HR) coating. It has two optical outputs, with twice the total output power. One of the optical outputs can be used as a monitor. The larger size of the CPM configuration can be an advantage for high frequency modelocking. At 350 GHz repetition rate, the SCPM configuration gives

a cavity length of only ~125 μm. The CPM configuration gives a cavity length of ~250 μm, which is easier to handle.

The SCPM configuration has the advantage of inherent pulse symmetry since there is only one pulse in the cavity. The SCPM configuration also has the advantage of smaller size, which is important for fabricating low repetition rate monolithic structures. Low repetition rates are useful for applications which interface with electrical signals, such as time division multiplexed optical transmission. Low repetition rates are necessary for applications like soliton transmission, which require a large energy per pulse but a limited average power. Fabrication of low repetition rate devices would be much more difficult with the CPM configuration, as the device would need to be twice as long. The SCPM configuration has the advantage of greater simplicity in the external cavity configuration, as only one lens and one external cavity mirror are needed.

4.3 Carrier Grating Equations

The effects of pulse collision in saturable absorbers can be studied using a simple model in which the absorption grating is assumed to be sinusoidal [3, 6]:

$$h = h_a + h_b \cos(2kx)$$

To be consistent with previous gain definitions, the grating is written in terms of the logarithmic gain parameter h, so the absorption term $\alpha = -h$. The DC absorption component is $-h_a$ and the sinusoidal absorption component due to the carrier grating is $-h_b$.

The equations for coherent pulse interaction [6] can be found from the coupling coefficients of a conductivity grating. The coupled equations for a short segment of length L are:

$$A_{out}^+ = \left(1 + \frac{h_a}{2}\right) A_{in}^+ - \frac{h_b}{4} A_{in}^-$$

$$A_{out}^- = \left(1 + \frac{h_a}{2}\right) A_{in}^- - \frac{h_b}{4} A_{in}^+$$

$$\frac{dh_a}{dt} = \frac{-\alpha_0 L - h_a}{\tau_c} - \frac{\left|A_{in}^+\right|^2 + \left|A_{in}^-\right|^2}{E_{sat}} h_a + \frac{\left|A_{in}^+\right|\left|A_{in}^-\right|}{E_{sat}} h_a$$

$$\frac{dh_b}{dt} = -\frac{h_b}{\tau_c} - \frac{\left|A_{in}^+\right|^2 + \left|A_{in}^-\right|^2}{E_{sat}} h_b + \frac{2\left|A_{in}^+\right|\left|A_{in}^-\right|}{E_{sat}} h_a$$

where A^+ and A^- are the forward and reverse traveling field amplitudes normalized to the square root of optical power. The unsaturated power transmission of the segment is $\exp(-\alpha_0 L)$. E_{sat} is the saturation energy of the semiconductor material when used as an amplifier which was defined in Chapter 3:

$$E_{sat} \equiv \frac{A/\Gamma}{g/v_g} E_{ph} = \frac{\text{optical mode area}}{\text{differential gain}} * \text{photon energy}$$

where A is the active region cross-sectional area, Γ is the optical confinement factor, g is the gain coefficient, v_g is the optical group velocity, and E_{ph} is the photon energy.

The counter-propagating pulses form standing waves in the saturable absorber. At the peak of the standing wave, the carrier generation rate is high, and at

91

the nulls, the carrier generation rate is low. The carrier grating causes periodic absorption which couples the forward and reverse traveling optical waves. Naturally, in the absence of a carrier grating (h_b=0) these equations reduce to the uniform carrier density case studied in Chapter 3.

4.4 CPM Analysis

In order to illustrate the effect of the carrier grating on the modelocking process, the three SCPM geometry structures shown in Fig. 4.5 are analyzed. The 'coherent CPM' case has an absorber at a high reflection mirror, and analyzes the coherent field interaction that causes grating formation. The 'incoherent CPM' case assumes that the forward and reverse traveling waves add incoherently, so no grating is formed. This can be done by setting the sinusoidal component of the grating gain h_b to zero. The 'no CPM' case has an absorber which is offset from the mirror by greater than the carrier recombination time, so that the absorber has to be bleached by the pulse on both the forward and reverse pass.

The calculated absorbed energy is shown in Fig. 4.6 for an unsaturated attenuation typically found in a saturable absorber dye of a dye laser. The round trip unsaturated power transmission is 0.8 for all three configurations. For high energy pulses, the absorbed energy is a factor of two smaller for the 'incoherent CPM' configuration than for the 'no CPM' configuration. Half as many carriers are needed to reach transparency, reducing the energy needed to bleach the saturable absorber by a factor of two. This is because the absorber is bleached twice, on both the forward and reverse pass of the optical pulse. This reduced energy enhances the effectiveness of the saturable absorber in the 'incoherent CPM' case lowering the modelocking pulse energy, which reduces the level of amplifier gain saturation as compared to the 'no CPM' configuration.

92

Optical Field Amplitude

Absorber Carrier Density

Absorber

forward wave

reverse wave

0 L   distance

**Coherent
CPM**

0   distance   L

N_0

mirror
side

**Incoherent
CPM**

0 L   distance

0   distance   L

Absorber

distance   0 L

No CPM

0   distance   L
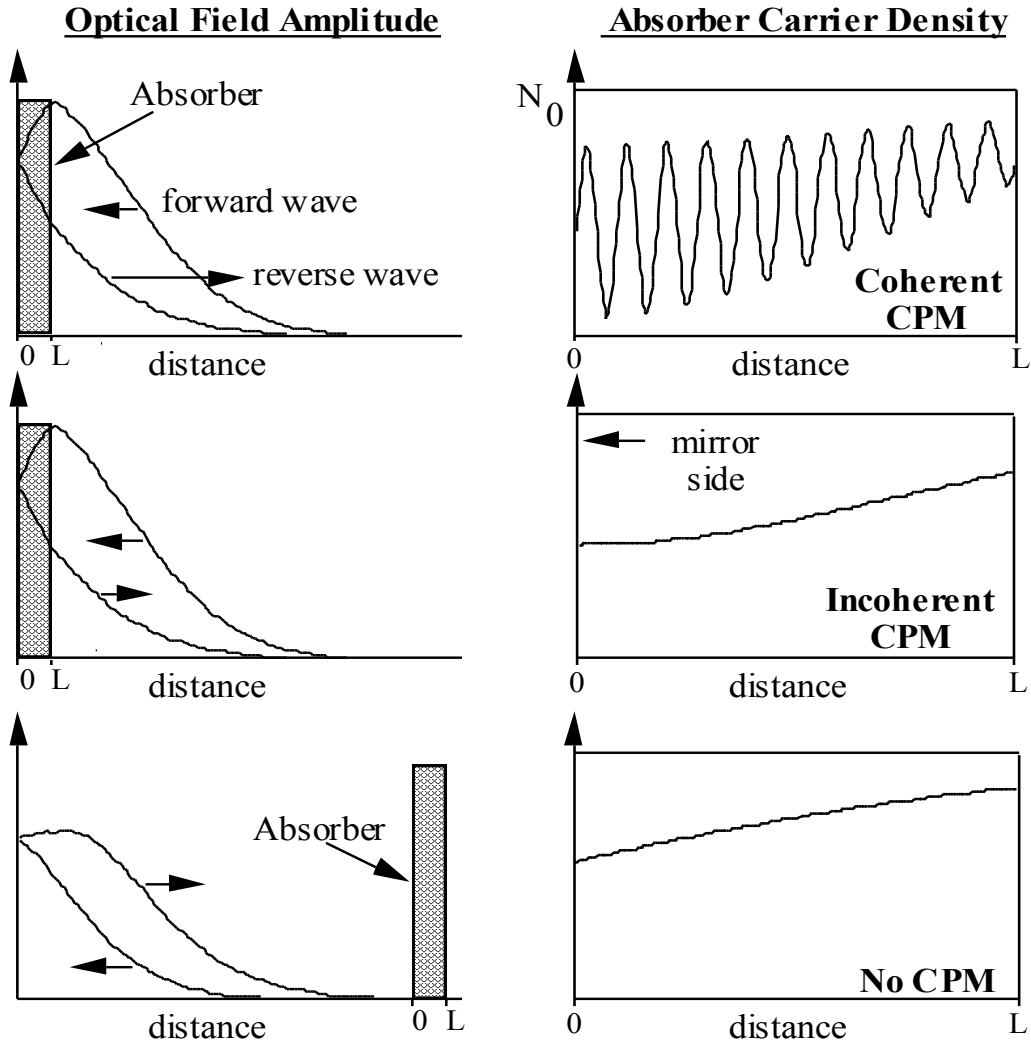
Fig. 4.5   Three configurations used for calculations of colliding pulse effects. The shaded region
in the optical field amplitude plot shows the region over which the absorber carrier
density is plotted. Unsaturated round trip power transmission=0.04. E_{in}/E_{sat}=2.

93
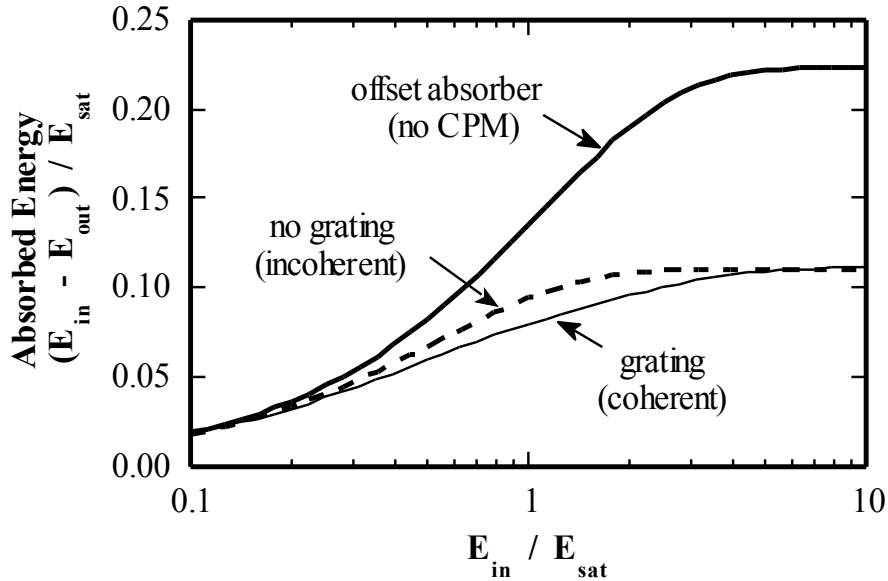
Fig. 4.6   Calculated absorbed energy in the saturable absorber for small unsaturated absorption
used with a dye laser (unsaturated transmission=0.8).

In passive modelocking, pulsewidth narrowing is due to the saturable absorber removing the front edge of the pulse, and provides a constant pulse shortening ratio as the pulsewidth is reduced. Pulsewidth narrowing on each pass is a fixed ratio which is limited by amplifier gain saturation. Pulsewidth broadening is dominated by self phase modulation [18], and the pulsewidth broadening ratio increases as the pulsewidth is reduced. The steady state pulsewidth occurs when the pulsewidth narrowing and broadening are equal for each round trip in the cavity. Due to the 'incoherent CPM' effect, the modelocked laser can be operated at a lower power, which reduces the pulse broadening mechanisms of amplifier gain saturation and self-phase modulation.

In order to take advantage of the 'incoherent CPM' improvement, the absorber does not have to be at the facet, where the pulses collide in the absorber. The

94

absorber must just be close enough to the facet so that the absorber does not have time to recover. This makes it a geometrical effect, rather than a coherent effect. Previous theoretical and experimental investigations lumped both of these effects together [4].

In the 'coherent CPM' configurations, there is an additional bleaching energy reduction due to the grating formation caused by the interaction of counter-propagating optical pulses in the saturable absorber. Since the carrier density does not have to be raised to transparency everywhere in the saturable absorber to reach a low loss state, the saturable absorber bleaches with a lower pulse energy than would be necessary if the standing waves did not exist. This allows modelocking with lower energy pulses, which reduces the pulse broadening mechanisms of amplifier gain saturation and self phase modulation.

The calculated absorbed energy is shown in Fig. 4.7 for a saturable absorber with the larger unsaturated attenuation typically found in semiconductor lasers. The round trip unsaturated power transmission is 0.04. The unsaturated gain per pass in the amplifier section of a semiconductor laser is much larger than in a dye laser. This means that the unsaturated absorption must also be higher than in a dye laser, due to the requirement that net gain in the cavity must be less than unity except during the passage of the pulse. The large initial absorption in the semiconductor saturable absorber attenuates the reverse traveling optical wave, causing a reduced standing wave. Only the section nearest the mirror receives the full benefit of coherent CPM, as this is the only section with a large standing wave. Thus the coherent CPM improvement due to the carrier grating is smaller for the semiconductor laser case than for the dye laser case.

95
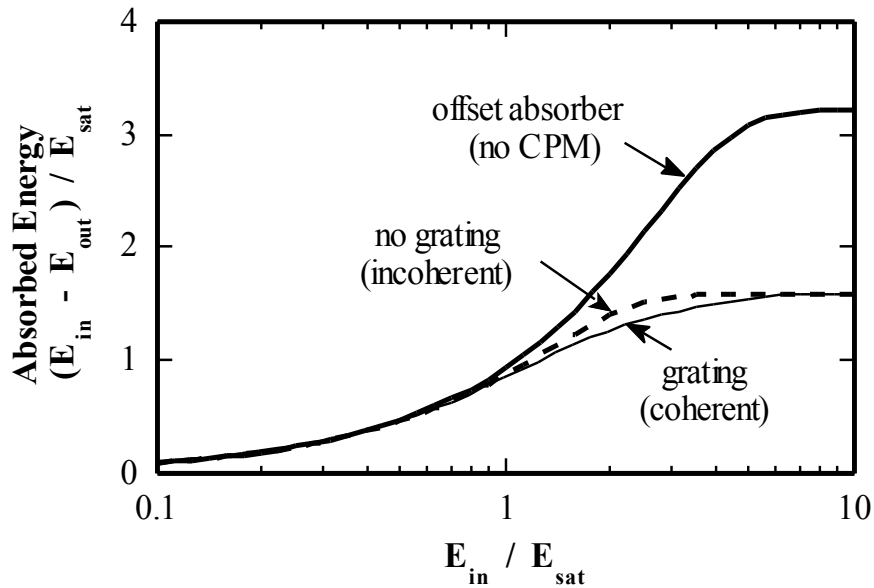
Fig. 4.7   Calculated absorbed energy in the saturable absorber for large unsaturated absorption used with a semiconductor laser.

The formation of a carrier grating in a semiconductor absorber is illustrated in Fig. 4.8. The carrier density and optical field amplitude are shown at three points in time. Initially the absorption is high (Fig 4.8a), so the optical field amplitude at the mirror side of the absorber is small, and the carrier generation rate is low. The reflected wave is also small, so the optical standing wave at the input side of the absorber is small, and carriers are generated uniformly with only a small modulation depth grating on this side of the absorber.

Optical Field Amplitude

Absorber Carrier Density

Absorber

forward
wave

reverse
wave

0 L   **distance**

N_0

mirror
side

(a)

0   **distance**   L

0 L   **distance**

N_0

(b)

0   **distance**   L

Mirror

0 L   **distance**

N_0

(c)

0   **distance**   L
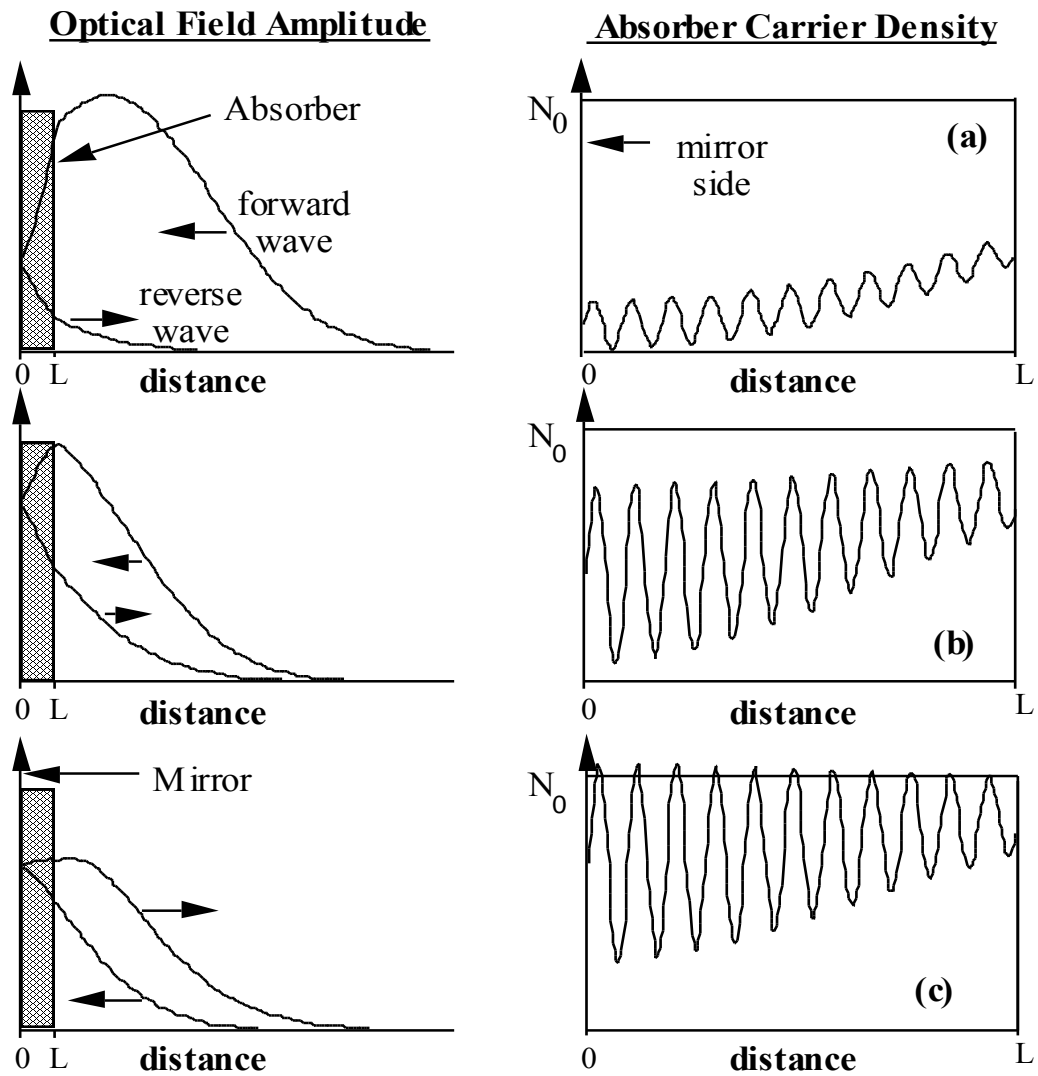
Fig. 4.8   Calculated grating buildup in a semiconductor laser absorber at three points in time. The
shaded region in the optical field amplitude plot shows the region over which the
absorber carrier density is plotted.   Unsaturated round trip power transmission=0.04.
E_{in}/E_{sat}=2.   The peak carrier density is higher than N_0 due to the sinusoidal grating
approximation.

As the input side of the absorber begins to saturate (Fig. 4.8b), carriers begin to be generated at the mirror side. A grating is formed on the mirror side because the optical standing wave ratio is high. The optical standing wave ratio is now also high on the input side of the absorber, but a large grating is not formed because this region has already been saturated.

As the optical pulse continues to propagate through the absorber (Fig. 4.8c), the relative modulation depth of the grating decreases as carriers are generated at the minimum points of the standing wave. Carrier diffusion will wash out the carrier grating after passage of the optical pulse. The computed carrier density has a maximum greater than the transparency value N_0 because of the numerical approximation of computing only the DC and sinusoidal grating components.

In the 'incoherent CPM' case, absorption recovery between forward and reverse optical passes will increase the energy required for modelocking. The absorber will have to be saturated again on the return trip of the optical pulse. If the absorber is placed close to the output facet, the bleaching energy will depend on the amount of absorber recovery between the forward and reverse pass. Fig. 4.9 shows the effect of going from no recovery (incoherent CPM) to full recovery (no CPM).

Reducing the output facet reflectivity will increase the effect of absorption recovery. As a smaller fraction of the optical energy is reflected, less energy is available to saturate the absorber on the return pass. Fig. 4.10 shows the absorbed energy for 50% absorber recovery between passes. For a mirror power reflectivity much below 30%, the bleaching energy increases substantially. This result is independent of the material or wavelength.
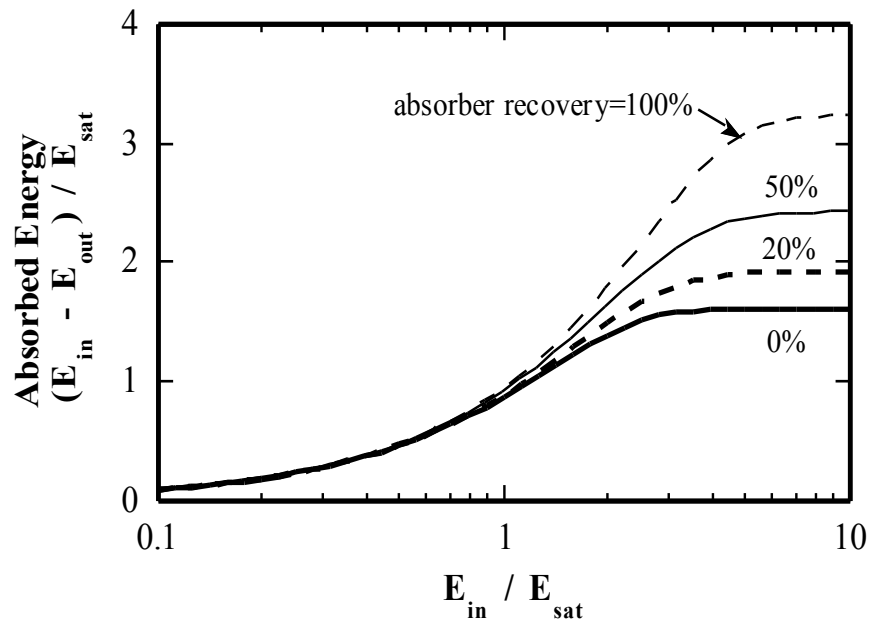
Fig. 4.9   Calculated absorbed energy for different amounts of absorption recovery. Mirror power reflectivity=100%. Unsaturated round trip power transmission=0.04.
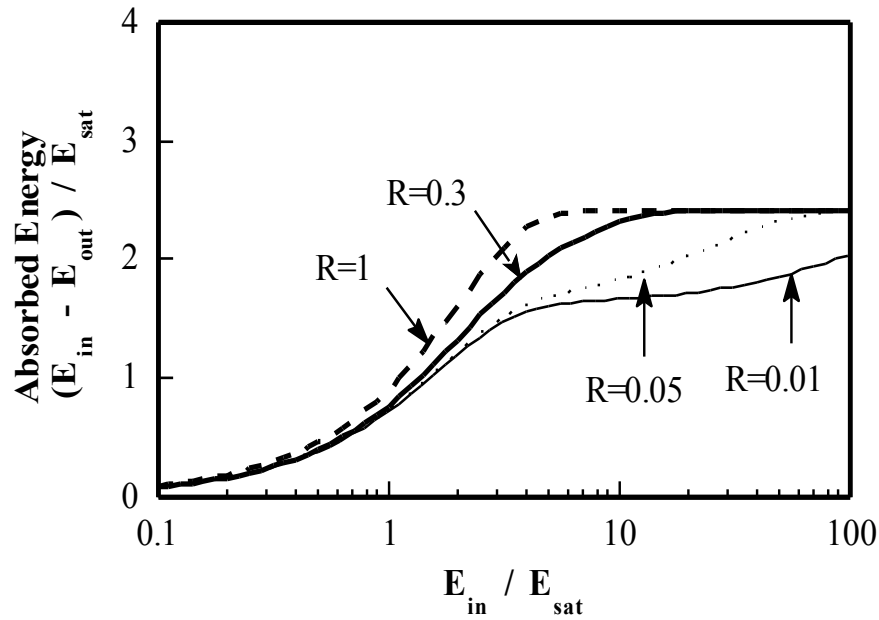
Fig. 4.10   Calculated absorbed energy for different output mirror power reflectivities. Carrier recovery=50% between passes. Unsaturated round trip power transmission=0.04.

The CPM grating analysis has shown that the grating does not play an important pulse shaping role for semiconductor lasers, so the pulsewidth should not depend strongly on the optical standing wave ratio at the facet. However, the geometrical position of the absorber is important, and the absorber should be close to the facet so that the optical round trip time is much less than the absorber recovery time. The absorber offset becomes more important as the output facet reflectivity is reduced.

4.5 Coherent CPM Comparison

The effect of coherent pulse collision on passive modelocking of semiconductor laser diodes was experimentally examined [19]. The SCPM configuration was used because the standing wave ratio can be varied through the mirror reflectivity, and the collision overlap can be reduced by offsetting the absorber region from the mirror. Unlike dye lasers which require a high-Q cavity, semiconductor laser diodes can be passively modelocked for a wide range of reflectivities of absorber side mirrors.

The multisection GaAs-AlGaAs lasers used in this experiment were fabricated using impurity induced disordering from silicon diffusion [20]. The bulk active region thickness was 82 nm, and the typical threshold current was 15 mA for a 500 μm device. The gain section and absorber section were separated by a 4 μm gap which was proton bombarded to achieve high contact isolation.

A GaAs device was modelocked using the linear cavity configuration shown in Fig. 4.11a. The laser gain length was 500 μm and the absorber length was 16 μm.

100

The device was antireflection (AR) coated and aligned in a 2 GHz external cavity. Passive modelocking was achieved by reverse biasing the 16 μm segment to act as a saturable absorber.

The experimental results for an absorber placed at the facet are shown in Fig. 4.11b. All three results were obtained from the same device by using the device with a cleaved output facet, adding a SiN quarter wave layer to make a low reflectivity output coating, and then adding a Si quarter wave layer to make a high reflectivity output coating. At a given pulsewidth, the average optical power increases as the facet reflectivity is reduced. As the field reflectivity is decreased from r=0.8 (high optical field standing wave ratio) to r=0.55 (medium optical field standing wave ratio), the output power increases due to the greater mirror transmittance, while the pulsewidth range remains the same. As the reflectivity is reduced to r=0.14 (low standing wave ratio), the output power for stable modelocking increases even further, leading to a small increase in minimum pulsewidth due to increased gain saturation and self phase modulation broadening. This small dependence of pulsewidth on the optical field standing wave ratio indicates that the coherent CPM effect is *not* an important pulse shaping mechanism.
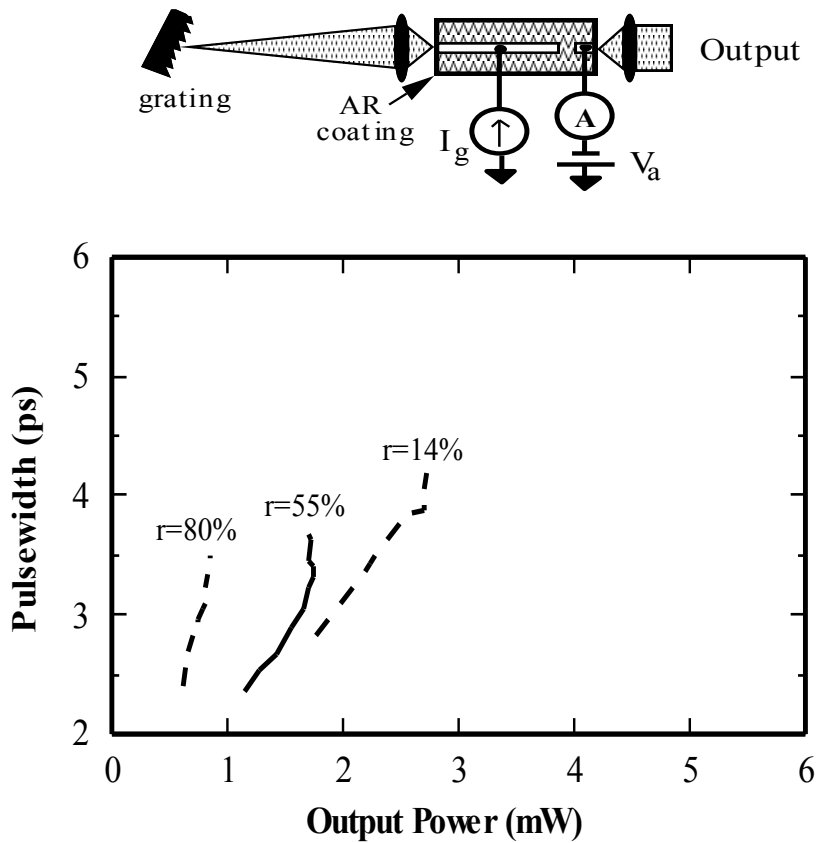
Fig. 4.11   (a) Experimental configuration for passive modelocking of a GaAs/AlGaAs semiconductor laser. (b) Measured dependence of the optical pulsewidth on the absorber mirror reflectivity. Lower mirror reflectivity gives higher output power, with somewhat wider output pulses.

4.6 Incoherent CPM Comparison

Modelocking with an absorber offset from the facet (Fig. 4.12a) was investigated to determine the effect of incoherent pulse collision. The absorber offset reduces the 'incoherent CPM' effect by allowing partial absorption recovery before the reverse pass through the absorber. The offset distance required to allow the absorber to recover is determined by the absorber recovery time. Devices were measured with absorber offset distances of 50 μm (1.3 ps round trip time) and 95 μm (2.5 ps round trip time). Both devices were from the same GaAs/AlGaAs wafer as the previous coherent CPM experiment shown in Fig. 4.11. The length of each device was also 500 μm.

The absorber recovery time measurement using a pump-probe experiment has been reported using GaAs/AlGaAs samples from the same wafer [21]. The measured recovery time constant for reversed biased samples was ~5 ps. The rapid recovery time is due to carriers being swept out of the active region by the applied electric field. This rapid recovery time allows an absorber offset of as little as 50 μm to give a significant amount of absorber recovery during the two passes of the optical pulse.

The devices with absorbers offset from the facet were modelocked in a 2 GHz external cavity. The experimental results are shown in Fig. 4.12b. For a 50 μm absorber offset, the minimum pulsewidth has broadened from 2.4 ps in the previous no-offset experiment to 3 ps. For a larger absorber offset of 95 μm, the minimum pulsewidth has broadened even further to 4 ps. At the same time, the output power is increasing due to the higher bleaching energy of the absorber. This shows that the 'incoherent CPM' effect is providing an important pulse shaping mechanism even for a small absorber offset corresponding to a short absorber recovery time.

103
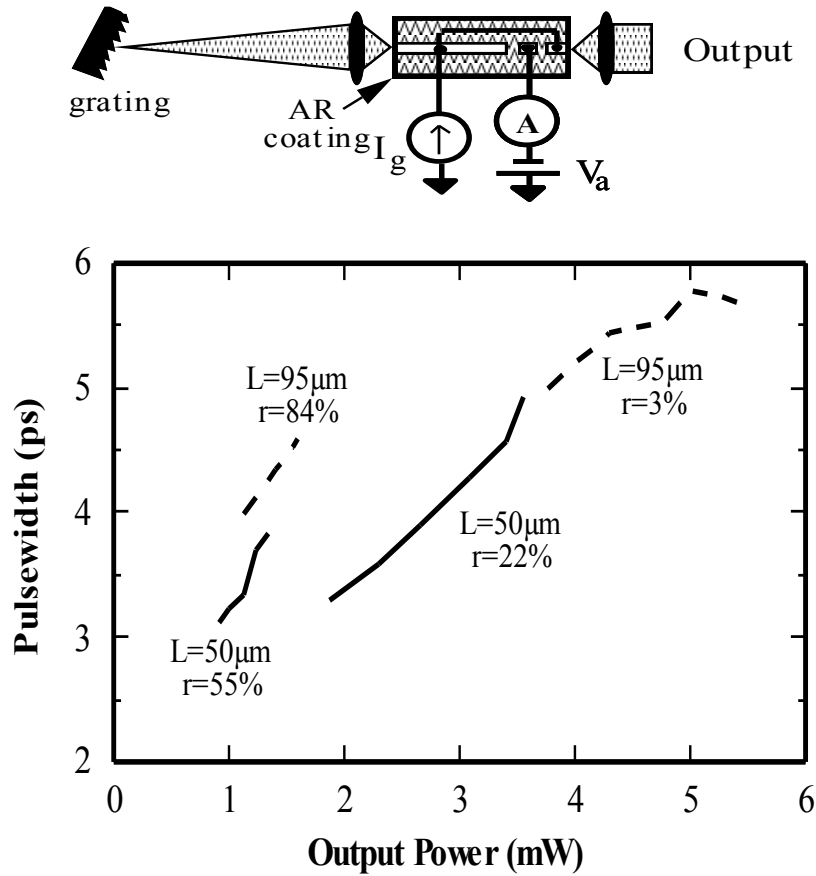
Fig. 4.12   (a) Experimental configuration for offset absorber investigation.   (b) Measured
dependence of optical pulsewidth on the absorber offset. A larger absorber offset gives
wider output pulses, with the effect more enhanced for lower facet reflectivity.

The offset absorber experiment shows the same trend as before of a low facet reflectivity producing high output power for stable modelocking, but at a wider pulsewidth. With an absorber offset of 95 µm and a mirror reflectivity of r=0.03, an average power of 5.5 mW was achieved with a pulsewidth of 5.5 ps. This gives a peak power of 500 mW, and pulse energy of 2.75 pJ. This technique produced much larger pulse energy than using an absorber next to a cleaved facet. Because of the low facet reflectivity, large pulse energy is needed in order to reflect enough energy to saturate the partially recovered absorber.

104

4.7 Incoherent CPM Pulse Compression

In the previous section, manipulation of the colliding pulse effect (though mirror reflectivity and absorber offset) was shown to give conditions with increased pulse energy. However, many applications require high peak power, so this technique is only useful if short pulses can still be generated.

Self phase modulation in modelocked semiconductor lasers results from gain saturation. Gain saturation is a result of carrier depletion, and is coupled to the phase index through the α parameter. The index change induces chirp on the pulses leading to a large optical spectral bandwidth. This increased bandwidth causes increased pulsewidth broadening in the amplifier section due to the finite gain-bandwidth of the semiconductor medium, and limits the optical pulsewidth. Short pulses can still be produced by removing the chirp. The chirped pulse can be compressed to a transform limited pulse by applying a phase correction vs. wavelength that is the negative of the phase distortion vs. wavelength of the optical output.

External cavity gratings were used to compress the pulses from the GaAs/AlGaAs laser with the 50 μm absorber offset in order to get short, high energy pulses. The laser was modelocked at a repetition rate of 3.3 GHz, an absorber bias voltage of -0.7 V, and a gain section bias current of 68 mA. The average power was 6.45 mW, which corresponds to 1.95 pJ of energy per pulse. The autocorrelation shown in Fig. 4.13 had a full width at half maximum (FWHM) of 7.1 ps, which corresponds to a 4.6 ps pulsewidth for a sech^2 pulse shape.

The optical spectral width is 3.3 nm, giving a time-bandwidth product of 6.6. An unchirped 4.6 ps sech^2 pulse has a time bandwidth product of 0.31, predicting an unchirped spectral width of only 0.15 nm. The wider actual spectrum indicates that

105

the output is strongly chirped, due to the self phase modulation in the gain and absorber sections.
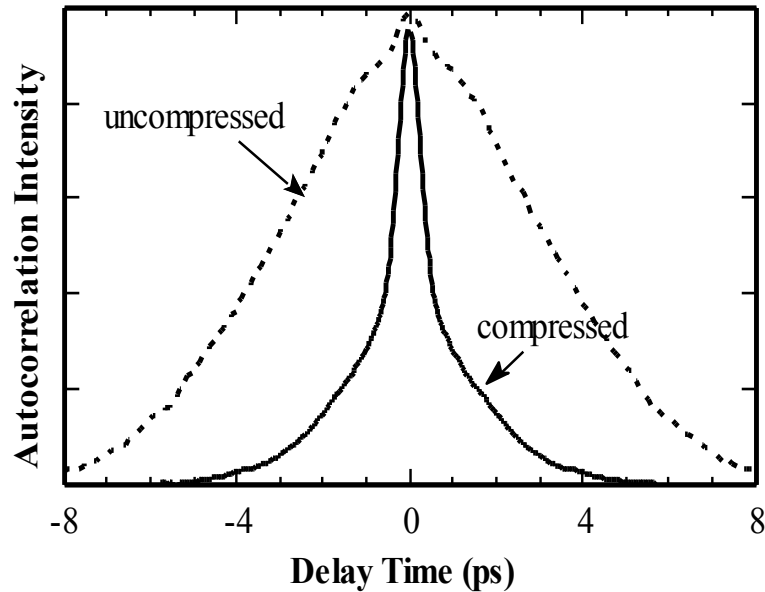
Fig. 4.13   Measured nonlinear autocorrelation of the modelocked semiconductor laser before and after pulse compression.   The pulse compressor compensates for quadratic phase distortion. Deconvolved pulsewidth is 0.57 ps.

Quadratic phase compensation with negative group velocity dispersion can be performed using two gratings in a two pass configuration [22]. The autocorrelation width after pulse compression with quadratic phase compensation is 0.88 ps corresponding to a deconvolved pulsewidth of 0.57 ps, assuming a sech^2 pulseshape. A comparison of the original and compressed pulse is shown in Fig. 4.13. The average power was 4.2 mW, which corresponds to 1.27 pJ of energy per pulse. The optical spectrum is the same as before compression, because the compressor changes only the phase of the optical spectrum. No spectral windowing was used to alter the relative spectral amplitude in the pulse compression process.

106

4.8 Summary

The effect of pulse collision in modelocked semiconductor diode lasers has been investigated. The colliding pulse effect is composed of two important effects - a coherent effect due to grating formation, and an incoherent geometrical effect. These effects were examined separately, both theoretically and experimentally. The incoherent colliding pulse effect is important because it reduces the bleaching energy of the absorber, and therefore reduces the pulse broadening effects of amplifier gain saturation and self-phase modulation. On the other hand, the improvement in pulse shaping from the coherent colliding pulse carrier grating effect is small for passive modelocking of semiconductor diode lasers.

The output facet reflectivity and absorber position were optimized to produce short pulses or give high output power. The shortest pulses were obtained with the absorber placed at the output mirror. The highest output power was obtained with an absorber offset from the output facet, along with a low reflectivity coating. This reduced the 'incoherent CPM' effect and requires modelocking to take place at a higher power level. The output from this higher power configuration was externally compressed to give pulses with a pulsewidth of 0.57 ps and a pulse energy of 1.27 pJ.

References

1.   G. H. C. New, "Pulse evolution in modelocked quasi-continuous lasers", J. Quantum Electron., **QE-10**, p. 115-124 (1974).

2.   I. S. Ruddock, B. J. Bradley, "Bandwidth limited subpicosecond pulse generation in modelocked CW dye lasers", Appl. Phys. Lett., **29**, p. 296-297 (1976).

3.   J. Herrmann, F. Weidner, B. Wilhelmi, "Theory of passive modelocking of CW dye lasers with contacted and non-contacted absorbers", Applied Physics B, **26**, p. 197-202 (1981).

4.   W. Dietel, "Transient absorber gratings shorten the pulses of a passively modelocked CW dye laser", Optics Communications, **43**, p. 69-71 (1982).

5.   D. Kuhlke, W. Rudolph, B. Wilhelmi, "Influence of transient absorber gratings on the pulse parameters of passively modelocked cw dye ring lasers", Appl. Phys. Lett., **42**, p. 325-327 (1983).

6.   M. S. Stix, E. P. Ippen, "Pulse shaping in passively modelocked ring dye lasers", J. Quantum Electron., **QE-19**, p. 520-525 (1983).

7.   A. E. Siegman, <u>Lasers</u>, University Science Books, Mill Valley CA, (1986).

8.   C. Harder, J. S. Smith, K. Y. Lau, A. Yariv, "Passive mode locking of buried heterostructure lasers with nonuniform current injection", Appl. Phys. Lett., **42**, p. 772-774 (1983).

9.   P. P. Vasilev, A. B. Sergeev, "Generation of bandwidth-limited 2 ps pulses with 100 GHz repetition rate from multisegmented injection laser", Electron. Lett., **25**, p. 1049-1050 (1989).

10.   P. A. Morton, J. E. Bowers, L. A. Koszi, M. Soler, J. Lopata, D. P. Wilt, "Monolithic hybrid modelocked 1.3 μm semiconductor lasers", Appl. Phys. Lett., **56**, p. 111-113 (1990).

11.   S. Sanders, L. Eng, J. Paslaski, A. Yariv, "108 GHz passive modelocking of a multiple quantum well semiconductor laser with an intracavity absorber", Appl. Phys. Lett., **56**, p. 310-311 (1990).

12.   P. G. May and M. Bierbaum, "Monolithic mode locking of long cavity GaAs-AlGaAs semiconductor lasers", J. Photonics Tech. Lett., **3**, p. 296-298 (1991).

13.   K. Y. Lau and J. Paslaski, "Condition for short pulse generation in ultrahigh frequency modelocking of semiconductor lasers", Photonics Tech. Lett., **3**, p. 974-976 (1991).

14.   D. J. Derickson, P. A. Morton, J. E. Bowers, "Comparison of timing jitter in external and monolithic cavity modelocked semiconductor lasers", Appl. Phys. Lett., **59**, p. 3372-3374 (1991).

15.   Y. K. Chen, M. C. Wu, T. Tanbun-Ek, R. A. Logan, M. A. Chin, "Subpicosecond monolithic colliding-pulse modelocked multiple quantum well lasers", Appl. Phys. Lett., **58**, p. 1253-1255 (1991).

16.   D. Kuhlke and W. Rudolph, "On chirped pulses from a cw dye laser in the colliding pulse modelocked regime", Optical and Quantum Electronics, **16**, p. 57-69 (1984).

17.   D. J. Derickson, J. G. Wasserbauer, R. J. Helkey, J. E. B. A. Mar, D. Coblentz, R. Logan, T. Tanbun-Ek, "A comparison of colliding pulse and self-colliding pulse monolithic cavity modelocked semiconductor lasers", Optical Fiber Communications Conference, San Jose, **ThB3** (1992).

18. D. J. Derickson, R. J. Helkey, A. Mar, J. R. Karin, J. G. Wasserbauer, J. E. Bowers, "Short pulse generation using multisegment modelocked semiconductor lasers", J. Quantum Electron., **28**, p. 2186-2202 (1992).

19. R. J. Helkey, D. J. Derickson, A. Mar, J. G. Wasserbauer, J. E. Bowers, R. L. Thornton, "Colliding pulse effects in modelocked semiconductor diode lasers", Conference on Lasers and Electro-Optics, Anaheim, **JTHB2** (1992).

20. R. L. Thornton, W. J. Mosby, T. J. Paoli, "Monolithic waveguide coupled cavity lasers and modulators fabricated by impurity induced disordering", J. Lightwave Tech., **6**, p. 786-792 (1988).

21. J. R. Karin, D. J. Derickson, R. J. Helkey, J. E. Bowers, R. L. Thornton, "Field-enhanced GaAs/AlGaAs waveguide saturable absorbers", Ultrafast Phenomena VIII, France, **MC21** (1992).

22. E. B. Treacy, "Optical pulse compression with diffraction gratings", J. Quantum Electron., **QE-5**, p. 454-458 (1969).

CHAPTER 5

MILLIMETER-WAVE GENERATION AND STABILIZATION

5.1 Optical Applications of Pulse Sources

This chapter examines the applications of optics to millimeter wave signal distribution, and methods of millimeter wave generation with semiconductor laser diodes. Optimum pulsewidth values for microwave to millimeter-wave harmonic generation are explored. Feedback is proposed for stabilizing the modelocking repetition rate of millimeter-wave monolithic devices with an external microwave reference. Feedback stabilization is demonstrated for an external cavity device.
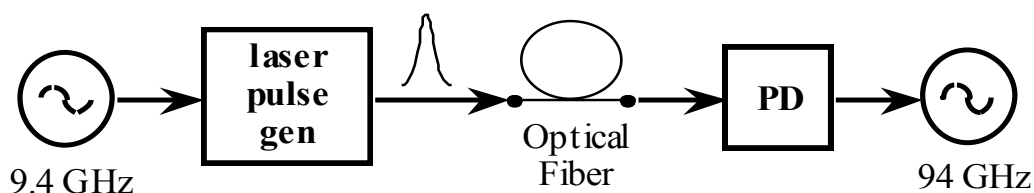
Fig. 5.1   Optical generation and distribution of electrical millimeter-wave signals from a lower frequency reference. The laser diode nonlinearity converts the input microwave electrical signal to a millimeter-wave optical modulation signal.

Semiconductor lasers offer a compact, reliable source of modulated light for transmission of microwave and millimeter wave signals. Applications include non-invasive generation and measurement of electrical signals, high reverse isolation for local frequency distribution [1], and signal transmission over long distances. The nonlinearity in modelocked lasers can be exploited to combine frequency multiplication and signal transmission as illustrated in Fig. 5.1.

111

One application of semiconductor lasers to signal transmission is in the fiber-optic distribution of control and reference signals for phased array radars. Because of the difficulties of wideband millimeter-wave modulation of light, a data mixing architecture [2] can be used for millimeter radar, in which reference and communication signals are distributed using separate fiber-optic links or a wavelength division multiplexed link. The reference channel distributes a single frequency millimeter-wave carrier, and the data channel provides microwave communication signals. The reference channel can be optimized for bandwidth, and the data channel for dynamic range. The frequency reference signal can be used for injection-locking of a local oscillator. Injection locking can be achieved by photodetection in the active region of the device, or with a photodetector coupled to the oscillator resonator. Injection locking is a simple technique that can give wide band noise reduction, but suffers from a small lock-in range and phase offsets between the reference and local oscillator. The optical signal can also be used as a reference for a phased locked loop. The phased locked loop has the advantage of a wider lock-in range and a controlled phase response, but is more complex and has a noise reduction range limited by the loop bandwidth.

Electrical signals on GaAs microstrip transmission lines can be measured with a pulsed optical probe using the electro-optic effect [3]. Complete on-wafer testing of monolithic millimeter wave integrated circuits (MMICs) can be performed using a pulsed optical source together with GaAs photoconductive switches to generate a test signal and a photoconductive switch or electro-optic probe to measure the response. Optical probing can also be used for wafer level testing of electrical oscillators. An optical probe has been used to generate harmonics that intermix with a 14.9 GHz oscillator output to phase lock it to an external reference [4].

112

5.2 Optical Generation Techniques

The three main techniques for millimeter wave signal generation using semiconductor lasers are shown in Fig. 5.2. These three techniques are: (a) heterodyning two optical sources, (b&c) frequency multiplication by optical comb generation, and (d) direct generation using a modelocked laser as an optical oscillator. An optical comb can be generated by gain-switching, Q-switching, or modelocking, which produce short optical pulses with frequency components far into the millimeter wave band. Alternatively, millimeter wave signals can be directly generated using passive modelocking to form a millimeter wave oscillator with an optical carrier.

A generation technique for applications requiring low harmonic distortion and wide electrical frequency tuning range is to optically heterodyne two continuous wave (CW) lasers [5]. When the sources are combined with the same polarization, the resulting optical field is amplitude modulated at the difference frequency between the optical sources. The difference frequency can be converted to an electrical signal in a photodetector. If distributed Bragg reflector (DBR) laser diodes are used as optical sources, tuning can be achieved by index changes in a Bragg reflector due to free carrier injection or temperature changes [6]. A tuning range of >100 GHz can typically be achieved, limited by discrete optical frequency shifts due to longitudinal mode hopping. This technique is used for frequency domain testing of optical detectors, because the modulation amplitude can be calibrated by separate optical power measurements of the two sources. However, typically the detector impulse response is usually not computed from the frequency response as the detector phase response is not as easily measured.

113

(a) optical
    heterodyne

Laser → Isolator →

Laser → Isolator →

3 dB coupler → output

tuning voltage

(b) gain switching

output

I_g ⊙ ⊙ I_{rf}

(c) external
    cavity
    modelocking

output

100 % Mirror

AR coating

⊙ ⊙ Ⓐ I_a

V_a

(d) mm-wave
    monolithic
    modelocking

I_g ⊙ Ⓐ I_a

V_{tune}
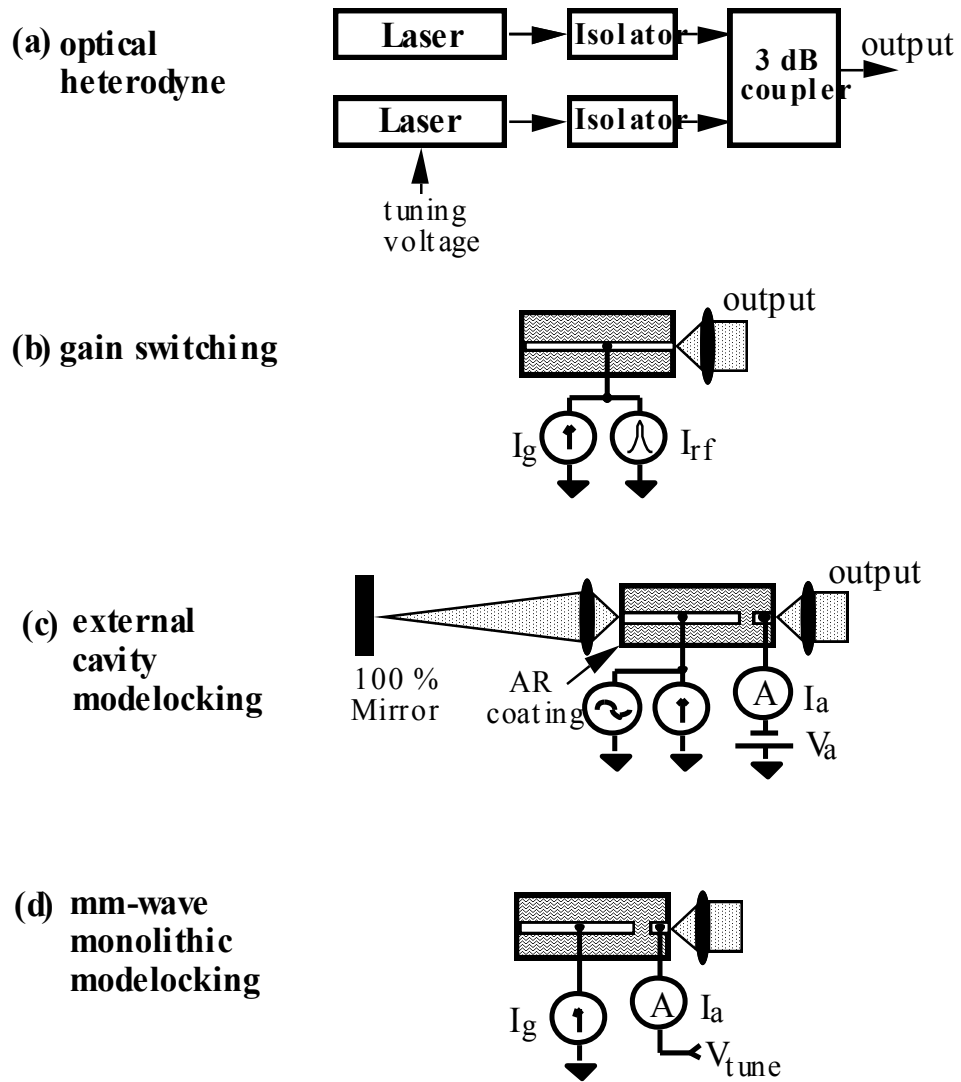
Fig. 5.2   Millimeter-wave optical generation techniques that do not require a millimeter-wave electrical reference.

114

The wide tuning range of the heterodyne technique is a disadvantage when used as a source for a stable millimeter wave reference signal. The phase noise of the beat signal is determined by the optical sources, which might have linewidths on the order of 10 MHz for semiconductor diode lasers. Because of the frequency sensitivity to the phase of the optical signal, the heterodyne method is not ideal for the generation of a stable millimeter wave reference signal.

Gain-switched lasers can be used to generate optical pulses from a sinusoidal electrical signal (Fig. 5.2b), which produces a comb of harmonics spaced by the repetition rate of the optical pulses. This harmonic generation requires an optical nonlinearity, which can be realized by biasing the laser below threshold and operating in the large signal regime. The carrier density is first driven far above threshold, giving large gain which causes the optical signal to rise rapidly. Gain saturation then brings the carrier density down and shuts off the optical pulse. An external cavity modelocked laser is shown in Fig. 5.2c. Modelocking uses pulse shaping similar to gain-switching, except that the resonant cavity allows the pulse shaping to occur over many round trips.

Monolithic cavity devices provide reduced size and a more stable cavity alignment compared to external cavity devices. A monolithic laser configuration is shown in Fig. 5.2d, where an integrated waveguide saturable absorber is used to initiate passive modelocking. The repetition rate of monolithic devices is determined by the length of the cavity. Repetition rates as low as 4.4 GHz have been demonstrated for 1 cm devices [7]. By decreasing the cavity length, very high pulse repetition rates can be achieved. In order for these high repetition rate devices to be useful, the devices should operate under CW pumping and produce distinct pulses [8, 9, 10]. Several groups have reported millimeter-wave repetition rate devices:

Frequency	Pulsewidth	Reference
65 GHz	3.5 ps	Paslawski and Lau (1991)
81 GHz	3.3 ps	Derickson et al. (1991)
350 GHz	0.64 ps	Chen et al. (1991)

Table 5.1   Millimeter-wave monolithic modelocked laser results under CW conditions.

These high repetition rate devices have potential applications such as clock generation and distribution, and millimeter-wave reference signal transmission. Such applications require synchronization to an external electrical source. The goal of pulse synchronization is to have the position of the optical signal envelope be exactly determined by an electrical reference. In practice, this is never completely achieved due to noise processes which cause random movement of the pulse position.

Two other techniques to obtain millimeter-wave modulation are 1) direct current modulation of a high speed laser, and 2) CW laser followed by an external amplitude modulator. Both of these techniques use a millimeter-wave electrical source as a reference, and therefore provide millimeter-wave signal distribution rather than generation. Signal generation is used here to refer to producing millimeter wave modulation without a millimeter wave electrical source.

The next section examines harmonic generation to produce millimeter-wave signals, and compares modelocking and gain-switching as optical sources. The rest of this chapter discusses feedback stabilization of modulated optical sources with electrical references.

5.3 Harmonic Generation

Gain-switching, Q-switching, and modelocking of semiconductor lasers all produce pulsed modulation. The heterodyne technique produces sinusoidal modulation. Pulsed modulation has the advantage that both frequency multiplication and modulation can be combined from the same source. In this way, millimeter reference signals can be generated from a lower frequency microwave source. The instantaneous optical power $P_{opt}(t)$ of a pulsed source can be described as an infinite series of Gaussian pulses:

$$P_{opt}(t) = \frac{\bar{P}T}{\sqrt{2\pi}\sigma_t} \sum_{m=-\infty}^{\infty} e^{-(t-mT)^2/2\sigma_t^2}$$

where $\bar{P}$ is the average optical power, T is the pulse repetition time, and σ_t is the rms duration of the Gaussian pulse.

For an ideal detector, the total electrical power at each harmonic frequency f can be found by converting the time domain description to a frequency domain Fourier series:

$$P_f = 2R_L \left(\frac{\eta q}{h\nu}\bar{P}\right)^2 e^{-(2\pi\sigma_t f)^2}$$

where P_f is the electrical power at a harmonic frequency f, R_L is the load resistance, η is the detector efficiency, q is the electron charge, h is Plank's constant, and υ is the optical frequency.

For a given average optical power, as the pulse gets shorter the electrical power at a given harmonic increases to a limiting value, the number of harmonics increases, and the total electrical power increases. As the repetition rate is reduced, the number of harmonics increases, the electrical power at each harmonic remains

117

the same and the total electrical power increases. The detector is nonlinear, converting optical power to electrical current. Decreasing the pulsewidth or repetition rate increases the peak optical power, which increases the conversion efficiency. High saturation energy can be extracted from a photodetector under reverse bias, where the applied DC field can supply electrical power.

Fig. 5.3 shows the theoretical electrical frequency response from optical comb generation with an ideal detector. A 3 ps optical pulse gives an electrical bandwidth greater than 100 GHz.

This previous discussion focused on the limitations that the modelocked source plays in generating harmonic energy. High speed photodetectors with adequate bandwidth to detect these optical pulses have been reported [11, 12]. However, the fundamental limitation now is the saturation characteristics of high speed photodetectors.

High speed p-i-n detectors have very low saturation limits [11]. These devices have a tradeoff between size and speed. To achieve higher speed, the device area must be decreased in order to reduce the capacitance. This results in a lower saturation energy. Unlike the transmitter limit discussed previously, the saturation power limit of the detector will depend on the repetition rate, as the detector saturation is based on the pulse energy rather than average power. Metal-semiconductor-metal (MSM) detectors have saturation energy densities similar to p-i-n devices but with a larger area, and so can produce somewhat larger electrical signals. These fundamental detector limits are being addressed with novel structures such as traveling wave photodetectors [13, 14].
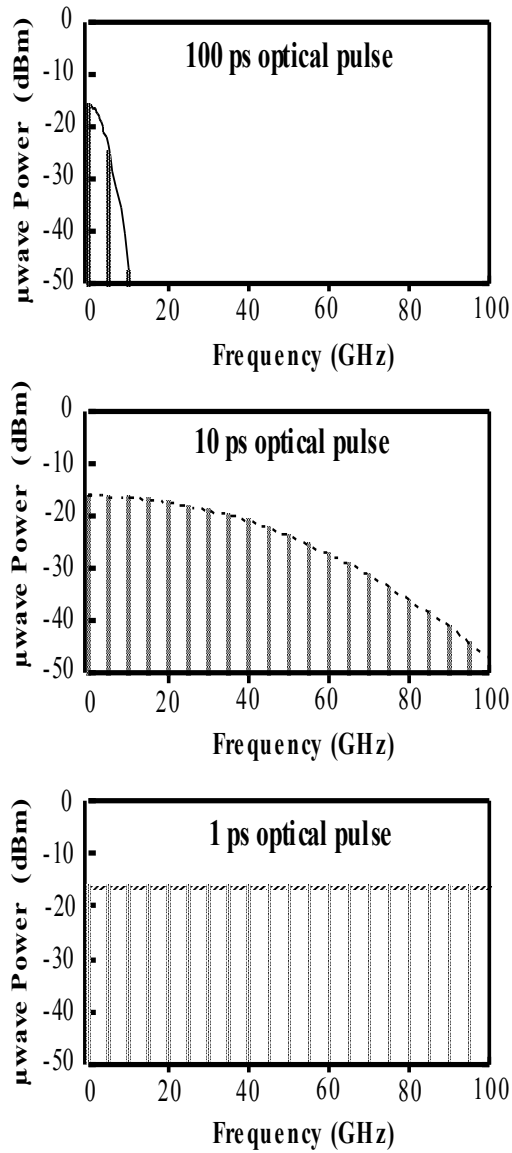
Fig. 5.3   Detected electrical power for a 5 GHz pulsed optical source and an ideal detector.

119

Another interesting possibility is the direct electrical generation from passively modelocked devices, which can have both electrical and optical outputs. With a multisegment device, the saturable absorber is also a photodetector. The carriers that are generated from bleaching the absorber are removed through the electrical contact. This is not the case with saturable absorbers formed by ion implantation in the facets, as the carriers are lost by recombination in the active region.

The electrical output signal from the absorber can be used for a local frequency monitor while the optical output can be used for remote frequency reference transmission. Unfortunately, the integrated absorber is heavily saturated by each pulse, leading to slow detector performance due to carrier screening of the electric field. However, high speed photodetector operation is possible by integrating a separate photodetector with lower optical injection than that in the saturable absorber. This could be done in a monolithic structure with an integrated cavity mirror before the detector. This mirror could be achieved with a cleaved coupled cavity, etched mirror [15], or integrated Bragg reflector [16].

5.4 Stabilization Theory

Pulses produced by passive modelocking are not synchronized to an external electrical reference. However, most modelocking applications require pulse synchronization. Such applications include time-division multiplexed optical transmission, millimeter-wave reference signal transmission, and optical computing. Depending on the implementation, applications such as nonlinear optical switching, photodetector testing, and electro-optic sampling may also require externally synchronized pulses.

Passive modelocking generates optical pulses at the round trip time of the optical cavity. Modelocking is caused by amplitude modulation which is internally generated by the saturable absorber. The saturable absorber produces both an electrical pulse and an optical pulse. The electrically generated waveform can be analyzed as an electrical oscillator with the optical cavity acting as a resonator.

The effect of noise on an oscillator can be described in the frequency domain using a complex phasor to represent the amplitude and phase of the optical envelope [17]. The amplitude is specified by the length of the phasor, and the phase is specified by the angle of the phasor. A phasor representing a signal is shown in Fig. 5.4, along with an additive noise phasor with a random phase and angle. The noise phasor can be broken up into two components. One component of the noise phasor is parallel to the signal phasor, and changes the signal amplitude. This component produces amplitude modulation (AM) and the result is called amplitude noise. The other component of the noise phasor is perpendicular to the signal phasor, and changes the signal phase. This component produces phase modulation (PM) and the result is called phase noise.
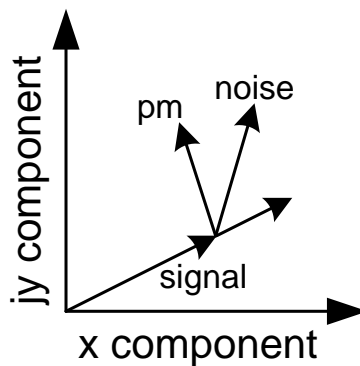
Fig. 5.4   Phasor description of the effect of additive noise on the phase and amplitude of the optical envelope.

121
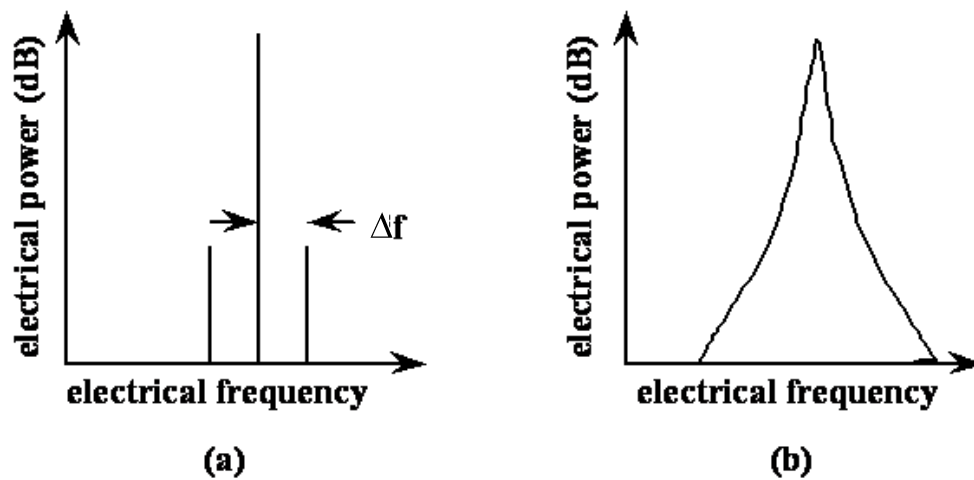
Fig. 5.5   (a) Phase noise due to carrier being modulated by a single noise frequency component.

(b) Phase noise due to carrier being modulated by a continuum of noise frequencies.

The phase modulation due to a single noise frequency causes two sidebands, one on each side of the signal (or carrier) frequency.   The two modulation components are equal in amplitude, and the frequency spacing from the carrier is equal to the noise modulation frequency. However, noise modulation is formed from a continuum of noise frequencies, giving a continuum frequency distribution of the phase noise.   Fig. 5.5 shows the effect of phase modulation due to a single noise frequency and due to a continuum of noise frequencies. Because phase modulation produces a symmetric frequency response, phase noise is frequently plotted for offset frequencies on just one side of the carrier.

A sinusoidal electrical or optical carrier oscillator can be modeled as an ideal oscillator with AM and PM modulation. The oscillator shown in Fig. 5.6 is a voltage controlled oscillator (VCO) with the phase modulation noise voltage in series with the tuning voltage. This model can be used for oscillators without a voltage control

input, by setting the input voltage to zero. The output voltage V(t) of an electrical oscillator can be described as:

$$V(t) = V_0(1 + g_{am}(t))\sin\left[2\pi f_{mod}(t - J_{pm}(t))\right]$$

where f_{mod} is the average oscillation frequency, g_{am} is the random amplitude modulation and $J_{pm}(t)$ is the random timing fluctuation.
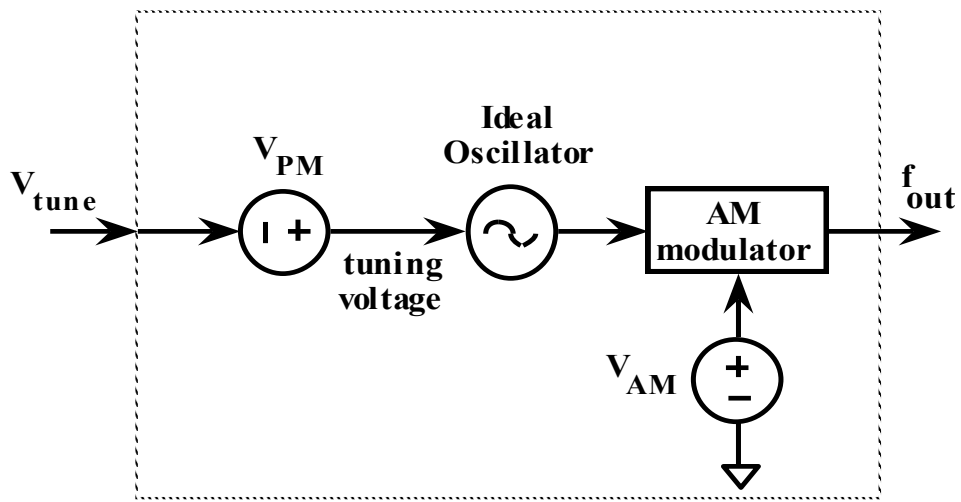
Fig. 5.6   Noise model of a voltage controlled oscillator. V_{pm} models the phase noise. V_{am} models the amplitude noise.

123

In a similar manner, the optical output power P(t) of a passively modelocked laser can be described as a series of pulses:

$$P(t) = \frac{\bar{P}T}{\sqrt{2\pi}\sigma_t} (1 + g_{am}(t)) \sum_{m=-\infty}^{\infty} e^{-(t-mT-J_{pm}(t))^2 / 2\sigma_t^2}$$

where $\bar{P}$ is the average intensity, $T \equiv 1/f_{mod}$ is the pulse repetition period, σ_t is the rms pulse duration, $g_{am}(t)$ is the random amplitude modulation, and $J_{pm}(t)$ is the random timing fluctuation of the pulse train.

For most applications the signal is used to extract frequency and timing information. The result of the amplitude modulation noise expressed by $g_{am}(t)$ is not as important as the frequency modulation in most applications. If AM noise degrades an application, the effect of the noise frequently can be eliminated by monitoring the optical amplitude in order to apply a normalizing correction to the system or measurement.

The phase modulation noise expressed by $J_{pm}(t)$, on the other hand, is usually more detrimental and cannot be as easily corrected. Phase noise causes time-varying changes in the arrival time of the optical pulse, called timing jitter. Timing jitter degrades the timing resolution, giving an effective pulsewidth larger than the actual pulsewidth. For many applications, there is little advantage in having the actual pulsewidth shorter than the root mean square (RMS) timing jitter.

Phase noise is more commonly described in the frequency domain. L(f) is defined as the ratio of the single sideband power in a 1 Hz bandwidth to the total signal power, at a frequency offset f away from the carrier frequency. The phase

124

noise is proportional to the Fourier transform of the timing jitter autocorrelation function [18]:

$$L(f) = \left(2\pi m f_{mod}\right)^2 \int_{-\infty}^{\infty} \left\langle J_{pm}(t) J_{pm}(t+\tau) \right\rangle e^{-j2\pi f\tau} d\tau$$

where $\langle ... \rangle$ is the mean expectation value function, f_{mod} is the fundamental pulse repetition frequency, m is the harmonic number at which the phase noise is being measured, and f is the frequency offset from the carrier frequency $m*f_{mod}$. The timing jitter distribution can be completely determined by either jitter measurements in the time domain or by phase noise measurements in the frequency domain.

It is usually more convenient to compute jitter by frequency domain measurements of the phase noise. The root-mean-squared (rms) jitter can be found by integrating the phase noise [17]:

$$\sigma_{timing\ jitter} \equiv \sqrt{\left\langle J_{pm}(t)^2 \right\rangle} = \frac{1}{2\pi m f_{mod}} \sqrt{2 \int_{f_{low}}^{f_{high}} L(f)\,df}$$

where f_{low} and f_{high} give the offset frequency range over which the timing jitter is defined. This equation gives the relation of the frequency domain description of the noise to the time domain description of the noise.

125

5.5 Phase Noise Integration Limits

In the phase noise integration of each decade of offset frequency, the integral of df increases by a factor of 10. L(f) must decrease by a factor of 10 every decade in order for each decade of frequency to have an equal phase noise contribution. This gives the timing jitter integration function an effective weight of 10dB/decade with respect to phase noise. If the phase noise slope is 11dB/decade, the timing jitter increases without limit as the lower integration limit is reduced. If the phase noise slope is 9dB/decade, the timing jitter increases without limit as the upper integration limit is increased.

Unstabilized oscillators such as passively modelocked semiconductor lasers have a phase noise slope of 20dB/decade [19, 20]. This is a consequence of the noise being generated from phase modulation by a white noise source. Fig. 5 shows the phase noise of an unstabilized oscillator with a slope of 20dB/decade, along with a contour of constant timing jitter with a slope of 10dB/decade. Since the system phase noise has a slope of greater than 10dB/decade, the timing jitter integral grows without limit as the lower integration frequency limit is decreased.

As a result, passively modelocked lasers have infinite timing jitter when integrating the complete phase noise contribution. However, because any measurement takes place over a finite amount of time, the timing jitter integral has an effective lower integration limit. The effective lower integration frequency limit is [17]:

$$f_{low} \approx \frac{1}{2 * (\text{measurement time})}$$

126
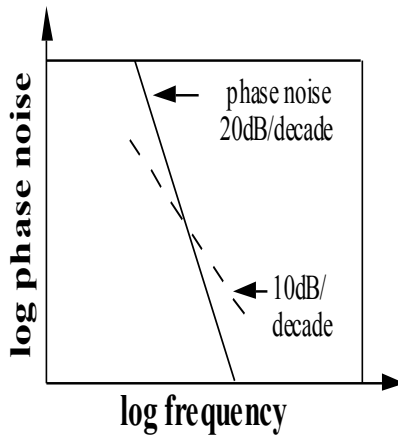
Fig. 5.7   Phase noise of a passively modelocked laser has a slope of 20dB/decade. The timing
jitter increases without limit as the lower integration limit is reduced.
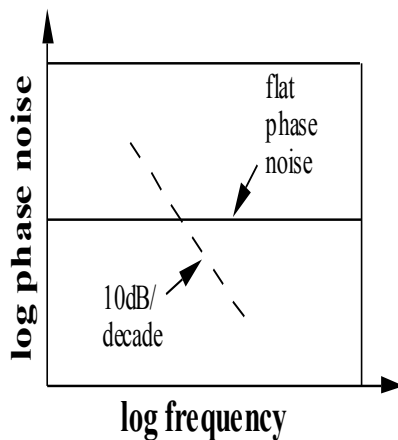
Fig. 5.8   Phase noise of a system with a flat noise floor. The timing jitter increases without limit
as the upper integration limit is increased.

The timing jitter integral can also become unbounded as the upper integration

limit is increased. Fig. 5.8 shows the phase noise of a system with a flat phase noise

floor. If the system phase noise has a slope of less than 10dB/decade, the timing

jitter integral grows without limit as the upper integration frequency limit is

increased. However, a flat noise floor does not contribute infinite timing jitter because the upper integration frequency has a maximum limit.

One upper integration frequency limit is the comb frequency spacing. The electrical spectrum of repetitive pulses is a comb of frequencies spaced at the repetition frequency f_{mod}. The maximum carrier offset frequency from the nearest harmonic is $f_{mod}/2$, before the offset frequency is smaller relative to a different harmonic. The level of broadband phase noise is only significant in systems with large uncorrelated pulse-to-pulse jitter. The resonant external cavity used in modelocking filters the broadband noise. The theory for computing timing jitter due to broadband noise has been developed for gain switched lasers [21].

Another upper integration frequency limit can be set by external noise filtering. Applications that select a single frequency component out of the many available electrical harmonics must have inherent bandpass filtering. An example is injection locking of a microwave oscillator, where the frequency determining resonator rejects signal energy outside of the small locking range of the oscillator. However, applications that require pulsed sources have no significant wide band noise limiting, as a large bandwidth is needed in order to include the pulse harmonics.

In order for the total timing jitter to be bounded, the phase noise should have a slope < 10dB/decade at low offset frequencies, and >10dB/decade at high offset frequencies. Fig. 5.9 shows the phase noise of a passively modelocked laser with a phase noise slope of 20dB/decade, which has been stabilized by a mechanism (described later) to an external reference oscillator at low offset frequencies. The peak timing jitter contribution comes from the transition corner where the slope is

equal to 10dB/decade. The total timing jitter has a bounded value which is found by integrating the noise contribution near the transition corner frequency.
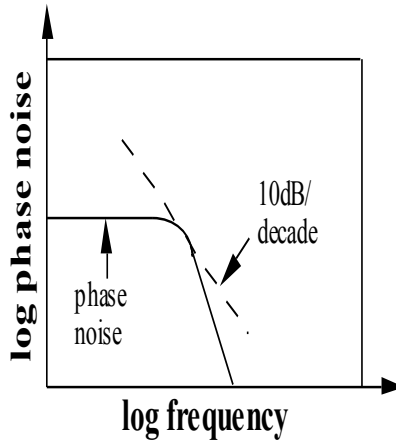
Fig. 5.9   Phase noise of a modelocked laser with low frequency stabilization. The total timing jitter has an upper bound which can be found by integrating the noise contribution near the corner frequency.
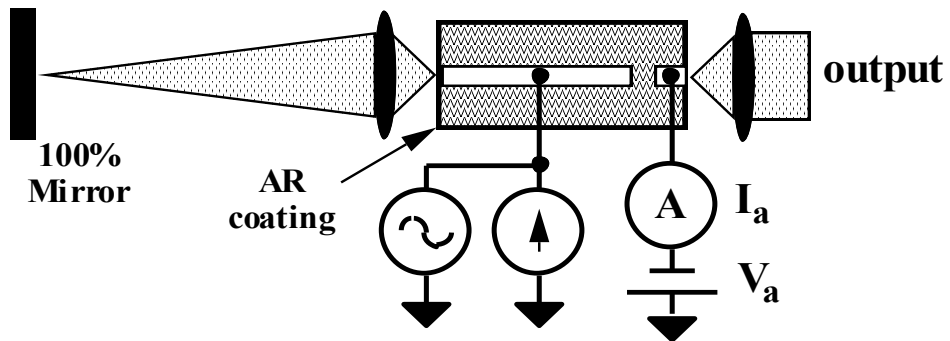
Fig. 5.10   Hybrid modelocking is the combination of active and passive modelocking.

129

5.6 Modulation Stabilization of Repetition Rate

Previously, pulse stabilization of passively modelocked semiconductor diode lasers has been done using gain modulation [22], which by itself produces active modelocking. The combination of active and passive modelocking is called hybrid modelocking.

Hybrid modelocking is shown in Fig. 5.10. In this figure, passive modelocking is caused by an integrated waveguide saturable absorber. Active modelocking is caused by current modulation of the gain region. The pulse shortening due to passive modelocking usually determines the pulsewidth, since the pulse shortening/pass remains constant as the pulsewidth decreases. In active modelocking, the pulse shortening/pass decreases as the pulsewidth decreases.

The addition of active modelocking acts as a pulse stabilizing mechanism. The electrical modulation signal shown in Fig. 5.11 acts as a restoring force on the optical pulse. If the optical pulse is not in the center of the modulation, the side of the pulse that is closer to the modulation center receives more gain. This nonsymmetric gain shifts the center of the optical pulse closer to the peak of the modulation.

The drawback of the gain modulation technique for repetition rate stabilization is that it is limited by the parasitics of the electrical contacts. For the millimeter-wave repetition rates that are possible for monolithic structures [8], another form of stabilization is desirable.

130
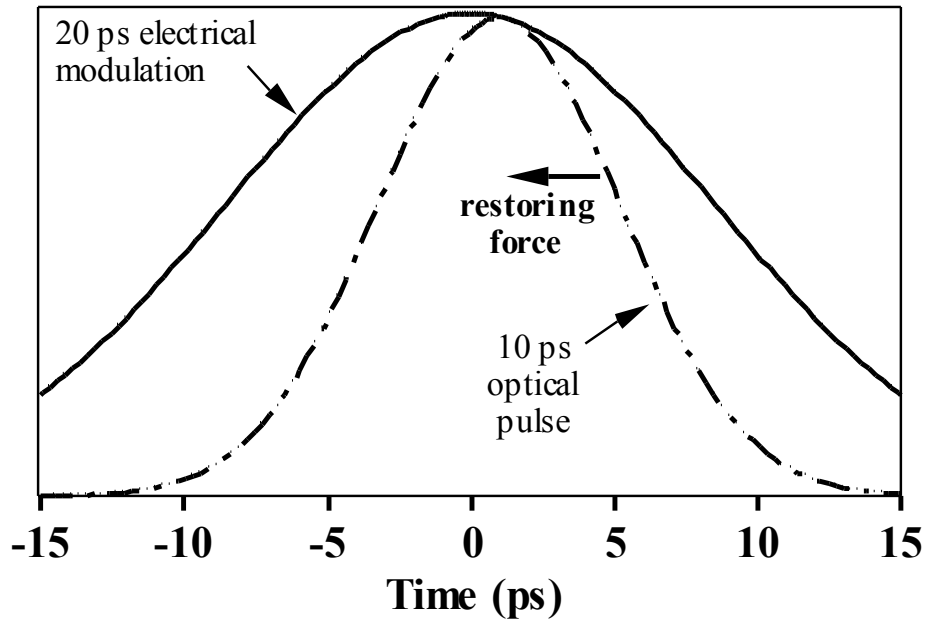
Fig. 5.11   Timing stabilization of an optical pulse is provided by a pulsed electrical modulation
signal. The modulation signal acts as a restoring force on the optical signal.

5.7 Feedback Stabilization of Repetition Rate

Besides amplitude modulation, another stabilization technique is the feedback
method shown in Fig. 5.12. This is a common method for stabilizing electrical
oscillators [23, 24]. The timing of the oscillator is compared to an external
frequency reference. An error signal is generated based on the timing difference
between the oscillator and reference frequency. $K_f(s)$ is the frequency dependent
transfer function used to determine the loop characteristics. This error signal is used
as feedback to a voltage control which changes the timing of the oscillator.

Ideally, the feedback should drive the error voltage to zero, which means the
oscillator and reference signal are perfectly synchronized in phase. In practice,
oscillator noise causes a time varying error voltage which is only partly canceled by

131

the feedback loop. The loop is considered locked when the average phase error is reduced to zero. The amount of oscillator noise that is not canceled by the feedback loop depends on the feedback loop parameters.
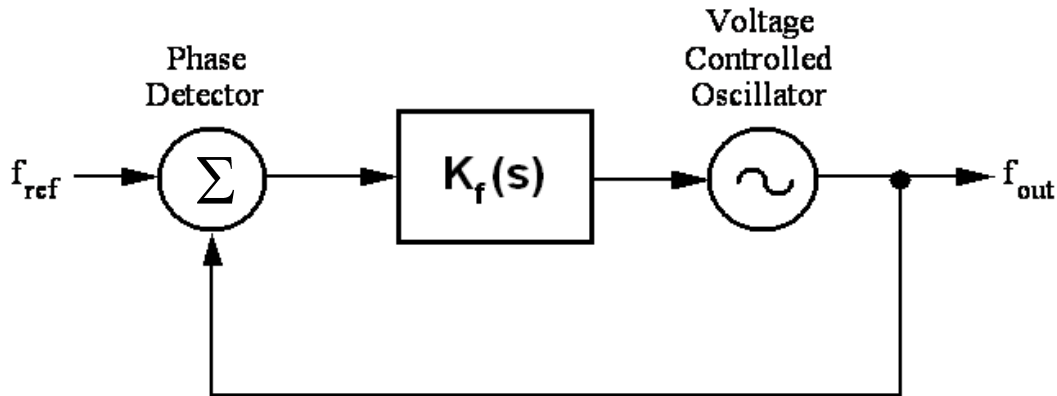
Fig. 5.12   Oscillator feedback stabilization technique.

The timing stabilization of optical sources has been demonstrated on an actively modelocked Nd:YAG laser [18]. The pulse shaping and primary timing stabilization was provided by an optical modulator. However, the low frequency amplitude modulation still allowed substantial pulse jitter due to pulse movement within the modulation timing window. The feedback mechanism was a phase shifter before the optical modulator, which shifted the modulation timing window to increase the effect of the modulator timing stabilization.

Repetition rate stabilization of passively modelocked dye and color center lasers has also been demonstrated using a piezoelectric element to control the cavity length [25]. This has the advantage of replacing a more complex optical modulator with a piezoelectric element for repetition rate tuning, but limits the loop bandwidth to a few kHz, which is too low for stabilizing semiconductor diode lasers.

132

Earlier, as part of this work, feedback was proposed as a means to stabilize millimeter-wave passively modelocked semiconductor lasers [26]. Fig. 5.13 shows a potential compact millimeter-wave source which includes the functions of optical modulation and frequency multiplication from a microwave reference. This type of source would be useful for signal distribution of millimeter-wave reference signals over optical fiber, in such systems as phased array radar [2].
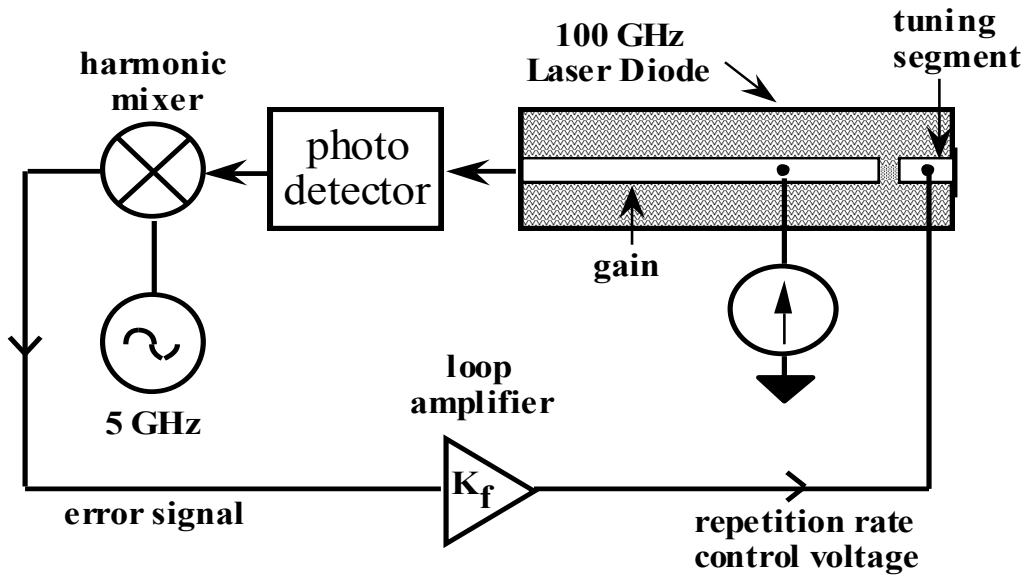
Fig. 5.13   Proposed stabilization of a 100 GHz monolithic modelocked device. The harmonic mixer performs frequency multiplication of the microwave source.

133
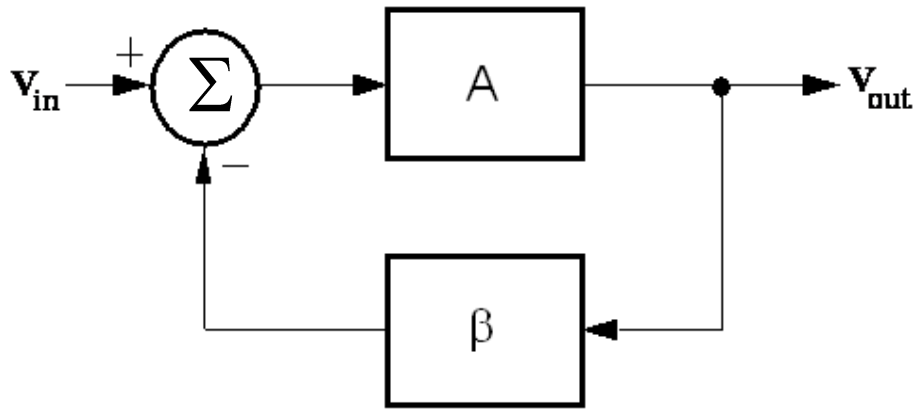
Fig. 5.14   Amplifier feedback stabilization.

The phase locked loop is a feedback system, analogous to the well known amplifier feedback method shown in Fig. 5.14. The closed loop transfer function H(s) is:

$$H(s) \equiv \frac{V_{out}}{V_{in}} = \frac{A}{1+A\beta}$$

where V_{in} is the input voltage, V_{out} is the output voltage, A is the unstabilized amplifier voltage gain, and β is the feedback network transfer function.   Gain stabilization due to negative feedback occurs over the frequency range for which $|1+A\beta|>1$. If the open loop gain $|A\beta|>>1$, then the closed loop gain H(s)=1/β. In this case, frequency and temperature variations in the gain have been removed by feedback.

If the open loop gain $|A\beta|<<1$, then the closed loop gain is equal to the unstabilized amplifier gain A. In this case the feedback has no effect. The variable s=j2πf is the complex frequency variable used in Laplace transform notation.

134

The stabilized oscillator that was shown in Fig. 5.12 has analogous values of $A = K_\phi * K_f * K_v / s$ and $\beta = 1$. K_ϕ / s is the phase detector transfer function, K_f is the feedback amplifier transfer function, and K_v is the voltage controlled oscillator transfer function. If a frequency detector were used in place of a phase detector, it would have a transfer function of Volt/Hz, while the voltage tuned oscillator has a transfer function of Hz/Volt. The product of the two transfer functions is a unit less number. However, a phase detector has a transfer function of Volt/radian, or Volt/Hz*sec. The implicit integration in the conversion of frequency to phase gives an additional 1/s term which needs to be included in the phase detector transfer function.

The operation of the loop can be analyzed when the loop is locked, so that $f_{out} = f_{ref}$. If an external sinusoidal phase perturbation θ_{in} is applied to the reference frequency, this causes a phase perturbation θ_{out} at the output given by:

$$H(s) \equiv \frac{\theta_{out}}{\theta_{in}} = \frac{K_\phi K_f K_v / s}{1 + K_\phi K_f K_v / s}$$

If the oscillator has an internal phase noise perturbation θ_n, the stabilized phase noise reduction function N(s) is given by [17]:

$$N(s) \equiv \frac{\theta_{out}}{\theta_n} = 1 - H(s) = \frac{1}{1 + K_\phi K_f K_v / s}$$

If $|1 + A\beta| > 1$, the phase noise of the source is reduced by the negative feedback of the loop. If $|1 + A\beta| < 1$, the feedback is positive, and the control loop enhances the oscillator phase noise, rather than reducing it.
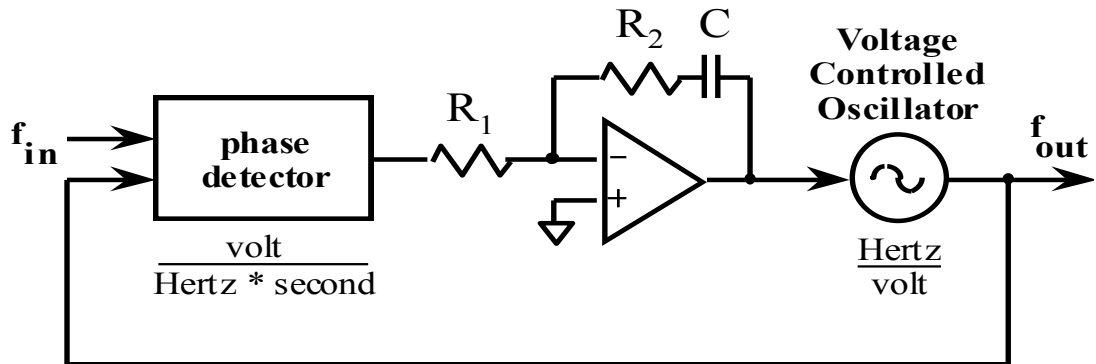
Fig. 5.15   Configuration of a type-2 feedback stabilization circuit.

A feedback stabilization example is shown in Fig. 5.15.   The feedback amplifier transfer function K_f is given by:

$$K_f(s) = \frac{1 + s/\omega_2}{s/\omega_1}$$

where $\omega_1 = 1/R_1 C$ and $\omega_2 = 1/R_2 C$.   This example is a type-2 second order phase-locked loop, which has an open loop response with two poles at the origin.   One pole is from the amplifier, and the other pole is from the inherent phase detector response. The resulting closed loop transfer function $H(s)$ and phase noise reduction function $N(s)$ are:

136

$$H(s) \equiv \frac{\theta_{out}}{\theta_{in}} = \frac{sK_\phi K_v \omega_1 / \omega_2 + K_\phi K_v \omega_1}{s^2 + sK_\phi K_v \omega_1 / \omega_2 + K_\phi K_v \omega_1}$$

$$N(s) \equiv \frac{\theta_{out}}{\theta_n} = \frac{s^2}{s^2 + sK_\phi K_v \omega_1 / \omega_2 + K_\phi K_v \omega_1}$$

The type-2 second order loop has an amplifier slope of 40dB/decade to the origin. This causes a 40dB/decade slope of the phase noise reduction function. Other control loop functions can be realized by choosing a different amplifier gain function $K(s)$.

These equations can be simplified using normalized design parameters ω_n and ζ:

$$\omega_n \equiv \sqrt{K_\phi K_v \omega_1} \qquad \zeta \equiv \frac{\omega_n}{2\omega_2}$$

The closed loop resonance frequency is given by ω_n, and the loop damping is given by ζ. The loop amplifier has two independent parameters, so these two feedback loop parameters can be specified independently.

In terms of the normalized design parameters, the transfer function and phase noise reduction function are:

$$H(s) \equiv \frac{\theta_{out}}{\theta_{in}} = \frac{1 + 2\zeta(s/\omega_n)}{1 + 2\zeta(s/\omega_n) + (s/\omega_n)^2}$$

$$N(s) \equiv \frac{\theta_{out}}{\theta_n} = \frac{(s/\omega_n)^2}{1 + 2\zeta(s/\omega_n) + (s/\omega_n)^2}$$

137

The noise suppression function N(s) is shown in Fig. 5.16 for several values of damping factor ζ.

Critical damping occurs when $\zeta=0.707$. For the under-damped case of $\zeta<0.707$, the noise with feedback will be higher than the open loop noise near the resonance frequency [18]. For the over-damped case of $\zeta>0.707$, the noise reduction is lower than for a critically damped loop with the same 3 dB noise suppression frequency.
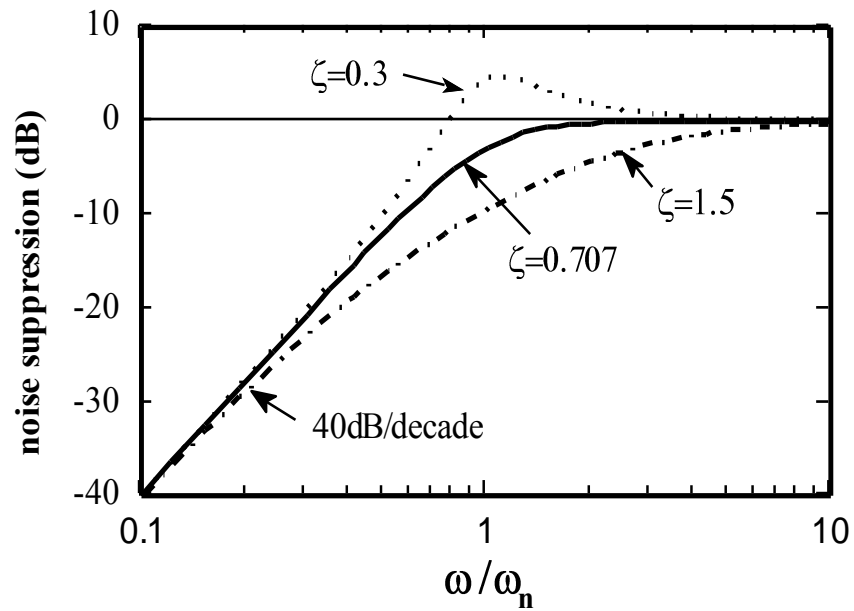
Fig. 5.16   Noise suppression function N(s) for different values of damping factor ζ.

5.8 Feedback Loop Stability

Feedback loops will become unstable if $A\beta=-1$, because then $H(s)\Rightarrow\infty$. The general condition for stability is that all the zeros of $(1+A\beta)$ all lie in the left-half of the complex frequency plane, or the frequency dependent curve of $A\beta$ does not enclose the point $(-1+j0)$ in the complex frequency plane [27]. A simpler condition for stability is that $|A\beta|<1$ when the phase angle $\angle A\beta=180°$. This is condition is sufficient to guarantee stability, but is not necessary.

A graphical method to examine the closed loop stability is the Bode plot [28]. This is a plot of the open loop gain and open loop phase angle. In order for the feedback system to be stable, the open loop gain should be reduced to unity before the open loop phase angle reaches $180°$. The open loop gain A is given in normalized design parameters by:

$$A(s) = \frac{K_\phi K_f K_v}{s} = \frac{1 + 2\zeta(s/\omega_n)}{(s/\omega_n)^2}$$

A Bode plot of the open loop response for a critically damped loop is shown in Fig. 5.17.

139
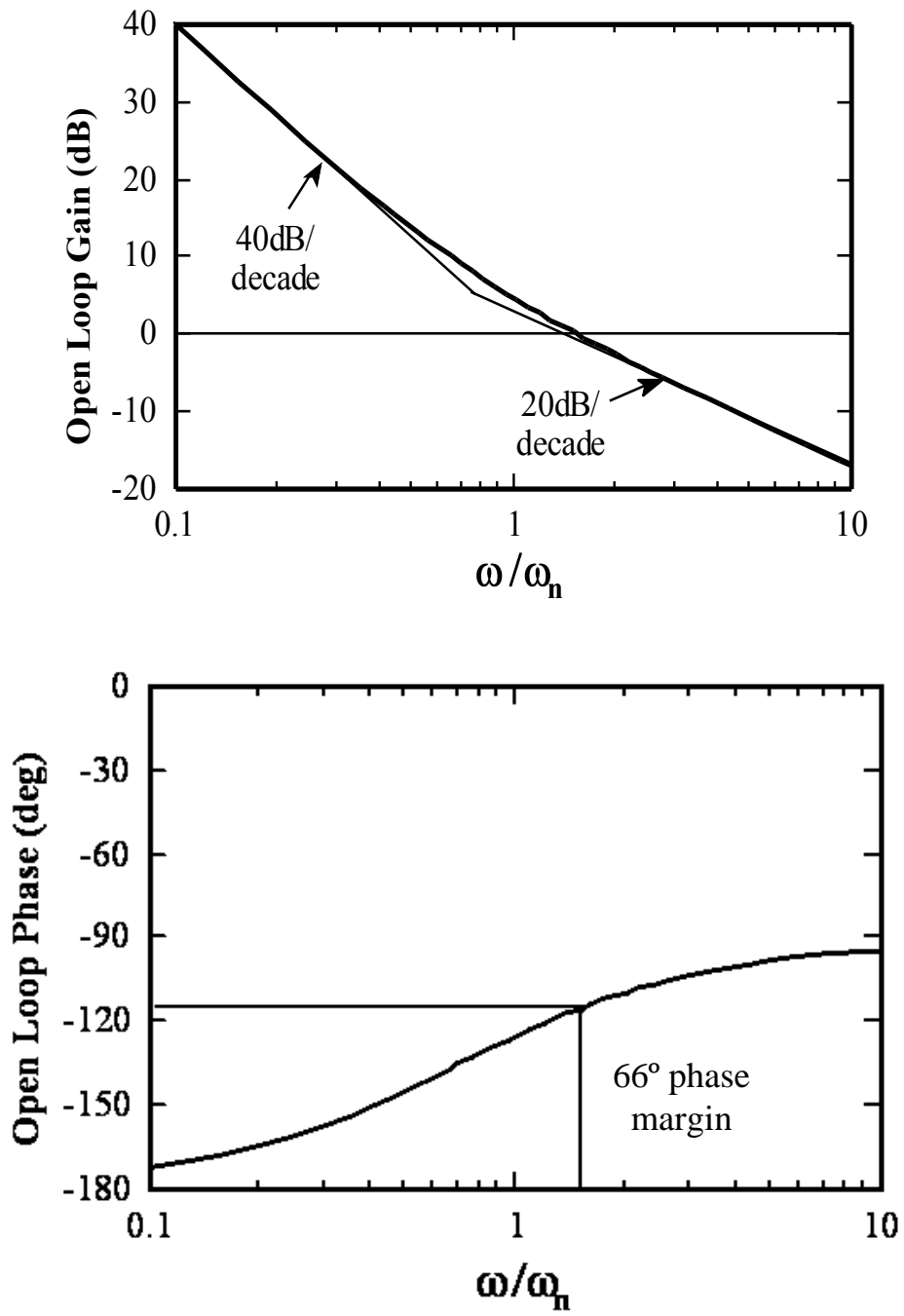
Fig. 5.17   Calculated Bode plot of the open loop response of a critically damped type-2 feedback
loop.

5.9 Repetition Rate Bias Tuning

In order to use feedback stabilization, it is necessary to have a bias dependent repetition rate. Several mechanisms can vary the pulse repetition frequency as a function of bias. One is carrier dependent changes in group velocity, which determines the pulse transit time. Another mechanism is a change in gain or absorption saturation. However, bias changes effect both the gain and phase response of a semiconductor medium. The α parameter is a measure of the ratio between the real and imaginary part of the index. Typical values of α are between 2 and 6.

Gain and absorber saturation cause effective time delays by shifting the pulse center. The time delay caused by absorber saturation is shown in Fig. 5.18. Changes in bias conditions alter the unsaturated gain, and the effective time delay Δt_{gain}, which changes the repetition rate.
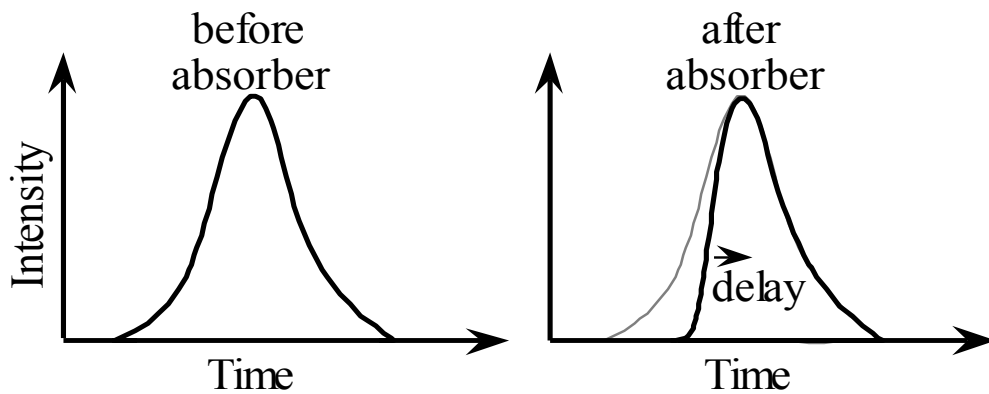
Fig. 5.18   Pulse delay due to saturable absorber.

141

A time delay shift Δt_{index} also results from the change in index associated with any gain change.

$$\Delta t_{index} = \frac{2 L_{seg} \Delta n}{c}$$

L_{seg} is the length of the tuning segment, Δn is the change in index due to a change in the carrier density, and c is the speed of light.

For timing jitter induced by spontaneous emission in these devices, the ratio of the amplitude and index components of time delay caused by spontaneous emission induced noise has been calculated by Derickson [29]. The same mechanism takes place for intentional bias changes as for noise-induced bias changes. The calculated time delay change due to gain saturation changes is ~10 times the time delay change due to index changes, when assuming a value of $\alpha = 4$. This means that gain saturation is the dominant repetition rate tuning mechanism.

5.10 Experimental Stabilization Results

For a monolithic multisection device with a uniform gain region (without using passive waveguide), the two parameters that can be varied are gain region current and absorber region voltage. The bias tuning range was measured using a 5 GHz modelocked semiconductor laser. The active device was a 360 μm long GaAs/AlGaAs bulk active region laser. Passive modelocking was initiated using an 8 μm integrated waveguide saturable absorber, which was placed at one facet. The other facet was antireflection coated and coupled to an external cavity. The optical pulses had a pulsewidth of 3 ps and a spectral width of 3 nm.

142
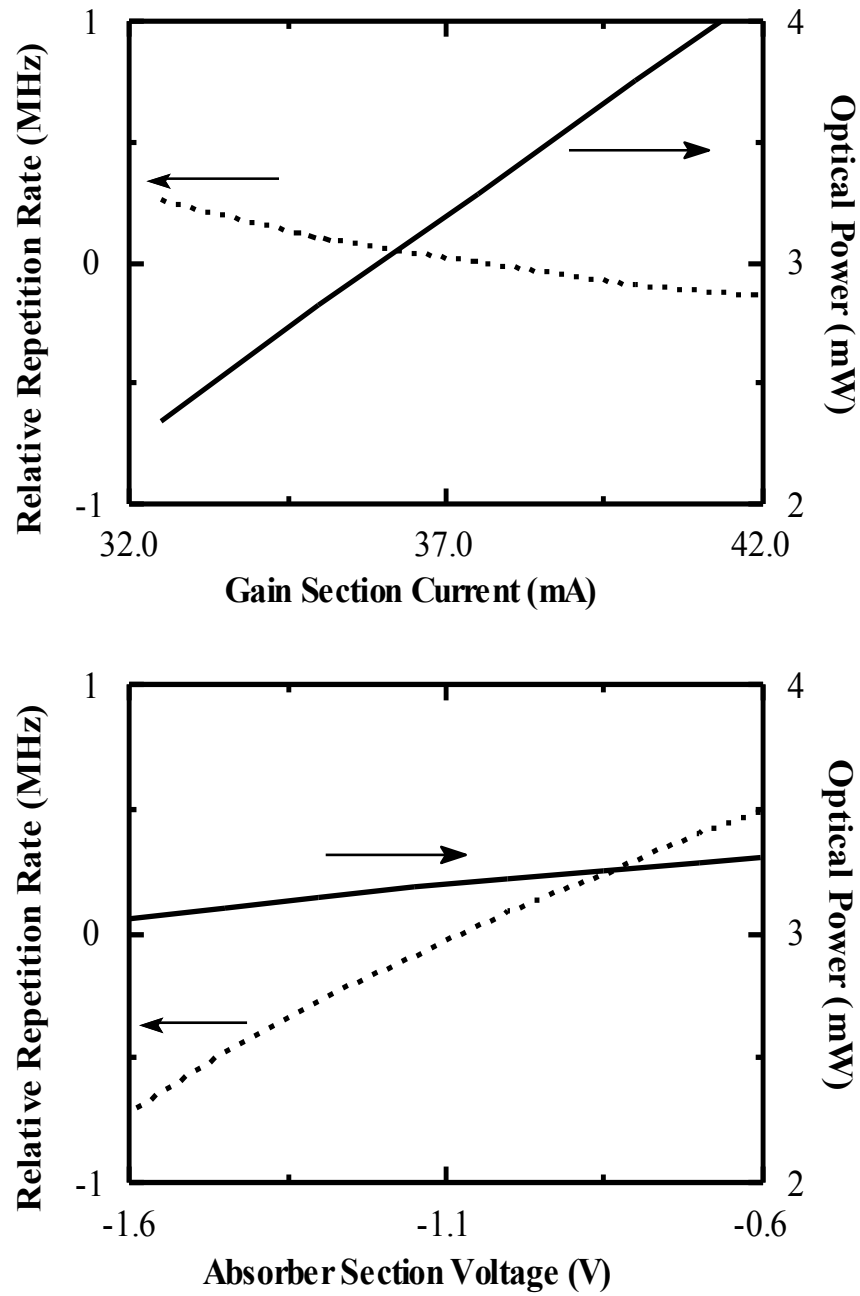
Fig. 5.19 Measured bias tuning of the repetition rate for a 5 GHz external cavity passively modelocked system using gain current tuning and absorber voltage tuning.

The results for bias tuning the gain and absorber regions are shown in Fig. 5.19. As the gain current was varied over a range of 8 mA, there was a large change in output power, and a small repetition rate tuning range. However, by varying the absorber bias over a range of 1 V, the repetition rate changed by 1.2 MHz. This corresponds to a change in the round trip time of 0.05 ps, or 1.7% of the optical pulse duration. There was little change in output power.
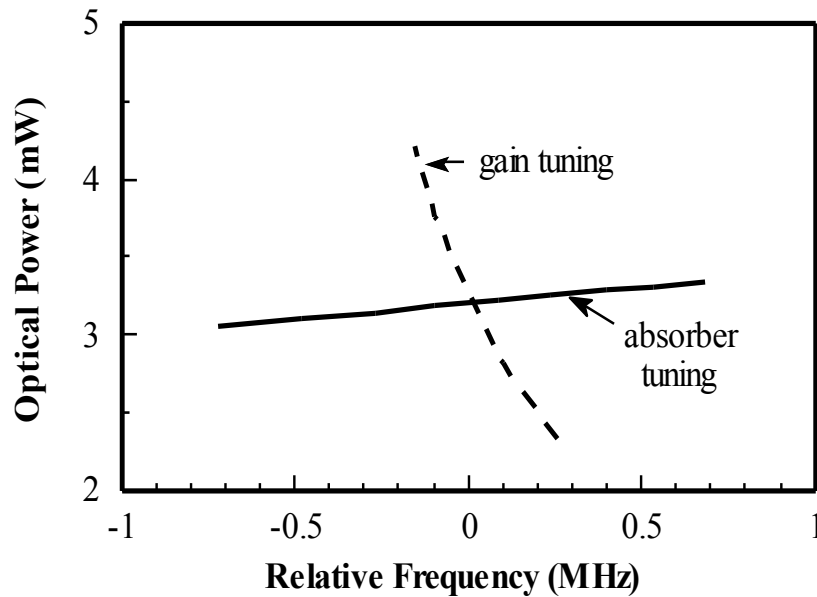
Fig. 5.20   Optical power dependence on repetition frequency for gain tuning and absorber tuning.

The important figures of merit for bias tuning mechanisms are Δf (the total tuning range) and dP/df (the rate of change of power with respect to tuning range). The gain and absorber tuning characteristics are plotted against the relative repetition frequency for gain and absorber tuning in Fig. 5.20. The total tuning range Δf is much larger for the absorber tuning. In addition, the ratio dP/df is smaller (0.2 mW/MHz for the absorber vs -5 mW/MHz for the gain region). This parameter is

144

important, as a constant power output prevents amplitude noise being generated as the bias voltage is changed to cancel out phase noise. The absorber bias is therefore a more appropriate control element for feedback stabilization.

The 5 GHz modelocked laser was stabilized using the experimental configuration shown in Fig. 5.21 [26]. This was the first demonstration of repetition rate feedback stabilization of a modelocked semiconductor laser. The saturable absorber performed the functions of pulse shaping, photodetection, and repetition rate tuning.

The reversed biased saturable absorber was used as a photodetector to monitor the pulse repetition rate. The pulse timing output was compared to both a microwave synthesizer and then a low frequency oscillator using a two-step down-conversion. The second comparison generated a DC error signal which passed through a type-II control loop, and was applied back to the saturable absorber to control the repetition rate. The 16 MHz IF frequency was chosen to be high enough so that the tuning range of the laser did not extend to the other sideband (5032 MHz would also mix down to a 16 MHz IF). This implementation has an advantage over previous feedback stabilization experiments in that the pulse shaping mechanism, the photodetector, and the tuning mechanism are all monolithically integrated along with the gain element into a single device.

5 GHz External Cavity Laser

Absorber   Gain   Antireflection coating

Out

Semiconductor Laser Diode

Stabilization Electronics

control voltage

photodetector signal

16 MHz amplifier

DC amplifier

5016 MHz   16 MHz
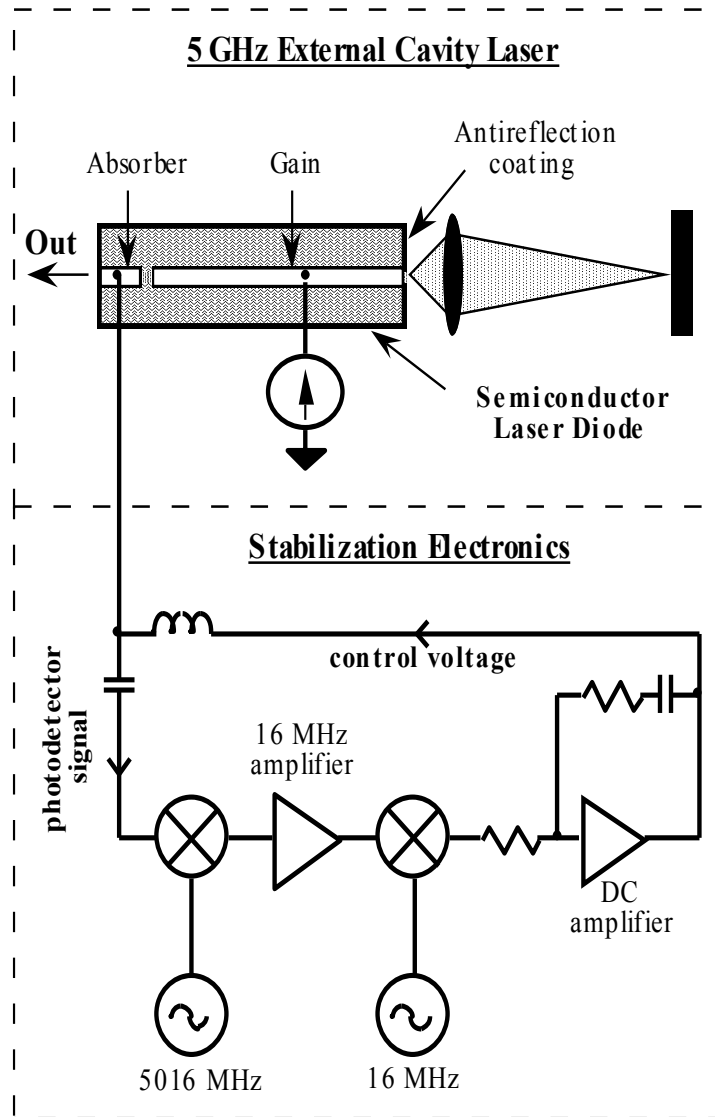
Fig. 5.21   Experimental feedback stabilization configuration. The short segment acts as a saturable absorber, a photodetector, and a repetition rate tuning element.

146

The two-step down-conversion that was used in this demonstration causes a small increase in the complexity of the low frequency components. However, this technique has several advantages. One advantage is that because amplifiers have 1/f noise that dominates at low frequencies, it is desirable to amplify the signal level as high as possible before the phase comparison that generates the DC error signal. Amplification is easier and less expensive at a lower intermediate frequency (IF=16 MHz). Also, the low frequency amplifier can reject amplitude modulation of the modelocked signal from the control loop, which can degrade the phase-lock stabilization.

Another advantage of the two-step down-conversion is that a digital phase/frequency comparator can be used for the phase detector. These devices do not have the out-of-lock error condition, which must be avoided when using analog phase comparators. Also, because the local oscillator (LO=5016 MHz) is different from the modelocked repetition rate, there is no gain modulation stabilization due to LO leakage through the mixer into the saturable absorber. This is important for this demonstration, as it shows that the repetition rate stabilization is only due to the feedback.

In this experimental demonstration, the 16 MHz oscillator for the second stage down-conversion is a crystal oscillator which is not phase-locked to the 5016 MHz microwave reference oscillator. Phase-locking the two oscillators is not important, as the phase noise is completely dominated by the microwave oscillator. However, most microwave oscillators are phase-locked to a low frequency reference which is externally available, so both of these references are usually available already phase-locked together.

147
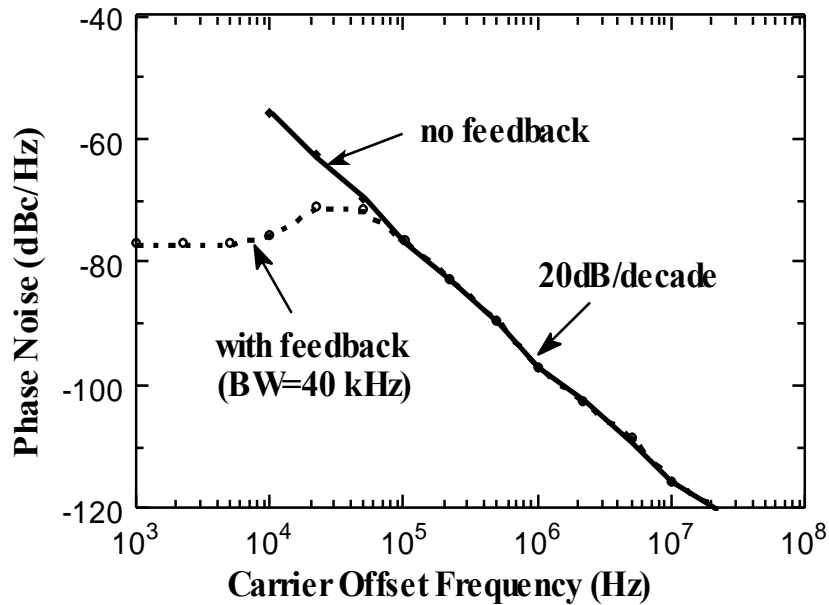
Fig. 5.22   Measured single sideband phase noise with and without feedback stabilization. Calculated stabilized timing jitter = 4 ps.

The measured phase noise is shown in Fig. 5.22 for both open loop (no feedback) and closed loop (with feedback) configurations. The unstabilized system has the characteristic 20dB/decade slope of the phase noise, which produces unbounded timing jitter for arbitrarily long measurement times. For a one second measurement interval, the unstabilized timing jitter was 1 ns.   For longer measurement times, the timing jitter would be even higher. The pulse interval is 200 ps for the 5 GHz repetition rate. A timing jitter of 1 ns implies that during a one second measurement, the number of pulses is 5×10^9, with an rms error of ± 5.

The loop feedback bandwidth for the closed loop configuration was 40 kHz. With repetition rate stabilization, the resulting timing jitter found from integrating all of the phase noise was 4 ps. Unlike the unstabilized case, the timing jitter does not continue to increase as the lower integration limit is reduced. The majority of the

148

timing jitter contribution came from the phase noise near the control loop corner frequency of 40 kHz.

In principle, increasing the loop bandwidth would increase the corner frequency and reduce the phase noise. In this case, however, the loop bandwidth could not be further increased because of instability caused by excess phase shift in the control loop. Timing jitter could be reduced even further by using higher frequency components and increasing the feedback loop bandwidth.

5.11 Summary

Applications of modelocked semiconductor lasers were examined. Fundamental transmitter limits for optical harmonic generation and transmission have been investigated. Short optical pulses provide the most energy for harmonic generation at a given harmonic frequency. However, as the pulsewidth decreases the electrical energy at a given harmonic increases to an asymptotic limit.

For an ideal detector, the amount of electrical power available at a particular frequency is independent of the pulse repetition frequency. For a real detector, the saturation energy is constant as the repetition frequency increases, limited by the detector recovery time. High repetition rates give a higher saturated electrical power.

A feedback technique has been proposed for stabilizing monolithic devices past the modulation frequency limit set by the contact parasitics. This is expected to be an important technique for using high repetition rate modelocked pulses in systems such as optical computing clock generation and millimeter-wave signal distribution. This technique has been demonstrated with a 5 GHz external cavity modelocked semiconductor laser. Timing jitter for a 1 second measurement interval was reduced from 1 ns to 4 ps.

149

References

1. D. B. Huff and J. P. Anthes, "Optoelectronic Isolator for Microwave Applications", IEEE Microwave Theory Tech., **38**, p. 571-575 (1990).

2. A. S. Daryoush, "Optical synchronization of millimeter-wave oscillators for distributed architectures", IEEE Microwave Theory Techniques, **38**, p. 467-476 (1990).

3. J. Wiesenfeld, "Electrooptic Sampling of High Speed Devices and Integrated Circuits", IBM J. of Research and Development, **34**, p. 141-161 (1990).

4. M. G. Li, E. A. Chauchard, C. H. Lee, H.-L. A. Hung, "Intermixing Optical and Microwave Signals in GaAs Microstrip Circuits for Phase-Locking Applications", IEEE Trans. Microwave Theory Tech., **38**, p. 1924-1931 (1990).

5. G. J. Simonis and K. G. Purchase, "Optical Generation, Distribution, and Control of Microwaves Using Laser Heterodyne", IEEE Trans. Microwave Theory Tech, **38**, p. 667-669 (1990).

6. M. Öberg, S. Nilsson, T. Klinga, P. Ojala, "A Three-Electrode Distributed Bragg Reflector Laser with 22 nm Wavelength Tuning Range", IEEE Photonics Tech. Lett., **3**, p. 299-301 (1991).

7. G. Raybon, P. B. Hansen, U. Koren, B. I. Miller, M. G. Young, M. Newkirk, P. P. Iannone, C. A. Burrus, J. C. Centanni, M. Zirngibl, "Two contact, 1 cm long, monolithic extended cavity laser actively mode-locked at 4.4 GHz", Electron. Lett., **28**, p. 2220-2221 (1992).

8. Y. K. Chen, M. C. Wu, T. Tanbun-Ek, R. A. Logan, M. A. Chin, "Subpicosecond monolithic colliding-pulse mode-locked multiple quantum well lasers", **58**, p. 1253 (1991).

9.   J. Paslawski, K. Y. Lau, "Parameter ranges for ultrahigh frequency mode locking of semiconductor lasers", Photon. Tech. Lett., **59**, p. 7-9 (1991).

10.   D. J. Derickson, R. J. Helkey, A. Mar, J. G. Wasserbauer, Y. G. Wey, J. E. Bowers, "Comb and signal generation above 100 GHz using optoelectronics", Photonics Systems for Antenna Applications Conference, (1991).

11.   Y. G. Wey, D. L. Crawford, K. Giboney, J. E. Bowers, M. J. Rodwell, P. Silvestre, M. J. Hafich, G. Y. Robinson, "Ultrafast Graded Double Heterostructure GaInAs/InP Photodiode", Applied Phys. Lett., **58**, p. 2156-2158 (1991).

12.   E. Özbay, K. D. Li, D. M. Bloom, "2.0 ps, 150 GHz GaAs Monolithic Photodiode and All-Electronic Sampler", IEEE Photonics Tech. Lett., **3**, p. 570-572 (1991).

13.   K. S. Giboney, M. J. W. Rodwell, J. E. Bowers, "Traveling-wave photodetectors", Photon. Tech. Lett., **4**, p. 1363-1365 (1992).

14.   J. E. Bowers, K. Giboney, Y. G. Wey, M. Rodwell, "New Concepts in 100 GHz high efficiency photodetectors", LEOS Topical Meeting on Optical Microwave Interactions, **M1.1** (1993).

15.   J. P. Donnelly, W. D. Goodhue, R. J. Bailey, G. A. Lincoln, C. A. Wang, G. D. Johnson, "High quantum efficiency monolithic arrays of surface-emitting AlGaAs diode lasers with dry-etched vertical facets and parabolic deflecting mirrors", Appl. Phys. Lett., **61**, p. 1487-1489 (1992).

16.   H. Kogelnik and C. V. Shank, "Coupled-wave theory of distributed feedback lasers", J. Appl. Phys., **43**, p. 2328-2335 (1972).

17.   W. P. Robins, <u>Phase Noise in Signal Sources</u>, Peter Peregrinus Ltd., London UK (1982).

18. M. Rodwell, D. Bloom, K. Weingarten, "Subpicosecond laser timing stabilization", IEEE J. Quantum. Electron., **25**, p. 817-827 (1989).

19. D. B. Leeson, "Simple model of a feedback oscillator noise spectrum", Proc. IEEE, **54**, p. 329-330 (1966).

20. W. F. Egan, <u>Frequency Synthesis by Phase Lock</u>, John Wiley & Sons, New York (1981).

21. D. A. Leep and D. A. Holm, "Spectral measurement of timing jitter in gain-switched semiconductor lasers", Appl. Phys. Lett., **60**, p. 2451-2453 (1992).

22. D. J. Derickson, P. Morton, J. E. Bowers, "Comparison of timing jitter in external and monolithic cavity modelocked semiconductor lasers", Appl. Phys. Lett., **59**, p. 3372-3374 (1991).

23. E. Labin, "Theorie de la synchronisation par controle de phase", Philips Res. Rept., **4**, p. 291-315 (1949).

24. J. Noordanus, "Frequency synthesizers-a survey of techniques", IEEE Trans. Communication Technology, **COM-17**, p. 257-271 (1969).

25. D. Walker, D. Crust, W. Sleat, W. Sibbet, "Reduction of phase noise in passively mode-locked lasers", IEEE J. Quantum. Electron., **28**, p. 289-296 (1992).

26. R. J. Helkey, D. J. Derickson, A. Mar, J. G. Wasserbauer, J. E. Bowers, R. L. Thornton, "Repetition frequency stabilization of passively modelocked semiconductor lasers", Electronics Letters, **28**, p. 1920-1921 (1992).

27. H. Nyquist, "Regeneration Theory", Bell System Tech. J., **11**, p. 126-147 (1932).

28. H. W. Bode, <u>Network Analysis and Feedback Amplifier Design</u>, D. Van Nostrand Company, New Jersey (1945).

29. D. Derickson, Ph.D. Thesis, University of California, Santa Barbara (1992).

CHAPTER 6

SUMMARY

6.1 Finished Work

A partial integration model was developed to allow more efficient numerical analysis of active and passive semiconductor mode locked lasers. It included important features such as nonuniform gain saturation and imperfect facet coating that are neglected in analytic solutions, but this model required much less computation time than finite difference numeric solutions. The partial integration method demonstrated more than 2 orders of magnitude improvement in computation time over previous finite difference solutions. One order of magnitude came from the improved computation time of unlocking the time and distance steps to reduce the number of computational grid points. The other order of magnitude came from the improved convergence of an exponential gain model. The photon density model was extended to include higher order effects. When using active modelocking, the finite gain-bandwidth of the laser medium was shown to be a limiting factor in producing subpicosecond pulses.

Analytic approximations to rate equations to gain and absorption regimes were developed in order to give useful expressions in limiting cases of large amplifier gain or strong bleaching of an absorber. Numerical convergence of the model was examined using various differential equation solution algorithms. A curved waveguide geometry was demonstrated to effectively eliminate secondary pulse formation. Tapered waveguides were shown to give increased output power.

154

The limits to extending this technique to higher power were analyzed. Large tapering rates can lead to degradation in modelocking performance for this configuration. The first compact optical source producing pulses <0.5 ps was demonstrated. The system produced pulsewidths of 0.45 ps after compression by a dispersive medium, which at the time were the shortest pulses produced by a semiconductor laser with an integrated saturable absorber.

Pulse collision effects in mode-locked semiconductor diode lasers were investigated. These effects can be important to pulse formation in solid-state and dye lasers. It was demonstrated that the colliding pulse effect is actually composed of two important effects - a coherent effect which arises from the grating formation and an incoherent geometrical effect. These effects were examined separately, both theoretically and experimentally. It was shown that the improvement in pulse shaping from the coherent colliding pulse carrier grating effect is *not* important. This is because the unsaturated absorption is much larger for semiconductor diode laser passive mode-locking than in the other passively modelocked systems that have been studied. It was shown that the incoherent colliding pulse effect *is* important because it reduces the bleaching energy of the absorber, and therefore reduces the pulse broadening effects of amplifier gain saturation and self-phase modulation. As part of the investigation, the output facet reflectivity and absorber position were optimized to give high output power or produce shorter pulses. The shortest pulses were obtained with the absorber placed at the output mirror. The highest output power was obtained with an absorber offset from the output mirror, in combination with a low reflectivity coating on the facet. This reduced the 'incoherent CPM' effect, requiring mode-locking to take place at a higher power level. The output from this

higher power configuration was externally compressed to give pulses with a pulsewidth of 0.57 ps and a pulse energy of 1.27 pJ.

Applications for modelocked semiconductor lasers were investigated. For harmonic generation and transmission, the fundamental limits imposed by the source were examined. A feedback technique was proposed for stabilizing monolithic devices past the modulation frequency limit set by the contact parasitics. This technique is expected to be important for using millimeter-wave repetition rate modelocked pulses in systems. This stabilization technique was demonstrated using an external cavity modelocked semiconductor laser at a 5 GHz repetition rate. Using stabilization, timing jitter was reduced from 1 ns to 4 ps for a 1 second measurement interval.

6.2 Further Work

The tapered waveguide results in Chapter 3 use a larger waveguide width at the absorber than the gain end to give higher output power. However, this is the opposite of the principle used in dye lasers, where the spot size in the absorber should be smaller than in the gain region. Another experiment would be to taper the waveguide in other direction to give a smaller spot size in absorber. This would increase, rather than decrease, the saturation ratio σ, leading to somewhat shorter pulsewidths. It should also improve monolithic modelocking, by increasing the modelocking bias parameter range.

This work discussed producing compact sources of subpicosecond optical pulses. However, it still is possible to reduce size of the source further. The size of the source can be drastically reduced by using a monolithic device. However, the grating pulse compressor required for high energy pulses then becomes the dominant

size constraint. Optical fiber can be used to compress upchirped pulses at wavelengths longer than the dispersion zero (such as 1.55 μm). The combination of monolithic source and fiber compressor should give an extremely small source of subpicosecond optical pulses.

6.3 Future Directions

During the course of this work, many of the problems involving modelocked semiconductor lasers have been solved, both here at UCSB and also by other research groups. The modelocking research done to date centers almost entirely on developing devices for systems applications, based on expected system needs. The important area that remains to be addressed is actual system demonstration. This is the stage where remaining device problems can be identified and resolved.

One important aspect that has been explored is generating the high peak power needed for nonlinear optics experiments. Peak power can be maximized with high pulse energy and short optical pulses. Peak optical power >160 W was achieved with 200 fs optical pulses using chirped pulse amplification followed by compression [8]. High average optical power of ~ 40 mW was demonstrated using tapered amplifier devices [9].

Another important aspect that has been explored is pushing the monolithic device technology to very high and low repetition rate extremes. High frequency results under CW conditions were obtained at 65 GHz [1], 81 GHz [2] and 350 GHz [3]. The upper limit on repetition rate is given by the onset of self-pulsation. Low repetition rates require waveguides with very low defect densities. Monolithic structures using passive waveguides achieved 4.4 GHz repetition rates using 1 cm devices [4]. Even lower repetition rates (700 MHz) were realized using a fiber cavity

[5], which gives a mechanically stable package with many of the advantages of monolithic devices.

Soliton propagation requires transform limited (unchirped) pulses. The laser chirp caused by self-phase modulation in semiconductor lasers needs to be eliminated using a narrow spectral filter, usually in an external cavity [6]. Transform limited results suitable for fiber transmission have been demonstrated with the filter integrated in a fiber [5] and in the laser structure using a modelocked DFB laser [7].

An important system area needing work is high data rate optical transmission. For high data rate optical transmission, results nominally >100GBit have been achieved [10] using a single external cavity multiplexed source. Using a single multiplexed source demonstrates high data rate capability of the link, but ignores important source-to-source timing jitter and repetition rate matching.

Further work is needed with monolithic cavity or fiber cavity devices, where multiple sources are used so that the full data bandwidth is completely realized.

References

1. J. Paslawski and K. Y. Lau, "Parameter ranges for ultrahigh frequency mode locking of semiconductor lasers", Photon. Tech. Lett., **59**, p. 7-9 (1991).

2. D. J. Derickson, R. J. Helkey, A. Mar, J. G. Wasserbauer, Y. G. Wey, J. E. Bowers, "Comb and signal generation above 100 GHz using optoelectronics", Photonics Systems for Antenna Applications Conference, Monterey CA (1991).

3. Y. K. Chen, M. C. Wu, T. Tanbun-Ek, R. A. Logan, M. A. Chin, "Subpicosecond monolithic colliding-pulse mode-locked multiple quantum well lasers", Appl. Phys. Lett., **58**, p. 1253 (1991).

4. G. Raybon, P. B. Hansen, U. Koren, B. I. Miller, M. G. Young, M. Newkirk, P. P. Iannone, C. A. Burrus, J. C. Centanni, M. Zirngibl, "Two contact, 1 cm long, monolithic extended cavity laser actively mode-locked at 4.4 GHz", Electron. Lett., **28**, p. 2220-2221 (1992).

5. P. A. Morton, V. Mizrahi, P. A. Andrekson, T. Tanbun-ek, R. A. Logan, P. Lemaire, D. L. Coblentz, A. M. Sergent, K. W. Wecht, P. F. Sciortino, "Mode-locked hybrid soliton pulse source with extremely wide operating frequency range", Photon. Technol. Lett., **5**, p. 28-31 (1993).

6. P. A. Andrekson, N. A. Olsson, M. Haner, J. R. Simpson, T. Tanbun-Ek, R. A. Logan, D. Coblentz, H. M. Presby, K. W. Wecht, "32 Gb/s optical soliton data transmission over 90 km", Photon. Tech. Lett., **4**, p. 76- (1992).

7. P. P. Iannone, G. Raybon, U. Koren, P. R. Prucnal, "Robust electrically tunable 1.5 μm mode-locked fiber-external-cavity laser", Appl. Phys. Lett., **61**, p. 1496-1498 (1992).

8. P. J. Delfyett, A. Dienes, J. P. Heritage, M. Y. Hong, Y. H. Chang, "Femtosecond hybrid modelocked semiconductor lasers and amplifier dynamics", Applied Physics **B**, to be published.

9. A. Mar, R. J. Helkey, J. E. Bowers, D. Mehuys, D. Welch, "Mode-locked operation of a master oscillator power amplifier", Lasers and Electrooptics Society Annual Meeting, **MSFL4.2**, San Jose (1993).

10. S. Kawanishi, H. Takara, K. Uchiyama, T. Kitoh, M. Saruwatari, "100 Gbit/s, 50 km optical transmission employing all-optical multi/demultiplexing and PLL timing extraction", Optical Fiber Communications Conference, **PD2-1**, San Jose (1993).

APPENDIX A

CHIRPED PULSE COMPRESSION

A.1 Spectral Broadening from Self-Phase Modulation

Self phase modulation results from index changes due to gain saturation. This gives a chirped pulse and broadens the optical spectrum. A chirped pulse is one in which the optical frequency changes with time. The increased optical bandwidth causes the finite gain-bandwidth to give an increased pulse broadening per pass, resulting in a longer optical pulse than would be expected from the wide optical gain-bandwidth available from semiconductor laser diodes. This short pulse potential can be recovered by removing the chirp with pulse compression.

A.2 Quadratic Phase Compensation

Quadratic phase compensation with negative group velocity dispersion can be performed using two reflection gratings in the two pass configuration shown in Fig. A.1 [1]. The angle of the reflected light is wavelength dependent, giving the gratings angular dispersion. The grating configuration gives a path length that is a function of wavelength, converting the angular dispersion of the gratings to spectral dispersion. The magnitude of the dispersion is proportional to the grating separation L_d. Since only $z>0$ is physically realizable, only one sign of dispersion is possible.
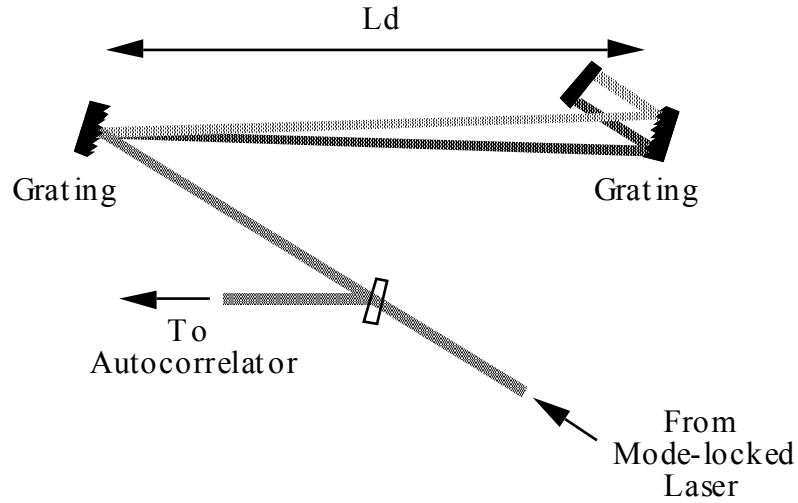
161

Fig. A.1   Grating pulse compressor providing negative group velocity dispersion.

Quadratic phase compensation of either sign can be obtained by adding two lenses between the gratings as shown in Fig. A.2 [2]. The lenses form a telescope which images the first grating at a point away from the grating. This effectively allows positive or negative grating separation, so that up-chirped or down-chirped signals to be compressed. The quadratic phase response for both lenses having the same focal length is given by:

$$\frac{d^2\phi}{d\omega^2} = k\beta^2(z_1 + z_2 - 2f)$$

where f is the focal length of the lenses, k is the free space wave vector, ß is an angular dispersion parameter of the grating, and z_1 is the distance between the input grating and the first lens, and z_2 is the distance between the second lens and second grating. In the case $z_1 = z_2 = f$, there is no linear dispersion component.
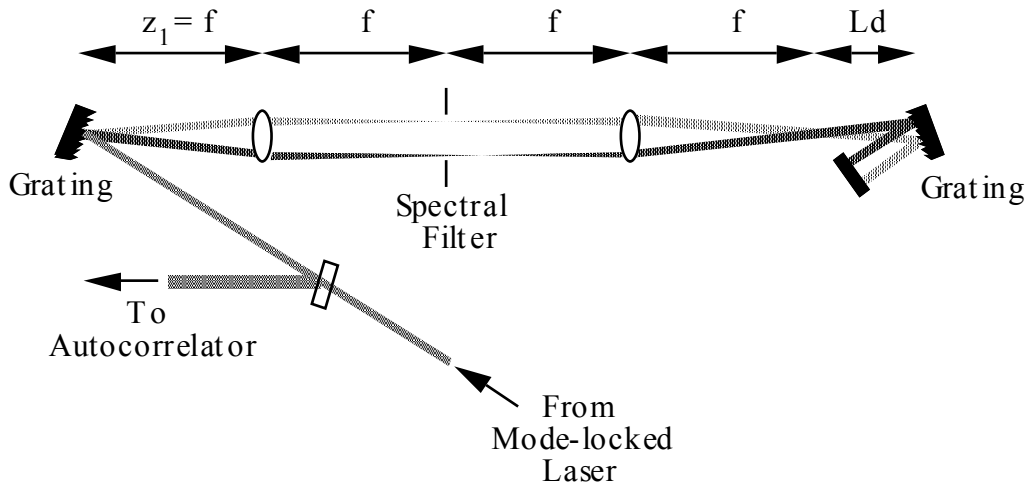
162

Fig. A.2   Telescope/grating pulse compressor providing adjustable positive or negative group velocity dispersion.

To illustrate grating/telescope pulse compressor operation, the simplest form is shown in Fig. A.2, where the first of the two identical lenses is spaced the focal length f from the first grating. The second lens must be spaced 2*f from the first lens. If the second grating spacing is set so that $L_d=0$, then all wavelengths travel the same distance, and there is no wavelength dispersion. The zero dispersion point has been imaged from the first grating in the previous example to a distance 4*f from the first grating when using the telescope. The telescope effectively allows a 'negative' grating separation which gives positive dispersion.

In addition, this more general telescope compressor has a Fourier plane between the two lenses where each optical frequency is focused at a separate point. This allows spectral windowing, in which the part of the optical spectrum that is not linearly chirped, and thus is not compressed, can be discarded by blocking the beam.

In the passive modelocking experiments, optimum pulse compression was obtained in the negative GVD dispersion region of the compressor. This indicates

that the output was up-chirped, with the leading edge of the pulse being lower in frequency than the trailing edge of the pulse. Because the signal is up-chirped, and no spectral windowing was needed, the chirp could be compensated by a two grating compressor without the lenses.

A.3 General Fourier Pulse Shaping

An area in which semiconductors can play an important role is in the area of Fourier pulse shaping. The sources in the past have been dye lasers or solid state lasers, due to the short optical pulses that are produced. However, the input pulse needs a large spectral bandwidth, which is achieved in semiconductor lasers as a result of the large amount of self-phase modulation.

Fourier pulse shaping is an extension of the quadratic chirp compensation which was discussed earlier. In this case, the pulse shape was changed by varying the linear component of the dispersion, with the goal of shortening the pulse. If higher orders of dispersion can be added, in principle any nonlinearly chirped pulse output can be compressed to a transform limited pulse. Higher order dispersion compensation is important for semiconductor lasers, which can have very large nonlinear chirp components.

A technique for arbitrary dispersion generation is shown in Fig. A.3. The spectrum of an optical signal is spread into its Fourier components by a grating, then each wavelength is brought to focus at a separate point. An arbitrary phase function can be imposed on the mirror by masking and etching a substrate to adjust the distance traveled by the optical beam. The mirror can be placed on either side of this programmable phase structure.

Besides short pulses, modelocked lasers can produce a variety of other optical waveforms. Examples are square pulses to avoid pulse breakup in optical switching and rapid periodic pulse trains to excite resonant systems such as atomic and molecular bonds. Producing short pulses by dispersion compensation is just a subset of a more general technique of Fourier pulse shaping. Arbitrary optical waveforms can be generated as well.
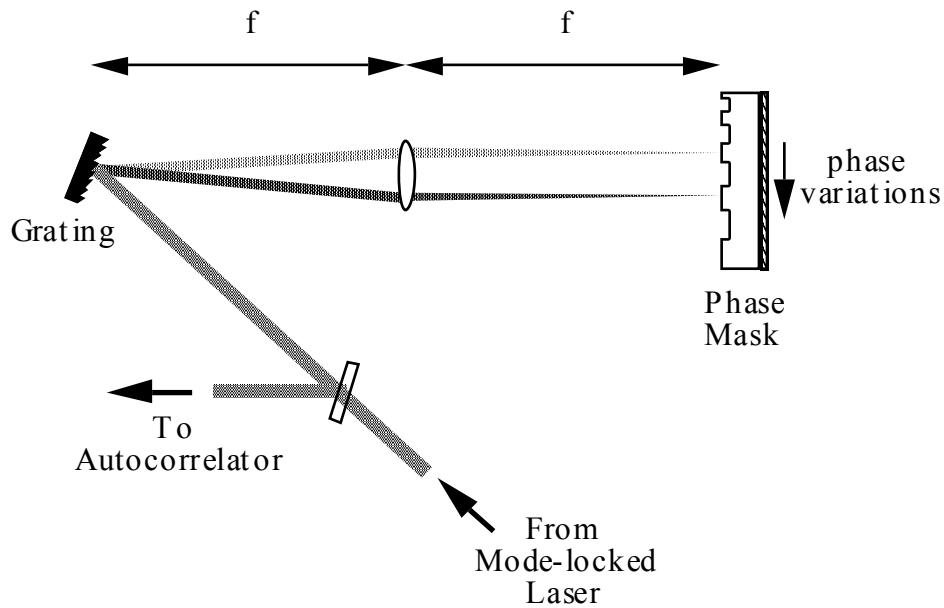

Fig. A.3   General Fourier pulse shaping network.

In general, any output function b(t) can be synthesized from any input function a(t) with the transfer function H(ω):

$$H(\omega) = \frac{B(\omega)}{A(\omega)}$$

where A(ω) and B(ω) are the Fourier transforms of a(t) and b(t) respectively.

The function H(ω) can be synthesized using the same Fourier plane manipulations used for pulse shaping. In practice however, the pulse shaping is only loss-less for phase manipulations. For amplitude shaping, the unwanted spectrum is discarded. To achieve low loss pulse shaping, the input spectrum should have a similar spectral width to the desired output spectrum.

Using a programmable phase mask, the phase linearity of the input waveform is not important as long as it is within the adjustable range. A transform limited or linearly chirped source is not needed. The source needs to provide the spectral width, which can done with semiconductor lasers.

References

1. E.B. Treacy, "Optical pulse compression with diffraction gratings", J. Quantum. Electron., **5**, p. 454 (1969).

2. O.E. Martinez, "3000 times grating compressor with positive group velocity dispersion: application to fiber compensation in 1.3-1.6 μm region", J. Quantum Electron., **23**, p. 59 (1987).

3. A.M. Weiner, Y. Silberberg, H. Fouchhardt, D.E. Leaird, M.A. Saifi, M.J. Andrejco, and P.W. Smith, "Use of Femtosecond Square Pulses to Avoid Pulse Breakup in All-Optical Switching", J. Quantum Electron., **25**, p. 2648-2655 (1989).

APPENDIX B

LIST OF SYMBOLS

A	optical mode cross-sectional area
A^+, A^-	electric field normalized to square root of power
α	chirping parameter
α_i	waveguide internal loss
β	optical phase propagation constant
β'	spontaneous emission into lasing mode
β_g	group propagation constant
β''	dispersion parameter
c	velocity of light in the vacuum
c_L	lens coupling efficiency
d	active region thickness
E	electric field normalized to square root of photon density
E_{bl}	energy to bleach absorber
E_{ph}	photon energy
E_{sat}	saturation energy
f	frequency
f_{mod}	modulation frequency
g	gain coefficient
g_{bw}	bandwidth parameter
G	exponential gain coefficient
G_e	amplifier pulse energy gain
G_f	final amplifier gain

168

G_o	initial amplifier gain
ΔG_{bw}	bandwidth gain reduction
ΔG_{im}	imaginary gain change
Γ	optical confinement factor
h	logarithmic gain coefficient
h_1-h_4	Runge-Kutta gain coefficients
H	feedback loop transfer function
η	electron to photon injection efficiency
j	imaginary number=sqrt(-1)
J	injection current density
K_ϕ	phase detector transfer function
K_f	feedback amplifier transfer function
K_v	voltage controlled oscillator transfer function
L	segment or device length
L(f)	single sideband phase noise in a 1 Hz bandwidth
λ	wavelength of operation of the laser
m	harmonic number
M	number of optical modes in pulse
n	optical phase index
n_g	group index
N	carrier density
N_{tr}	transparency current
ν	optical frequency
ω	optical frequency (radians/sec)
ω_n	feedback loop bandwidth
ω_o	center optical frequency

P	optical power
π	3.14159...
q	electron charge
R_c	cavity mirror reflectivity
R_g	gain facet reflectivity
S	photon density
σ	gain/absorber saturation energy ratio
σ_t	rms pulsewidth
$\sigma_{timing\ jitter}$	rms timing jitter
t	time
τ	normalized integration time
τ_n	carrier recombination lifetime
θ	phase angle
θ_n	noise induced phase perturbation
U_{in}	input pulse energy
v_g	group velocity
ζ	feedback loop damping parameter